Charles University in Prague
Faculty of Mathematics and Physics

MASTER THESIS

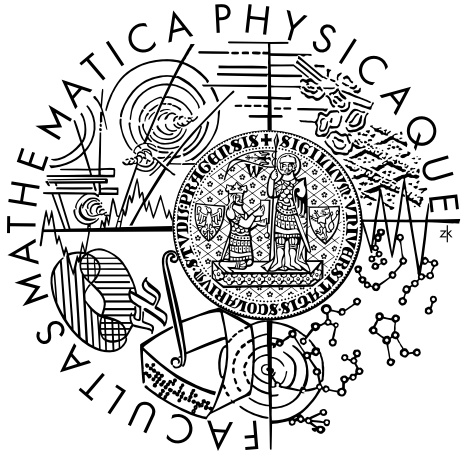

Pavel Motloch

Resumovaná chirální poruchová teorie a studium K_{l4} rozpadů

Institute of Theoretical Physics

Supervisor of the master thesis: RNDr. Jiří Novotný, CSc.
Study programme: Physics
Specialization: Theoretical Physics

Prague 2012

I would like to thank my supervisor RNDr. Jiří Novotný, CSc. for all his help and patience, Mgr. Marián Kolesár, Ph.D. for sharing with me his older Mathematica files, Prof. Johan Bijnens for sending me computer versions of his results, Mgr. Martin Zdráhal and RNDr. Karol Kampf, Ph.D. for fruitful discussions and my parents for all the support.

I declare that I carried out this master thesis independently, and only with the cited sources, literature and other professional sources.

I understand that my work relates to the rights and obligations under the Act No. 121/2000 Coll., the Copyright Act, as amended, in particular the fact that the Charles University in Prague has the right to conclude a license agreement on the use of this work as a school work pursuant to Section 60 paragraph 1 of the Copyright Act.

In Prague date 08/03/2012

Název práce: Resumovaná chirální poruchová teorie a studium K_{l4} rozpadů

Autor: Pavel Motloch

Katedra: Ústav teoretické fyziky

Vedoucí diplomové práce: RNDr. Jiří Novotný, CSc., Ústav částicové a jaderné fyziky

Abstrakt:
V isospinové limitě jsme v resumované chirální poruchové teorii vypočítali formfaktory F a G rozpadů K_{l4} do řádu $O(p^4)$. Odvodili jsme výrazy pro reparametrizaci nízkoenergetických konstant L_1 – L_3 pomocí experimentálních pozorovatelných a tyto jsme použili k získání hodnot nízkoenergetických konstant z nejnovějších experimentálních dat. Poté jsme odhadli teoretickou chybu výsledku a vyšetřovali závislost na parametrech X, Z spontánního narušení chirální $SU(3)\times SU(3)$ symetrie a poměru kvarkových hmot. Dále diskutujeme konvergenci formfaktorů v resumovanné chirální poruchové teorii a naznačujeme, že přidání σ jako explicitního stupně volnosti do chirální poruchové teorie by mohlo výrazně vylepšit konvergenci chirálních řad.

Klíčová slova:
Efektivní teorie pole, Resumovaná chirální poruchová teorie, Nízkoenergetické konstanty, Semileptonové rozpady kaonů

Title: Resummed chiral perturbation theory and study of K_{l4} decays

Author: Pavel Motloch

Department: Institute of Theoretical Physics

Supervisor: RNDr. Jiří Novotný, CSc., Institute of Particle and Nuclear Physics

Abstract:
The F and G formfactors of K_{l4} decays are calculated to $O(p^4)$ in isospin limit in Resummed Chiral Perturbation Theory. Formulae for reparametrization of low-energy constants L_1 – L_3 in terms of physical observables are derived. They are used to obtain values of these low-energy constants from recent experimental data, theoretical error of the result is estimated and dependence on parameters X, Z of spontaneous symmetry breaking of $SU(3) \times SU(3)$ chiral symmetry and quark mass ratio r is investigated. Convergence of the formfactors in Resummed Chiral Perturbation Theory is discussed and it is suggested that inclusion of σ as an explicit degree of freedom into Chiral Perturbation Theory could significantly improve overall covergence of chiral series.

Keywords:
Effective field theories, Resummed Chiral Perturbation Theory, Low-energy constants, Semileptonic kaon decays

Contents

Introduction

The kaon decays have historically played a very important role in helping us understand the world of particle physics. Their investigation led to discovery of third flavor, parity and CP violations, quark mixing and the GIM mechanism. Today, kaon decays remain very important as useful tools which aid us in search for the origin of CP violation and as important probes of physics beyond the Standard Model. For a comprehensive review see [1] and [2].

Theoretical understanding of these decays is hindered by the fact that these decays are goverend by the Quantum Chromodynamics (QCD), which is nonperturbative in the low-energy region; nonperturbative effects include quark confinement and spontaneous breaking of the chiral symmetry. One possible way how to overcome nonperturbative nature of QCD at low energies is to investigate the low-energy hadron physics in the framework of Chiral Perturbation Theory (χPT), which is a systematic expansion of decay amplitudes in terms of momenta and light quark masses [3], [4] (review). It parametrizes the dynamics of low-energy hadrons in terms of a number of parameters called low-energy constants, which are related to the order parameters of the chiral symmetry breaking. Precise knowledge of these low-energy constants is crucial for successful theoretical predictions of χPT.

Because of the specific value of the s-quark mass, pattern of chiral symmetry breaking can be different in the limit of QCD with two and three massless quarks due to vacuum fluctuations of $s\overline{s}$ pairs [5]. This could lead to a suppression of order parameters of the spontaneous symmetry breakdown of the chiral symmetry — especially chiral condensate and Goldstone boson decay constant — in the three flavor χPT which could induce instabilities in the chiral series. If this scenario is realized in the Nature and the suppression of order parameters really occurs, then standard formulation of χPT is built on invalid assumptions. Almost ten years ago, Resummed Chiral Perturbation theory (RχPT) was introduced [5]. This approach to χPT is based on careful selection of "good" observables and cautious manipulation with the chiral series and is capable of correct description of the low-energy hadronic dynamics even in the scenario with strong suppression of the order parameters.

Semileptonic kaon K_{l4} decays hold a substantial position from the point of view of χPT. Their dynamics depends strongly on low energy constants $L_1 - L_3$ of the χPT Lagrangian and investigation of these semileptonic decays represents a very convenient way how to determine these constants [6]. Moreover, understanding of semileptonic kaon decays enables us to understand $\pi - \pi$ decay at low energies which provides a welcomed consistency check of the theory. Recently, precise experimental data about K_{l4} decays were published by E865 [7] and NA48/2 [8] collaborations.

The main aim of this thesis is to calculate the formfactors F, G of the semileptonic kaon decay $K^+ \to \pi^+\pi^- l^+\nu_l$ in the isospin limit to next-to-leading order in RχPT and use the result to obtain values of low-energy constants L_1 – L_3 from the experimental data. Values of these low-energy constants were already determined within the standard treatment of χPT, however the latest fit of the low-energy constants brought controversial results which are incompatible with expectations based on Zweig rule [9]. If this rule is violated, then the low energy constants L_4, L_6 and combination $2L_1 - L_2$ are not suppressed and treatment of the chiral series should be done in the formalism of RχPT, where all aspects of alternative spontaneous symmetry breaking scenario can be taken into account. Within RχPT the semileptonic kaon decays were not investigated so far and this thesis should fill the gap.

The thesis is organized as follows. In Sect. 1 – 3 we give introduction on effective field theories, Chiral Perturbation Theory and its resummed variant RχPT and phenomenology of semileptonic kaon decays. In Sect. 4 we present our method of calculations and give results on the formfactors F and G of the K_{l4} decays. In Sect. 5 we at first use this result in reparametrization of L_1 – L_3 in terms of physical observables and parameters of the chiral symmetry breaking. From the resulting expressions we then calculate values of low-energy constants L_1 – L_3 and estimate the theoretical error arising from higher orders not included in our calculation. In the end we discuss unsatisfactory convergence of the result for higher energies and suggest possible cure.

Chapter 1

Effective Field Theories

When we investigate a problem, it is always convenient to focus only on phenomena that are important for the problem at hand. In many cases it is theoretically possible to include full multitude of interactions that affect the solution in only the tiniest but this approach is not very practical and usually does not brings about much to understand the problem. Effective field theories are one of the manifestations of this doctrine in the world of particle physics and we are going to give a brief overview of them in this chapter.

Effective field theory is always a simplification of some more complete — fundamental — theory. In some cases we know this theory, as in the case of Fermi theory of weak interactions, in others we do not. Among this second group we may count the Standard Model, which we believe would turn out to be part of some "Theory of Everything", which should be able to describe all four currently known interactions. This second group of theories will not be treated in this thesis.

Each fundamental theory contains a set of particles which differ in their rest masses. Often the differences in the masses are significant, as we can see from Table 1 where we listed masses of the six quarks of the Standard Model [10].

quark	mass [MeV]
down	2.3 ± 0.7
up	4.8 ± 0.7
strange	95 ± 5
charm	1275 ± 25
bottom	4180 ± 30
top	173500 ± 1400

Table 1: Quark masses

The basic idea that stands behind transformation from the fundamental theory to an effective theory is that of an energy scale Λ[1], which naturally sorts all particles into light and heavy,

$$m_l \ll \Lambda < M_h \ . \tag{1.1}$$

For the effective theory to be any good, we need a significant mass gap separating masses of heavy particles from investigated energy scale $E < \Lambda$, because then we

[1] Or equivalently the distance scale.

are able to consider the light particles as the only dynamical degrees of freedom and treat presence of heavy particles effectively:

As there is not enough energy for the heavy particles to go on-shell, they can manifest themselves only as virtual exchange particles in the interaction. Corresponding propagator

$$\Delta(p) \sim \frac{i}{p^2 - M_h^2} \tag{1.2}$$

may then be for $p^2 < \Lambda^2$ expanded as

$$\Delta(p) \sim -\frac{i}{M_h^2}\left(1 + O\left(\frac{p^2}{M_h^2}\right)\right) \ . \tag{1.3}$$

We see that exchange of heavy particles is really suppressed — by the factor M_h^{-2} — and we can also read off M_h as radius of convergence of the momentum expansion[2]. If there were no gap separating mass M_h from the investigated energy scale E, we could not expect to obtain a well behaving convergence of the result and heavy particles would have to be included explicitly as dynamical degrees of freedom.

In full theory, we cope with fields of heavier excitations by "integrating them out" from the action[3]. As a result, nonlocal interactions of light particles appear in our theory which are in the low energy region[4] reproduced by an infinite tower of local interactions of light particles in the effective theory. These interactions can be organized as an expansion in $\frac{E}{\Lambda}$, where E stands for the typical energy of the process in question. Coupling constants of the effective low energy Lagrangian then reflect properties of the heavy particles. Because we are interested in the energy region where $E \ll \Lambda < M_h$, we expect that Lagrangian terms scaling with higher powers of energy are suppressed in comparison with the terms scaling with lower powers of energy.

The same reasoning may be applied to the whole Feynman diagrams constructed from the effective Lagrangian, which leads to organization of diagrams with respect to their importance for the investigated process.

Expansion in the powers of energy gives us means of performing rough estimates on which terms in the Lagrangian are relevant to our calculation if we demand relative accuracy ϵ. By setting

$$\left(\frac{E}{\Lambda}\right)^k \approx \epsilon \tag{1.4}$$

we see that for demanded precision we have to include at least terms with

$$k \approx \frac{\log(1/\epsilon)}{\log(\Lambda/E)} \ . \tag{1.5}$$

Similarly to performing perturbative expansion in inverse masses of the heavy particles, analogous treatment is possible to carry out for very light particles with

[2]In case that respective couplings do not depend on M_h.

[3]The theoretical basis for this procedure is so-called Appelquist-Carazzone theorem [11], which is however not valid for all Quantum Field Theories. Spontaneously broken gauge theories serve as an example of such a theory [12].

[4]Under the threshold of heavy particles production.

masses $m_l \ll \Lambda$. Because their masses are much smaller than other energies in the problem, in the first approximation we can set $m_l = 0$. Inclusion of nonzero m_l can then be executed as a perturbation in m_l/Λ.

Regarding the particle content two more things has to be said before going further:

- There may be light particles we do not consider relevant for the investigated problem. In such case, we do not include corresponding degrees of freedom into the theory.

- In asymptotically free theories with confinement low energy degrees of freedom (bound states) may be different from the degrees of freedom of the fundamental theory (which are confined and not directly accessible).

Simply deciding which particles are integrated out, ignored or included into the effective theory does not suffice. Problem is that at any given order, effective Lagrangian would in general contain a very large number of terms which can be constructed from the chosen fields. This setting would have only very little predictive power and we thus need something that would restrict the variety of possible Lagrangian terms. The guiding principle turns out to be the symmetries of the underlying fundamental theory, which we want to reproduce with our effective theory. This assertion lies on a famous conjecture by Weinberg [13]:

> "... if one writes down the most general possible Lagrangian, including all terms consistent with assumed symmetry principles, and then calculates matrix elements with this Lagrangian to any given order of perturbation theory, the result will simply be the most general possible S-matrix consistent with analyticity, perturbative unitarity, cluster decomposition and the assumed symmetry principles." ,

which restricts possible terms only to those which comply with the symmetry principles of the underlying theory.

To our knowledge, this theorem has never been proven, despite being used in lying groundworks to a couple of physical theories, such as Chiral Perturbation Theory (χPT) or String Theory. However, we are not aware of any doubts concerning its validity, with Weinberg himself claiming "which I cannot imagine could be wrong." If we hence include into the Lagrangian all terms that comply with the symmetries of the fundamental theory, we expect that our effective theory will be able to reproduce the fundamental theory by a correct choice of constants of the effective Lagrangian, because the fundamental theory is a theory satisfying criteria of the Weinberg's conjecture.

There is a cost to the transition from fundamental to effective theory, which is closely connected to the limited validity of the effective theory — effective theory is by its construction not power-counting renormalizable. Fortunately this is not an issue, because the theory can be renormalized order-by-order [14]. For example in the case of χPT if we use a renormalization scheme that preserves symmetries of the effective theory, renormalization of the one-loop graphs calculated from the leading order (LO) vertices produces counterterms which are of a next to leading order (NLO). Because of the preserved symmetries, each counterterm must have its counterpart in the next-to-leading Lagrangian, because into the

Lagrangian we included all terms of the given symmetry. The one loop divergences can then be absorbed into the next to leading order Lagrangian by shift in the corresponding low energy constants. At higher levels and number of loops, the argument proceeds analogously and may be used to prove the order-by-order renormalizability.

Chapter 2

Chiral Perturbation Theory

2.1 QCD with massless quarks

Chiral perturbation theory is an low energy effective theory to the QCD. Before we get to the construction of χPT, we first summarize basics of the underlying theory. For a more complete review see [10], [15], [16].

Constituents of QCD are six massive Fermionic fields with spin $\frac{1}{2}$ called quarks, usually organized into a vector

$$q = \big(u, \quad d, \quad s, \quad c, \quad t, \quad b\big)^T \ , \tag{2.1}$$

and non-Abelian spin 1 gauge fields called gluons. The gauge group of the theory is $SU(3)$; apart from flavor index, each quark carries additional quantum number called color. With these constituents we may write Lagrangian of the theory

$$\mathcal{L}_{QCD} = \overline{q}\,(i\not{D} - M_{QCD})\,q - \frac{1}{4}G^{\alpha}_{\mu\nu}G^{\alpha\mu\nu} \ , \tag{2.2}$$

where as usual $\not{D}$ is covariant derivative (in the color space), M_{QCD} is a matrix in the flavor space encompassing quark masses and $G^{\alpha}_{\mu\nu}$ are gulon field strengths.

Quantum Chromodynamics is an asymptotically free theory. The coupling constant of QCD grows with decreasing energy, which makes a thorough analysis of QCD dynamics in the low energy limit an arduous task[1]. To understand the hadronic physics below the energy scale

$$\Lambda_H \approx 1\,\mathrm{GeV} \tag{2.3}$$

it is more instructive to employ the machinery of effective field theories and investigate only the "important". The first step in the way from QCD to an χPT is integrating out three heaviest quarks — charm, bottom and top — from the theory. From Table 1 we see that their masses are well above the chosen energy scale Λ_H and we expect that the error introduced by this is of an order $\approx (E/1300\,\mathrm{MeV})^2$. After this, we switch to the chiral limit, where the masses of the three lightest quarks are set to zero. As the light quark masses are small in comparison with Λ_H, we expect that these masses could be introduced into the theory in a perturbative way. In the next section we show how this can be done.

[1]The coupling constant reaches infinite value at energy scale $\Lambda_{QCD} \approx 250\,\mathrm{MeV}$ [17].

After the two steps described above, we get a Lagrangian

$$\mathcal{L}^0_{QCD} = \overline{q} i \not{D} q - \frac{1}{4} G^\alpha_{\mu\nu} G^{\alpha\mu\nu} \ , \tag{2.4}$$

where we have only three (massless) quarks

$$q = \begin{pmatrix} u \\ d \\ s \end{pmatrix} \ . \tag{2.5}$$

These may be decomposed into right and left handed components

$$q_{R,L} = \frac{1}{2}(1 \pm \gamma_5) q \ , \tag{2.6}$$

which may be used to rewrite the Lagrangian to

$$\mathcal{L}^0_{QCD} = \overline{q_L} i \not{D} q_L + \overline{q_R} i \not{D} q_R - \frac{1}{4} G^\alpha_{\mu\nu} G^{\alpha\mu\nu} \ . \tag{2.7}$$

This Lagrangian has a global symmetry [18]

$$SU(3)_L \times SU(3)_R \times U(1)_V \times U(1)_A \ . \tag{2.8}$$

The $U(1)_A$ symmetry

$$\begin{array}{rcl} q_R & \rightarrow & \exp(i\alpha) q_R \\ q_L & \rightarrow & \exp(-i\alpha) q_L \end{array} \tag{2.9}$$

is not conserved at a quantum level due to the Abelian anomaly (for pedagogical introduction see [18]). The $U(1)_V$ symmetry

$$\begin{array}{l} q_R \rightarrow \exp(i\alpha) q_R \\ q_L \rightarrow \exp(i\alpha) q_L \end{array} \tag{2.10}$$

corresponds to the baryon number and is manifested trivially in the meson sector, as mesons are combinations of a quark and antiquark [16]. The remaining group — chiral group $G = SU(3)_L \times SU(3)_R$ — is the symmetry of the Lagrangian (2.7) that we want to reproduce with our effective theory.

If we parametrize operations from this group

$$G = (g_R, g_L), \quad g_{R,L} \in SU(3) \ , \tag{2.11}$$

then transformations from G act on quarks as

$$\begin{array}{rcl} q_R & \rightarrow & g_R \, q_R \\ q_L & \rightarrow & g_L \, q_L \ . \end{array} \tag{2.12}$$

Group G has an important subgroup $SU(3)_V$, which consists of the symmetry operations

$$H = (g, g), \quad g \in SU(3) \ . \tag{2.13}$$

The Noether currents of the chiral group are [4]

$$J^{a\mu}_A = \overline{q}_A \gamma^\mu \frac{\lambda_a}{2} q_A \quad (A = L, R;\ a = 1, ..., 8) \tag{2.14}$$

and correspodning Noether charges

$$Q_A^a = \int d^3x \, J_A^{a0} \ . \tag{2.15}$$

As was shown by Vafa and Witten [19], the state of the lowest energy in the chiral limit is necessarily invariant under the charges of the vector current

$$J_V^{a\mu} = J_L^{a\mu} + J_R^{a\mu} = \overline{q}\gamma^\mu \frac{\lambda_a}{2} q \ . \tag{2.16}$$

Regarding the charges of the axial current

$$J_A^{a\mu} = J_L^{a\mu} - J_R^{a\mu} = \overline{q}\gamma^\mu\gamma^5 \frac{\lambda_a}{2} q \ , \tag{2.17}$$

there are two distinct possibilities [4]:

- Wigner-Weyl realization of the chiral group with symmetric ground state. In this case, spectrum contains degenerate multiplets of G.
- Nambu-Goldstone realization of the chiral group. In this case the ground state is asymmetric and spectrum contains degenerate multiplets of only $SU(3)_V \in G$.

By a single look at the physically observed spectrum [10] we can rule out the first possibility, as the lightest parity counterpart to the lightest meson $\pi(140)$ can be $a_0(980)$ with much higher energy. We are hence left with Nambu-Goldstone realization of the chiral group corresponding to the pattern

$$G = SU(3)_L \times SU(3)_R \to H = SU(3)_V \ . \tag{2.18}$$

There are also theoretical arguments giving evidence for this possibility [20]. Because the vacuum breaks the invariance of the Lagrangian down to $SU(3)_V$, eight massless Goldstone bosons are expected to appear in the theory [21]. They must be spinless, have negative parity and form an $SU(3)_V$ octet. These are precisely the properties of the eight lightest particles in the spectrum — octet of pseudoscalar mesons (π, K, η) — and this suggests that we should identificate these mesons with the Goldstone bosons of the QCD with massless quarks. The fact that these mesons are not massless in the real world does not constitute a problem because inclusion of quark masses to the Lagrangian breaks chiral symmetry explicitly. Later we will show that meson masses squared are proportional to the masses of the three lightest quarks and hence Goldstone bosons masses really vanish in the limit $m_{u,d,s} \to 0$. Because in reality quark masses are relatively small in comparison to Λ_H, pseudoscalar mesons constitute the lightest particles in the theory, $M_{\pi,K,\eta} \ll \Lambda_H \sim 1\,\mathrm{GeV}$ and are separated from other hadrons by a mass gap.

As a next step we introduce external hermitian matrix fields $v^\mu(x), a^\mu(x), s(x)$ and $p(x)$, couple them to quark fields

$$\mathcal{L} = \mathcal{L}_{QCD}^0 + \overline{q}\gamma^\mu(v_\mu + a_\mu\gamma_5)q - \overline{q}(s - ip\gamma_5)q \tag{2.19}$$

and promote the chiral symmetry from global to local.

The Lagrangian (2.19) gives rise to the generating functional Z defined as

$$\begin{aligned} \exp(iZ) &= \langle 0_{out}|0_{in}\rangle_{v,a,s,p} \\ &= \int \mathcal{D}q\,\mathcal{D}\overline{q}\,\mathcal{D}G_\mu \exp\left(i\int d^4x\mathcal{L}\right) , \end{aligned} \tag{2.20}$$

where $\langle 0_{out}|0_{in}\rangle$ is vacuum-to-vacuum transition amplitude in the presence of external fields. If we knew the generating functional explicitly, we would be able to simply generate Green functions of the Noether currents by performing functional derivatives at $v = a = p = s = 0$. Because we are not able to do it, we must conform to the formalism of effective field theories and reproduce the functional order by order.

As shown by Leutwyler [22], invariance of the generating functional under a local transformation of the external fields is equivalent to the Ward identities obeyed by the Green functions of the theory. This hold only in the absence of anomalies, which must be taken care of specially.

To simplify notation it is customary to introduce linear combinations of axial and vector fields

$$\begin{aligned} r_\mu &= \frac{v_\mu + a_\mu}{2} \\ l_\mu &= \frac{v_\mu - a_\mu}{2} . \end{aligned} \tag{2.21}$$

which under the action of the group G (2.11) have to transform as

$$\begin{aligned} r_\mu &\to g_R\, r_\mu\, g_R^{-1} + i g_R\, \partial_\mu g_R^{-1} \\ l_\mu &\to g_L\, l_\mu\, g_L^{-1} + i g_L\, \partial_\mu g_L^{-1} \\ s + ip &\to g_R(s+ip)g_L^{-1} \end{aligned} \tag{2.22}$$

to conserve invariance under local transformations from G.

External fields enable us to easily incorporate quark masses into our calculations. Instead of taking derivative at $s = 0$, we have to expand s around matrix containing quark masses,

$$M = \begin{pmatrix} m_u & 0 & 0 \\ 0 & m_d & 0 \\ 0 & 0 & m_s \end{pmatrix} , \tag{2.23}$$

by setting

$$s = M + \dots . \tag{2.24}$$

Weak interactions can be similarly introduced through expanding[2] ([4])

$$l_\mu = -\frac{g}{\sqrt{2}}(W_\mu^\dagger T_+ + h.c.) + \dots . \tag{2.25}$$

Here matrix T_+ contains Cabibbo-Kobayashi-Maskawa factors

$$T_+ = \begin{pmatrix} 0 & V_{ud} & V_{us} \\ 0 & 0 & 0 \\ 0 & 0 & 0 \end{pmatrix} . \tag{2.26}$$

[2]We did not consider interactions from Quantum Electrodynamics (QED), so we expand r_μ around zero.

2.2 Effective theory

In the region below Λ_H hadronic spectrum contains first of all octet of pseudoscalar mesons π, K and η which are identified with the pseudo-Goldstone bosons of the QCD with three light quarks. Interactions among these mesons can be easily understood based on symmetry arguments as we show in the following paragraphs. Apart from them, below scale Λ_H we can find vector mesons together with controversial wide resonances $f_0(500)$ and $K^*(800)$ [10]. They can be potentially included into the theory, however they are not explicit degrees of freedom of the χPT. Their possible inclusion is also based on symmetry arguments and a specific example — inclusion of the resonance $f_0(500)$ — will be discussed later in the text.

It is possible to arrange pseudo-Goldstone bosons into a single matrix with simple transformation properties. The derivation starts with realization that Goldstone bosons "live" on the coset G/H, because the subgroup H is associated with the generators of whole G which leave the ground state invariant. We can then denote coordinates of the Goldstone fields in the coset space G/H as ϕ^a $(a = 1, \ldots, 8)$. To remove the ambiguity, we choose a coset representative [14] $\overline{\xi}(\phi) \equiv (\xi_L(\phi), \xi_R(\phi)) \in G$. The chiral transformation $g = (g_L, g_R) \in G$ changes Goldstone fields to

$$\xi_L(\phi) \to g_L \xi_L(\phi) h^\dagger, \quad \xi_R(\phi) \to g_R \xi_R(\phi) h^\dagger \ . \tag{2.27}$$

Here we introduced compensating transformation $(h, h) \in H$, which brings the result back to the chosen coset representative. Knowing that we may introduce

$$U(\phi) = \xi_R(\phi) \xi_L^\dagger(\phi) \ , \tag{2.28}$$

which transforms as

$$U(\phi) \to g_R U g_L^\dagger. \tag{2.29}$$

It is then customary to take the canonical choice of coset representative with $\xi_R(\phi) = \xi_L^\dagger(\phi) \equiv u(\phi)$. The Goldstone fields can then parametrized by 3×3 unitary matrix

$$U(\phi) = u(\phi)^2 = \exp(i\sqrt{2}\Phi/F_0) \tag{2.30}$$

with the field [3]

$$\Phi(x) = \begin{pmatrix} \frac{\pi^0}{\sqrt{2}} + \frac{\eta}{\sqrt{6}} & \pi^+ & K^+ \\ \pi^- & -\frac{\pi^0}{\sqrt{2}} + \frac{\eta}{\sqrt{6}} & K^0 \\ K^- & \overline{K^0} & -\frac{2\eta}{\sqrt{6}} \end{pmatrix} \ . \tag{2.31}$$

As U has convenient transformation properties with respect to G (2.29), it is one of the building blocks of the χPT Lagrangian.

With respect to local invariance, the gauge fields v_μ, a_μ can enter the theory only through covariant derivatives of U [3],

$$\begin{aligned} D_\mu U &= \partial_\mu U - i r_\mu U + i U l_\mu \\ &= \partial_\mu U - i\{a_\mu, U\} + i[U, v_\mu] \end{aligned} \tag{2.32}$$

or the field strength tensors

$$\begin{aligned} F^L_{\mu\nu} &= \partial_\mu l_\nu - \partial_\nu l_\mu - i[l_\mu, l_\nu] \\ F^R_{\mu\nu} &= \partial_\mu r_\nu - \partial_\nu r_\mu - i[r_\mu, r_\nu] \ . \end{aligned} \tag{2.33}$$

Finally we rescale the scalar sources by an unconstrained constant to define

$$\chi = 2B_0(s + ip), \tag{2.34}$$

which transforms in a known way under chiral group.

Now we have all parts which can be used to construct the Lagrangian and we know their transformation properties with respect to the chiral group. The only remaining question is which order to assign to distinct terms in the Lagrangian and how to assess the importance of various Feynman diagrams.

The Lagrangian terms are organized according to the increasing number of derivatives and quark masses,

$$\mathcal{L}_{eff} = \mathcal{L}_2 + \mathcal{L}_4 + \mathcal{L}_6 + \dots \ , \tag{2.35}$$

where subscript gives number of derivatives and where each quark mass is counted as a derivative of the second order. This expansion is in fact expansion in the powers of energy we mentioned in the first chapter, because each derivative brings down a power of four-momentum[3]. The counting rule which counts quark mass as two powers of momentum is based on the identity $p^2 = M^2$ and leading order formulae for meson masses (given further), which state that to this order squared mass of any pseudo-Goldstone boson is proportional to the first power of quark masses, $M^2_{\pi,K,\eta} \sim m_q$. In expansion (2.35) there are no terms odd in momentum, because of the Lorentz invariance and the counting rule for quark masses.

For brevity we say that a variable is of an order $O(p^k)$ if in our scheme it is counted as k powers of momentum. Specifically momentum is of an order $O(p)$ and mass has order $O(p^2)$. In the next paragraph we take a look at the remaining quantities.

Field U contains no derivative or quark mass, thus we count it as a quantity of order $O(1)$. As noted before, space derivative of a field ϕ is of an order $O(p)$. Because of this, derivative $\partial_\mu U$ is also of an order $O(p)$. If we want all terms in the definition of the covariant derivative (2.32) to be of the same order, we must define left and right external fields r_μ, l_μ to be qualities of order $O(p)$ and then naturally the covariant derivative itself must be of this order. Field strengths — which contain two powers of $O(p)$ fields l_μ, r_μ — must be $O(p^2)$. Finally, χ is counted in the same way as s, which is the external field that is expanded around the matrix of the quark masses. Therefore for consistency we must postulate χ to be of an order $O(p^2)$. Table 2 summarizes our counting rules.

Element	Power of momentum
U	$O(1)$
$D_\mu U$	$O(p)$
$F^{L,R}_{\mu\nu}$	$O(p^2)$
χ	$O(p^2)$

Table 2: Power counting convention

[3]This can be best seen in the momentum representation where taking space derivative is equal to multiplication of momentum times imaginary unit.

To sort Feynman diagrams we investigate behavior of their amplitudes under rescaling of all momenta (of both real and virtual particles), quark and physical masses according to

$$\begin{aligned} p &\to t\,p \\ m_q &\to t^2\,m_q \\ M_i &\to t M_i\ , \end{aligned} \tag{2.36}$$

where we introduced a shorthanded notation $q = u, d, s$.

Under this rescaling amplitude of any given diagram is a homogenous function of t,

$$A(t\,p_i, t\,M_i, t^2\,m_q) = t^D A(p_i, M_i, m_q)\ . \tag{2.37}$$

Smaller value of D suggests larger importance of the diagram in the low energy region $E \ll \Lambda_H$.

By analyzing the diagram we find that dependence on t appears in one of three ways — from a vertex, from an internal propagator or from integration over the loop momenta. If we recall that energy scales as $E \sim t$, contribution from vertices has just been discussed. Scaling of the propagators is trivial and depends on the kind of the particle; for scalar particles propagators behave as $\sim t^{-2}$. Finally, integration over the unconstrained loop momenta scales as fourth power of momentum, thus we get contribution $\sim t^4$. Putting all these contributions together we get[4]

$$D = \sum_k 2k \cdot N_k - 2N_I + 4N_L\ . \tag{2.38}$$

Here we denoted N_I number of internal lines, N_L number of loops and N_k number of vertices with Lagrangian interaction from $\mathcal{L}_{2k}$, which scale as E^{2k}. Employing the well-known formula for the number of loops in the graph

$$N_L = N_I - \sum_k N_k + 1 \tag{2.39}$$

we get final result

$$D = 2 + \sum_k 2(k-1) \cdot N_k + 2N_L\ , \tag{2.40}$$

usually called Weinberg's power counting scheme [4]. It may be used to find out, which Feynman diagrams — containing which vertices and how many loops — are necessary to calculate if we want to achieve given precision expressed through coefficient D and related to ϵ in a manner analogous to (1.4).

Now we know all pieces which may be used to construct the Lagrangian, their transformation properties and orders $O(p^k)$. Theorem quoted in Chapter 1 states that to completely describe the dynamics of pseudo-Goldstone bosons we should write the most general Lagrangian consistent with the chiral symmetry.

The lowest order at which we are able to set up a contribution is $O(p^2)$. To this order the χPT Lagrangian is uniquely given by [3]

$$\mathcal{L}_2 = \frac{F_0^2}{4}\langle \partial_\mu U^\dagger \partial^\mu U + \chi U^\dagger + U^\dagger \chi \rangle\ , \tag{2.41}$$

[4]Here we assume only scalar particles can propagate as virtual particles, generalization to other fields is trivial.

with $\langle . \rangle$ denoting trace of a matrix. At the lowest order the Lagrangian of the χPT contains two constants unconstrained by the symmetry — F_0 and B_0. These are related to the most important order parameters of the chiral symmetry breaking:

The F_0 is the Goldstone boson decay constant and corresponds to the leading order contribution to the pion decay constant. As a rough estimate, we thus expect [10]

$$F_0 \approx F_\pi = 92.2\,\mathrm{MeV}\ . \tag{2.42}$$

The constant B_0 is related to the so-called chiral condensate $\langle 0|\overline{u}u|0\rangle_0$ by the formula

$$B_0 = -\frac{\langle 0|\overline{u}u|0\rangle_0}{F_0^2}\ . \tag{2.43}$$

The nonzero value of the chiral condensate generates meson masses in the leading order — by expanding the Lagrangian (2.41) using parametrization (2.30) we can read off coefficients standing at the quadratic terms in the fields, which leads to the LO contribution of the masses in the isospin limit

$$\begin{aligned} \overset{\circ}{M}{}_\pi^2 &= 2\hat{m}B_0 \\ \overset{\circ}{M}{}_K^2 &= (\hat{m}+m_s)B_0 \\ \overset{\circ}{M}{}_\eta^2 &= \frac{2}{3}(\hat{m}+2m_s)B_0\ , \end{aligned} \tag{2.44}$$

where we introduced $\hat{m} = \frac{1}{2}(m_u + m_d)$.

Leading order masses satisfy the Gell-Mann Okubo relation

$$4\overset{\circ}{M}{}_K^2 = 3\overset{\circ}{M}{}_\eta^2 + \overset{\circ}{M}{}_\pi^2\ , \tag{2.45}$$

which is very well satisfied by the experimental data [3].

Relations (2.44) are not sufficient to obtain values of the quark masses and B_0, because scaling

$$\begin{aligned} B_0 &\to xB_0 \\ m_{u,d,s} &\to m_{u,d,s}/x \end{aligned} \tag{2.46}$$

leaves masses (2.44) invariant. However, we are able to use the leading order results for an estimate of the ratio of the quark masses, because

$$\frac{\overset{\circ}{M}{}_K^2}{\overset{\circ}{M}{}_\pi^2} = \frac{\hat{m}+m_s}{2\hat{m}} \to \frac{m_s}{\hat{m}} \approx 25.9\ . \tag{2.47}$$

2.3 Next to leading order

At next to leading order $O(p^4)$ Weinberg's power counting formula (2.40) indicates that at this order computation of the generating functional contains two distinct contributions:

- Tree level graphs with one vertex from the most general effective chiral Lagrangian $\mathcal{L}_4$ of order $O(p^4)$ and arbitrary number of vertices from $\mathcal{L}_2$

- One-loop graphs associated with the lowest order Lagrangian $\mathcal{L}_2$

Moreover, as the anomaly is of this order, we have to add a functional Z_{WZ} which reproduces the anomalous behavior of the QCD generating functional under the chiral gauge transformation.

The most general effective Lagrangian of the order $O(p^4)$ with desired symmetry is [3]

$$\begin{aligned}\mathcal{L}_4 &= L_1\langle D_\mu U^\dagger D^\mu U\rangle^2 + L_2\langle D_\mu U^\dagger D_\nu U\rangle\langle D^\mu U^\dagger D^\nu U\rangle + \\ &+ L_3\langle D_\mu U^\dagger D^\mu U D_\nu U^\dagger D^\nu U\rangle + L_4\langle D_\mu U^\dagger D^\mu U\rangle\langle U^\dagger\chi + \chi^\dagger U\rangle + \\ &+ L_5\langle D_\mu U^\dagger D^\mu U(U^\dagger\chi + \chi^\dagger U)\rangle + L_6\langle U^\dagger\chi + \chi^\dagger U\rangle^2 + \\ &+ L_7\langle U^\dagger\chi - \chi^\dagger U\rangle^2 + L_8\langle\chi^\dagger U\chi^\dagger U + U^\dagger\chi U^\dagger\chi\rangle - \\ &- iL_9\langle F_R^{\mu\nu} D_\mu U D_\nu U^\dagger + F_L^{\mu\nu} D_\mu U^\dagger D_\nu U\rangle + L_{10}\langle U^\dagger F_R^{\mu\nu} U F_{L\mu\nu}\rangle + \\ &+ H_1\langle F_{R\mu\nu}F_R^{\mu\nu} + F_{L\mu\nu}F_L^{\mu\nu}\rangle + H_2\langle\chi^\dagger\chi\rangle\ . \end{aligned} \tag{2.48}$$

As we see, constants $H_{1,2}$ do not contribute to the dynamics of pseudoscalar mesons and are not directly measureable. They are included to serve as counterterms in the renormalization of one-loop graphs. Lagrangian $\mathcal{L}_4$ then contains ten additional low energy constants L_1 – L_{10}, which parametrize our ignorance of the precise QCD dynamics. Values of low energy constants L_i should in principle be obtainable from analytic solutions to QCD, however due to lack of these solutions up to now, we are forced to obtain values of L_i by comparing theoretical calculations with experimental data or by some approximate methods. In the next section we provide a basic introduction into fitting the low energy constants.

The functional that reproduces the anomaly was constructed by Wess and Zumino [23] and Witten [24]. Because its explicit form is important for theoretical soundness of χPT but not for our calculations, we do not give full explicit form here. It may be found for example in [25]. We give here only the term that is relevant for K_{l4} decays,

$$\mathcal{L}_{WZ} = -\frac{\epsilon^{\mu\nu\alpha\beta}}{12\pi^2}\langle U\partial_\mu U^\dagger\partial_\nu U\partial_\alpha U^\dagger l_\beta\rangle\ . \tag{2.49}$$

Finally, we have to include contribution from one loop graphs with vertices from $\mathcal{L}_2$. This may be done in the standard way by the method of evaluating Feynman diagrams with vertices from $\mathcal{L}_2$ or alternatively by using expansion of U around the solution to the classical equations of motion, as did authors of [3]. In this latter approach, Lagrangian terms with third and higher power of quantum fields[5] are neglected, which enables Gaussian integration over the quantum fields. Details may be found in the original article or in the chapter describing our calculations.

As usual, one loop graphs in the dimensional regularization scheme give us infinite contributions which have to be taken care of. In the first chapter we sketched the general approach in effective field theories, here we give a specific example. Using Gaussian integration over pseudo-Goldstone boson fields, we are able to obtain an explicit result for the one-loop contribution to the generating functional Z_{loop} up to order $O(p^4)$.

[5]Difference between a field and the respective solution to the equations of motion.

If we use dimensional regularization in d dimensions, we get a result that can be written schematically as

$$Z_{loop} = \int d^4x \, \frac{R}{d-4} + \text{regular part} \ , \tag{2.50}$$

where regular part contains no singularity in the limit $d \to 4$. Because dimensional regularization preserves chiral symmetry and one-loop results start at an order $O(p^4)$ (2.40), the expression R defined in (2.50) has the general form of the $O(p^4)$ Lagrangian $\mathcal{L}_4$. Infinities at the one-loop level can be hence absorbed by a renormalization of the low energy constants L_i,

$$L_i = L_i^r(\mu) + \Gamma_i \lambda_\infty \ . \tag{2.51}$$

Constants Γ_i may be found in [3], variable λ_∞ contains the singularity

$$\lambda_\infty = \frac{\mu^{d-4}}{(4\pi)^2} \left(\frac{1}{d-4} - \frac{1}{2}(\log(4\pi) + \Gamma'(1) + 1) \right) \ . \tag{2.52}$$

As the renormalization scale we in this text use consistently

$$\mu = 770 \, \text{MeV} \ . \tag{2.53}$$

From now on, whenever we write L_i we mean the renormalized value of the low energy constant, $L_i^r(\mu)$, renormalized at scale μ given above.

To summarize - if we want to calculate contribution to the generating functional up to the order $O(p^4)$, we must include tree graphs with all vertices from $\mathcal{L}_2$; tree graphs with one vertex from $\mathcal{L}_4$ or $\mathcal{L}_{WZ}$ and remaining vertices from $\mathcal{L}_2$ and finally one-loop graphs with vertices from $\mathcal{L}_2$.

2.4 Low energy constants

The variation of the loop contribution under a rescaling of μ provides a natural order-of-magnitude estimate of chiral symmetry breaking scale

$$\Lambda_\chi \sim 4\pi F_\pi \sim 1.2 \, \text{GeV} \ . \tag{2.54}$$

If we recall that we perform an expansion in

$$\frac{p^2}{\Lambda_H^2} \sim \frac{p^2}{\Lambda_\chi^2} = \frac{p^2}{(4\pi F_\pi)^2} \tag{2.55}$$

and compare typical term $\sim \frac{F_\pi^2}{4} p^2$ in $\mathcal{L}_2$ with a typical term $\sim L_i p^4$ in $\mathcal{L}_4$, we obtain a crude estimate [14]

$$L_i \sim \frac{1}{4(4\pi)^2} = 1.6 \cdot 10^{-3} \tag{2.56}$$

of what should be typical magnitude of the low energy constants L_i. Rough estimates of the magnitude of the leading order constants F_0 and B_0 were discussed in the previous sections.

All these constants parametrize unknown dynamics in the nonperturbative regime. Their values can be obtained using QCD-inspired models [26], meson-resonance saturation [27] and lattice QCD [28]. However, by far the most typical is some usage of experimental input and fitting it to next to leading order calculations.

In this section we describe experimental determination of values of L_i in the standard χPT, where it is assumed that next to leading order corrections are much smaller than leading order results and that the same relation holds between next to leading and next to next to leading corrections (NNLO)[6].

First, before the next to next to leading formulae were available, theorists relied on a number of observables that depend on values of L_i.

To obtain values of L_4, L_5 and F_0, NLO results for the decay constants of pions, kaons and eta were used [3]:

$$\begin{aligned} F_\pi &= F_0\left(1-2\mu_\pi-\mu_K+\frac{4M_\pi^2}{F_\pi^2}L_5+\frac{8M_K^2+4M_\pi^2}{F_\pi^2}L_4\right) \\ F_K &= F_0\left(1-\frac{3}{4}\mu_\pi-\frac{3}{2}\mu_K-\frac{3}{4}\mu_\eta+\frac{4M_K^2}{F_\pi^2}L_5+\frac{8M_K^2+4M_\pi^2}{F_\pi^2}L_4\right) \\ F_\eta &= F_0\left(1-3\mu_K+\frac{4M_\eta^2}{F_\pi^2}L_5+\frac{8M_K^2+4M_\pi^2}{F_\pi^2}L_4\right)\ , \end{aligned} \tag{2.57}$$

where

$$\mu_P=\frac{M_P^2}{32\pi^2F_\pi^2}\log\left(\frac{M_P^2}{\mu^2}\right)\ . \tag{2.58}$$

We have three equations with three unknown parameters and we can easily solve the system of equations to get $F_0, L_{4,5}$. In reality, the η decay constant is not known very precisely, which would introduce large uncertainty into the result if we used F_η in our determination. Therefore it is a standard procedure to use only F_π and ratio F_K/F_π (which depends solely on L_5) and obtain the value of L_4 from another source. In the older fits [3], [29] arguments based on Zweig rule were used, leading to conclusion $L_4 \approx 0$. These arguments lead also to $L_6 \approx 0$.

To obtain value of L_9, pion's electromagnetic formfactor is used. This formfactor depends on momentum transfer in the way

$$F_V^{\pi^\pm}(q^2)=1+\frac{1}{6}\langle r^2\rangle_V^{\pi^\pm}q^2+\dots\ , \tag{2.59}$$

where at NLO electromagnetic radius reads [4]

$$\langle r^2\rangle_V^{\pi^\pm}=\frac{12L_9}{F_0^2}-\frac{1}{32\pi^2F_0^2}\left(2\log\left(\frac{M_\pi^2}{\mu^2}\right)+\log\left(\frac{M_K^2}{\mu^2}\right)+3\right)\ . \tag{2.60}$$

From the known experimental value of the radius we are able to obtain the value of L_9.

The low energy constant L_{10} can be pinned down through investigation of semileptonic tau decays [9]. Another possibility is to analyse $\pi \to e^+\nu\gamma$ [3], which depends on combination $L_9 + L_{10}$. From known value of L_9 we are then able to calculate the value of L_{10}.

[6]Description of the position of L_i in the Resummed Chiral Perturbation Theory will be explained in the next chapter.

To get values of L_1 – L_3 it is usual to use formfactors of semileptonic kaon decays, which are discussed in detail in the next chapter. Alternative possibility is to use data about $\pi\pi$ scattering lengths [9].

Finally the constants L_7, L_8 are determined from relations between meson masses. At NLO, we have [3]

$$\begin{aligned}\frac{4M_K^2 - M_\pi^2 - 3M_\eta^2}{M_\eta^2 - M_\pi^2} &= -2 \cdot \frac{4M_K^2\mu_K - M_\pi^2\mu_\pi - 3M_\eta\mu_\eta}{M_\eta^2 - M_\pi^2} \\ &\quad - \frac{6}{F_0^2}(M_\eta^2 - M_\pi^2)(12L_7 + 6L_8 - L_5) \end{aligned} \tag{2.61}$$

and

$$\frac{M_K^2}{M_\pi^2} = \frac{m_s + \hat{m}}{2\hat{m}} \left(1 - \mu_\pi + \mu_\eta + \frac{8}{F_0^2}(M_K^2 - M_\pi^2)(2L_8 - L_5)\right) . \tag{2.62}$$

Because we already know L_5, the only remaining ingredient we must provide to obtain L_7 and L_8 is the ratio of quark masses $m_s/\hat{m}$. This ratio can not be obtained from χPT calculations (at $O(p^4)$) because of an accidental symmetry[7] of $\mathcal{L}_2 + \mathcal{L}_4$ under the change

$$\begin{aligned} \mathcal{M} &\to \alpha\mathcal{M} + \beta(\mathcal{M}^\dagger)^{-1} \det \mathcal{M} \\ B_0 &\to B_0/\alpha \\ L_6 &\to L_6 - \xi \\ L_7 &\to L_7 - \xi \\ L_8 &\to L_8 + 2\xi \ , \end{aligned} \tag{2.63}$$

where we used

$$\xi = \frac{\beta F_0^2}{32\alpha B_0} . \tag{2.64}$$

Above α and β are arbitrary constants. By various choices of β, we are able to nontrivially change quark mass matrix $\mathcal{M}$ and thus the ratio of the quark masses. This ratio must then be provided from other source, such as calculations on a lattice. After we specify the ratio $m_s/\hat{m}$, we are able to extract values of L_i in the suggested way.

So far we discussed original attempts which were focused on determination of L_i using physically accessible observables from NLO expressions. Now we restrict our attention to the newest fit [9], which presents some improvements. First of all, the fit includes a larger number of observables. Instead of the smallest number of observables necessary to obtain values of L_i constants, the authors of [9] decided to include larger set of following observables which they want to reproduce with the χPT calculations:

- masses and decay constants of pseudoscalar mesons
- ratio F_K/F_π
- quark mass ratio $m_s/\hat{m}$

[7] Called Kaplan-Manohar ambiguity, [30].

- K_{l4} formfactors
- $\pi\pi$ scattering lengths and slopes
- πK scattering lengths and slopes
- pion scalar formfactor

The quark mass ratio deserves a short note — it is calculated as either

$$\left.\frac{m_s}{\hat{m}}\right|_1 = \frac{2m_{0K}^2 - m_{0\pi}^2}{m_{0\pi}^2} \tag{2.65}$$

or

$$\left.\frac{m_s}{\hat{m}}\right|_2 = \frac{3m_{0\eta}^2 - m_{0\pi}^2}{2m_{0\pi}^2} \ , \tag{2.66}$$

where $m_{0\phi}$ stands for physical mass of the ϕ meson minus NLO and NNLO corrections. Because of course no direct experimental data on this ratio exist, results of calculations on the lattice are used instead.

Second difference from the original approach is that article [9] uses NNLO formulae. The basic idea behind the fit is to generate various sets of low energy constants and compare how well each set reproduces the experimental data. As variable sorting the sets of low energy constants,

$$\chi^2 = \sum \left(\frac{x_{i(meas)} - x_{i(calc)}}{\Delta x_i} \right)^2 \tag{2.67}$$

is used. Here $x_{i(meas)}$ means experimental value of variable x_i, $x_{i(calc)}$ stands for this variable calculated using given set of low energy constants. Finally, Δx_i are errors of the experimental values. The set minimizing χ^2 — best reproducing the experimental data — is used as the final set of low-energy constants.

This approach should in principle be more precise than simple NLO results, however it presents a major shortcoming. The most general χPT Lagrangian at NNLO level contains 94 additional low energy constants C_i which enter $x_{i(calc)}$ and which are probably impossible to obtain from purely experimental input. The authors of [9] used three distinct ways to obtain these low energy constants

- the resonance saturation model [27]
- study based on first principles of QCD [31]
- random choice of C_i

In the first two approaches the C_i were fixed and only LO and NLO low energy constants were altered to find the best possible χ^2. In the last approach, C_i were given freedom to carry out a random walk and combination leading to smallest χ^2 was searched for using a Monte Carlo type algorithm.

Constant	Value
$10^3 L_1$	0.88 ± 0.09
$10^3 L_2$	0.61 ± 0.20
$10^3 L_3$	-3.04 ± 0.43
$10^3 L_4$	0.75 ± 0.75
$10^3 L_5$	0.58 ± 0.13
$10^3 L_6$	0.29 ± 0.85
$10^3 L_7$	-0.11 ± 0.15
$10^3 L_8$	0.18 ± 0.18

Table 3: Values of low energy constants L_i

Various assumption lead to various sets of low energy constants, the main new result of the article [9] is the set of low energy constants summarized in the Table 3.

2.5 Convergence problems and Resummed χPT

As presented in the previous chapter, χPT with massive quarks is an expansion in masses of the quarks around the χPT in the chiral limit. Because masses of down and up quarks are small in comparison with Λ_H and even masses of the pseudoscalar mesons, we expect a very good convergence of calculated observables in the two-flavor χPT. By two flavor χPT we understand effective theory to QCD, where we perform an expansion in quark masses around the $SU(2) \times SU(2)$ chiral limit with massless up and down quark while we keep m_s at its physical value. Direct calculations in the two-flavor χPT confirm these expectations about good convergence [32].

Position of the strange quark is somewhat different. Its mass is small enough in comparison to Λ_H to be used as an expansion parameter in three flavor χPT, where we perform an expansion around the $SU(3) \times SU(3)$ chiral limit with massless up, down and strange quarks. By comparing Λ_H with the kaon mass we expect convergence given by the ratio $M_K^2/\Lambda_H^2 \sim 0.3$. However, mass of the strange quark is of order Λ_{QCD} which means s quark is not heavy enough to suppress loop effects of massive $\overline{s}s$ vacuum pairs. This can have interesting consequences in the different chiral dynamics of two- and three-flavor χPT [5].

The difference could lie in a possible relative enhancement of chiral order parameters of two-flavor χPT

$$\begin{aligned} \Sigma(2) &= -\lim_{m_u, m_d \to 0} \langle \overline{u}u \rangle \Big|_{m_s = physical} \\ F(2)^2 &= -\lim_{m_u, m_d \to 0} F_\pi^2 \Big|_{m_s = physical} \end{aligned} \tag{2.68}$$

with respect to chiral order parameters

$$\begin{aligned} \Sigma(3) &= \lim_{m_s \to 0} \Sigma(2) \\ F(3)^2 &= \lim_{m_s \to 0} F(2)^2 \end{aligned} \tag{2.69}$$

in the three-flavor χPT.

These variables should satisfy paramagnetic inequalities

$$\begin{aligned} \Sigma(2) &> \Sigma(3) \\ F(3)^2 &> F(2)^2 \ , \end{aligned} \tag{2.70}$$

with the difference proportional to the mass of the strange quark [5],

$$\Sigma(2) = \Sigma(3) + m_s \cdot \lim_{m_s \to 0} \int d^4x \langle \overline{u}u(x)\overline{s}s(0)\rangle_c \tag{2.71}$$

and analogously for F. If the hypothesis about substantial vacuum fluctuations is true, then the three flavor condensate $\Sigma(3)$ could be numerically considerably smaller than the two flavor condensate and similarly for $F(3)$. This suppression of $SU(3) \times SU(3)$ order parameters could lead to a particular instability of the three-flavor χPT as order parameters are connected to the parameters of the LO three-flavor χPT Lagrangian

$$\begin{aligned} F(3) &= F_0 \\ \Sigma(3) &= B_0 F_0^2 \ . \end{aligned} \tag{2.72}$$

For a long time analyses were based on an explicit assumption that the effect of vacuum fluctuations of the $\overline{s}s$ pairs on order parameters is small and it was assumed that the order parameters are such that $F_0 \approx F_\pi$ and $2\hat{m}\Sigma(3) \approx M_\pi^2 F_\pi^2$. In such case, corrections due to nonzero m_s can be considered to be small perturbations.

Based on this assumption, standard χPT calculations consisted of two steps. First, the calculated quantity was written as an expansion in the masses of the light quarks

$$A = \sum_{i,j,k} m_u^i m_d^j m_s^k A_{ijk}(m_u, m_d, m_s; B_0, F_0, L_i, \ldots) \ . \tag{2.73}$$

The right hand side of (2.73) is called "strict chiral expansion". The dots represent higher order low energy constants, explicit dependence of A_{ijk} on masses of the quarks was introduced to cover the chiral logarithms which arise from Goldstone boson masses in the loops. The second step consists in inversion of the expressions [3] for the pion mass

$$\begin{aligned} M_\pi^2 = 2\hat{m}B_0 \Bigg(1 + \mu_\pi - \frac{1}{3}\mu_\eta + \frac{16\hat{m}B_0}{F_0^2}(2L_8 - L_5) + \\ + (2\hat{m} + m_s)\frac{16B_0}{F_0^2}(2L_6 - L_4) + \ldots\Bigg) \ , \end{aligned} \tag{2.74}$$

pion decay constant

$$F_\pi = F_0 \left(1 - 2\mu_\pi - \mu_K + \frac{8\hat{m}B_0}{F_0^2}L_5 + \frac{8(2\hat{m} + m_s)B_0}{F_0^2}L_4 + \ldots\right) \tag{2.75}$$

and ratio of kaon and pion masses

$$\frac{M_K^2}{M_\pi^2} = \frac{m_s + \hat{m}}{2\hat{m}} \left(1 - \mu_\pi + \mu_\eta + \frac{8}{F_0^2}(m_s - \hat{m})B_0(2L_8 - L_5) + \ldots\right) \ . \tag{2.76}$$

Because usually it was assumed that the LO contribution is decisive and vacuum fluctuations of the strange quark pairs are small, variables in the parentheses were supposed to be very close to one. It was then possible to obtain inversions that were to NLO linear in L_i, for example

$$\begin{aligned} 2\hat{m}B_0 &= M_\pi^2 \left(1 - \mu_\pi + \frac{1}{3}\mu_\eta - \frac{8M_\pi^2}{F_\pi^2}(2L_8 - L_5) - \right. \\ &\left. - \frac{8M_\pi^2 + 16M_K^2}{F_\pi^2}(2L_6 - L_4) - \dots\right) . \end{aligned} \tag{2.77}$$

Using these inversions, quantities other than M_π^2, M_K^2 and F_π^2 which were used in the determination can be expressed[8] as an expansion in powers of physical masses M_P^2 and logarithms $\log(M_P^2)$, with coefficients depending on the low energy constants of NLO and higher orders. Because the resulting relations are linear in the low energy constants[9], we are able to obtain their values from a sufficiently large number of experimental variables. As we saw, this agenda is crucially dependent on the assumption that NLO corrections are small in comparison to the LO contribution; if this assumption does not hold and the leading and next to leading contributions are of a similar size, $A_{LO} \sim A_{NLO}$, the standard treatment of the chiral series does not work.

To investigate how much the vacuum fluctuations of $\overline{s}s$ pairs affect the expansions we define quantities

$$\begin{aligned} X &= \frac{2\hat{m}B_0F_0^2}{M_\pi^2F_\pi^2} \\ Z &= \frac{F_0^2}{F_\pi^2} , \end{aligned} \tag{2.78}$$

which incorporates information about the convergence of the expansions of F_π^2 and $F_\pi^2M_\pi^2$. It is customary to introduce one more quantity,

$$Y = \frac{X}{Z} = \frac{2\hat{m}B_0}{M_\pi^2}, \tag{2.79}$$

which tells us about the convergence of the expression for the pion mass.

In the standard treatment it was assumed that the leading order saturates the series and thus it was expected that

$$X, Z \sim 1 . \tag{2.80}$$

Recent results limit ranges for these quantities as ([33], [34])

Source Type	PACS - CS Subset Lattice calculations	RBC/UKQCD Subset Lattice calculations	Descotes - Genon RχPT
X	(0.59 ± 0.21)	(0.20 ± 0.14)	$X \leq 0.83$
Y	(0.90 ± 0.22)	(0.43 ± 0.30)	$Y \leq 1.1$
Z	(0.66 ± 0.09)	(0.46 ± 0.04)	$0.18 \leq Z \leq 1$

Table 4: Recent values of X, Y, Z

[8] In the usually considered isospin limit.

[9] Again — only to next-to-leading order; in NNLO we get contributions from tree graphs with two vertices from L_4, which depend on L_i quadratically. In such case, we may use for example the least squares method to obtain values of L_i [9].

From these values we see that the assumption (2.80) might not be valid and thus the standard treatment could be based on invalid assumptions.

To cope with the shortcoming of the standard treatment, Resummed χPT was introduced [5].

It assumes that chiral series of observables that are linearly related to the low energy correlation functions in the domain of their analyticity far away from singularities have satisfactory convergence properties. These are for example F_π^2, $F_\pi^2 M_\pi^2$ or decay amplitudes of processes with pseudo-Goldstone bosons, multiplied by appropriate powers of pseudo-Goldstone boson decay constants. Apart from these, observables which are obtainable from the generating functional $Z[v, a, p, s]$ by linear operations are also considered as convergent in a satisfactory manner. We will call all these observables "good", to distinguish them from other observables which we will call "dangerous". Each observable can be written as a sum of leading order, next to leading order contributions and the residual term

$$A = A_{LO} + A_{NLO} + A\delta_A \ , \tag{2.81}$$

the residual term contains contributions from the higher orders. In RχPT, we assume that "good" observables fulfill condition

$$|\delta_A| \ll 1 \tag{2.82}$$

which means that NNLO and higher contributions are small. We call observables fulfilling condition (2.82) "globally convergent".

On general grounds we expect that for "good observables",

$$\delta_A \sim \frac{M_K^4}{\Lambda_H^4} = 0.1 \ . \tag{2.83}$$

However, magnitudes of remainders for certain quantities[10] are constrained by the $SU(2) \times SU(2)$ low energy theorems to be of order $O(M_\pi^2 M_K^2)$ or even $O(M_\pi^4)$. In such cases, we expect even better convergence than 10%. On the other hand, certain quantities start their expansions in NLO. In such case, our expectations on the reminder are worse as the NLO and NNLO expansions can differ in only a single power of m_s. Our estimate on δ_A in such case is

$$\delta_A \sim \frac{M_K^2}{\Lambda_H^2} = 0.3 \ . \tag{2.84}$$

With defined NNLO reminder, we can show that observables depending non-linearly on the generating functional could exhibit poor convergence. As an example we take ratio of two "good" observables, which can be formally expanded in the form

$$\frac{A}{B} = \frac{A_{LO}}{B_{LO}} + \frac{A_{LO}}{B_{LO}} \left(\frac{A_{NLO}}{A_{LO}} - \frac{B_{LO}}{B_{NLO}} \right) + \frac{A}{B} \delta_{A/B} \tag{2.85}$$

with

$$\delta_{A/B} = \frac{(1 - X_B)(X_A - X_B)}{X_B^2} + \frac{\delta_A}{X_B} - \frac{X_A \delta_B}{X_B^2} \ , \tag{2.86}$$

[10] Such as certain remainders in the low energy $\pi\pi$ scattering [5].

where we introduced

$$X_A = \frac{A_{LO}}{A} \ . \tag{2.87}$$

We see that if $X_B \ll 1$, the size of the reminder can be numerically large even for $\delta_A, \delta_B \approx 0$. This proves that performing nonlinear operations with "good observables" can produce observables which are not globally convergent. Using such observables leads to problems with precision, as higher order remainders δ_A are always present in the final expressions in RχPT. Very large higher order remainders δ_A then lead to imprecise results of calculations. When we operate in the space of observables expressible from generating functional linearly, we are able to control the remainders and keep their magnitudes at reasonable values.

To provide a specific example of a "dangerous" observable which may not be globally convergent we can mention square of the pion mass, which can be written as a ratio of two good observables

$$M_\pi^2 = \frac{F_\pi^2 M_\pi^2}{F_\pi^2} \ . \tag{2.88}$$

It is customary to include one modification of the "strict chiral expansion" (2.73). Instead of writing $O(p^2)$ masses as arguments of loop functions[11], we will replace these by the physical values of the masses [5], [35]. This is motivated by correct position of branching points of scattering amplitudes and can be circumvented by performing a dispersive analysis. From the point of view of the convergence of the series for variable A, this replacement results in redefinition of the higher order reminder δ_A. It is the series

$$A = A_{LO} + A'_{NLO} + A\delta'_A \ , \tag{2.89}$$

where arguments of loop functions in A_{NLO} were replaced by physical values, which is assumed to be globally convergent. From now on we will assume that this replacement was performed in all expansions and will not write the apostrophes explicitly[12]. We will label resulting series as "bare", to distinguish them from the unaltered "strict" chiral expansions.

The inversion of chiral series for pion mass and decay constant and ratio of kaon and pion masses which is crucial in the standard treatment is not allowed from the point of view of RχPT, because it relies on inverting variables which is considered "dangerous".

In RχPT variables X, Z and quark masses ratio

$$r = \frac{m_s}{\hat{m}} \tag{2.90}$$

are used as a free parameters which determine the LO low energy constants directly,

$$\begin{aligned} F_0^2 &= F_\pi^2 Z \\ 2\hat{m}B_0 &= M_\pi^2 Y \\ 2m_s B_0 &= r M_\pi^2 Y \ . \end{aligned} \tag{2.91}$$

[11] Functions J^r and $\overline{J}$, see Appendix B.

[12] A_{LO} contains no loop functions and apostrophe is hence not needed there.

This way, we have three more parameters to pin down, however advantage of this approach is that we avoid performing the "dangerous" inversions and are able to deal even with observables with $X_A \ll 1$.

In general, all potentially "dangerous" observables should be kept in the "resummed" form where replacement according to (2.91) was performed but no perturbative expansion was done. All maniuplations of these observables and their respective series must be purely algebraic, which enables us to control the error introduced into our calculations by (in principle unknown) remainders.

To summarize the method of Resummed Chiral Perturbation Theory [35]:

- Confine to the space of "good" observables and observables obtainable from them using linear operations. Do not perform perturbative expansion of "dangerous" observables and keep them in the resummed form.
- Carefully define the bare expansion
- Instead of inverting formulae for physical parameters, use X, Z and r to reexpress leading order Lagrangian parameters F_0, $\hat{m}B_0$ and m_sB_0.
- All operations with the series should be purely algebraic.

If we stick to these rules, we can work even with quantities with $X_A \ll 1$.

To obtain values of the low energy constants L_i, bare expansions of various "good" observables are calculated and LO low energy constants are replaced according to (2.91). If we now set the resulting resummed series equal to the experimental values of the observables, we are able to algebraically solve the system of equations for values of L_i. The solution in general depends on experimental values of the observables — especially meson masses and decay constants — values of X, Z, r and the remainders δ parametrizing our ignorance of the higher order contributions. The solutions for the constants $L_4 - L_8$ and L_9 were calculated before [5], [33], [35] and the resulting formulae are given in the Appendix C. This work fills the gap by reparametrizing the low energy constants $L_1 - L_3$ in terms of the experimental data.

Chapter 3

Phenomenology of Kl_4 Decays

3.1 Basics

Semileptonic kaon decays have been in extensive detail covered in [36]. This section summarizes the relevant pieces of the K_{l4} phenomenology from the mentioned article. Immense importance of these processes for χPT lies in a fact that formfactors of Kl_4 decays strongly depend on low energy constants $L_1 - L_3$ and represent a very convenient way for their experimental determination.

There exist three semileptonic decays, which differ in kinds of kaons and pions involved. These are

$$\begin{aligned} K^+(k) &\rightarrow \pi^+(p_1)\ \pi^-(p_2)\ l^+(p_l)\ \nu_l(p_\nu)\ , \\ K^+(k) &\rightarrow \pi^0(p_1)\ \pi^0(p_2)\ l^+(p_l)\ \nu_l(p_\nu)\ , \\ K^0(k) &\rightarrow \pi^0(p_1)\ \pi^-(p_2)\ l^+(p_l)\ \nu_l(p_\nu)\ ;\ l = e, \mu\ . \end{aligned} \tag{3.1}$$

The matrix element for $K^\beta \rightarrow \pi^a \pi^b l^+ \nu_l$ is defined as [15]

$${}_{out}\langle \pi^a \pi^b l^+ \nu_l | K^\beta \rangle_{in} = (2\pi)^4 \delta^4(k - p_1 - p_2 - p_l - p\nu) \cdot iT(K^\beta \rightarrow \pi^a \pi^b l^+ \nu_l) \tag{3.2}$$

and is related to the decay rate of the process through

$$d\Gamma = \frac{1}{2M_K(2\pi)^8} \sum_{spins} |T|^2 \delta^4(k - p_1 - p_2 - p_l - p\nu) \frac{d^3p_1}{2p_1^0} \frac{d^3p_2}{2p_2^0} \frac{d^3p_l}{2p_l^0} \frac{d^3p_\nu}{2p_\nu^0}\ . \tag{3.3}$$

In the low energy region we are interested in, the W boson can be integrated out and the interaction Lagrangian reduces to a current-current interaction [37]

$$\mathcal{L}_W = \frac{G_F}{\sqrt{2}} J_W^\mu J_{W\mu}^\dagger\ , \tag{3.4}$$

where weak current comprises of leptonic and hadronic currents,

$$J_W^\mu = J_l^\mu + J_h^\mu\ . \tag{3.5}$$

The matrix element for a K_{l4} decay can be then factorized as

$$T = \frac{G_F}{\sqrt{2}} \langle l^+(p_l)\nu_l(p_\nu)|J_l^\mu|0\rangle \cdot \langle \pi^a(p_1)\pi^b(p_2)|J_{h\mu}|K^\beta(k)\rangle\ . \tag{3.6}$$

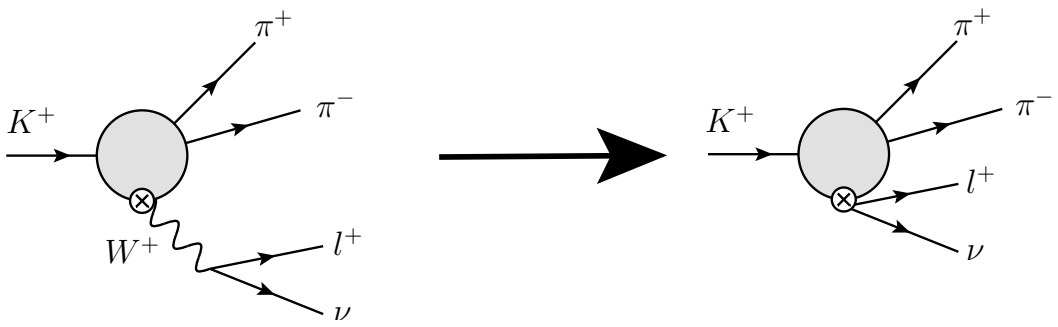

Figure 1: Integrating out exchange of W^+ boson.

Leptonic current is known to be

$$\langle l^+(p_l)\nu_l(p_\nu)|J_l^\mu|0\rangle = \overline{u}(p_\nu)\gamma_\mu(1-\gamma_5)\nu(p_l)\ , \tag{3.7}$$

hadronic current gets vector and axial contributions

$$\langle \pi^a(p_1)\pi^b(p_2)|J_\mu^h|K^\beta(k)\rangle = V_{us}^*(V_\mu - A_\mu)\ , \tag{3.8}$$

where we introduced

$$I_\mu = \langle \pi^a(p_1)\pi^b(p_2)|I_\mu^{4-i5}(0)|K^\beta(k)\rangle\ ;\ I = V, A \tag{3.9}$$

and where V_{su}^* is the corresponding element of the Cabibbo-Kobayashi-Maskawa matrix.

Superscript on the operators V, A refers to the Gell-Mann matrices,

$$\lambda^{4-i5} = \frac{1}{\sqrt{2}}(\lambda^4 - i\lambda^5)\ . \tag{3.10}$$

Explicitly

$$\begin{aligned} V_\mu^{4-i5} &= \frac{1}{\sqrt{2}}\,\overline{s}\gamma_\mu u \\ A_\mu^{4-i5} &= \frac{1}{\sqrt{2}}\,\overline{s}\gamma_\mu\gamma^5 u\ . \end{aligned} \tag{3.11}$$

Putting all this together, we get T matrix element

$$T = \frac{G_F}{\sqrt{2}}V_{us}^*\overline{u}(p_\nu)\gamma_\mu(1-\gamma^5)v(p_l)(V^\mu - A^\mu)\ . \tag{3.12}$$

Matrix element V_μ is governed by the Wess-Zumino term (2.49) and does not have any connection to the low energy constants L_1 – L_3 we are trying to pin down [3]. We will thus fully focus our attention on the axial current. WZ term does not contribute to the matrix element of the axial current and we will thus not mention it from now on.

All our calculations were done in the isospin limit, where masses of down and up quarks are set equal. At the same time we turned off Quantum Electrodynamics by setting $\alpha_{QED} = 0$. Now we show that in the isospin limit, it suffices to know the dynamics of the first decay in (3.1) to describe all three semileptonic kaon decays. To show it, we introduce isospin doublets

$$A_\mu^\alpha = \begin{pmatrix} A_\mu^{4-i5} \\ A_\mu^{6-i7} \end{pmatrix} = \frac{1}{\sqrt{2}}\begin{pmatrix} \overline{s}\gamma_\mu\gamma^5 u \\ \overline{s}\gamma_\mu\gamma^5 d \end{pmatrix}$$

$$K^\beta \;=\; \begin{pmatrix} |K^+\rangle \\ |K^0\rangle \end{pmatrix} \;. \tag{3.13}$$

With these we can introduce general object

$$M_\mu^{a,b;\alpha,\beta}(p_a,p_b,k) = \frac{1}{\sqrt{2}}\langle \pi^a(p_a)\pi^b(p_b)|A_\mu^\alpha(0)|K^\beta(k)\rangle \;, \tag{3.14}$$

where $a,b = 1,2,3$ are cartesian indexes of pion triplet and α,β are spinor indexes of isospin doublets.

In the limit of conserved isospin, $M^{a,b;\alpha\beta}$ is an invariant object:

$$\begin{aligned}
\sqrt{2}M_\mu^{a,b;\alpha,\beta}(p_a,p_b,k) &= \langle \pi^a(p_a)\pi^b(p_b)|A_\mu^\alpha(0)|K^\beta(k)\rangle \\
&= \langle \pi^a(p_a)\pi^b(p_b)|U^\dagger U A_\mu^\alpha(0) U^\dagger U|K^\beta(k)\rangle \\
&= R_c^a(U)R_d^b(U)U_\gamma^\beta\langle \pi^c(p_a)\pi^d(p_b)|U A_\mu^\alpha(0)U^\dagger|K^\gamma(k)\rangle \\
&= \sqrt{2}R_c^a(U)R_d^b(U)U_\gamma^\beta(U^*)_\delta^\alpha M_\mu^{c,d;\delta,\gamma}(p_a,p_b,k) \;.
\end{aligned} \tag{3.15}$$

Here U was arbitrary transformation from the (isospin) $SU(2)$ group; $R_c^a(U)$ and U_γ^β are representations of the transformation on the space of the pion triplet and kaon doublet.

Because of the invariance, we can write the structure of M as

$$M_\mu^{a,b;\alpha,\beta} = A_\mu(p_a,p_b,k)\delta^{ab}\delta^{\alpha\beta} + B_\mu(p_a,p_b,k)\epsilon^{abc}\sigma^{c,\alpha\beta} \;, \tag{3.16}$$

where σ are Pauli spin matrices.

As pions are bosons, Bose symmetry forces

$$\begin{aligned}
A_\mu(p_a,p_b,k) &= A_\mu(p_b,p_a,k) \\
B_\mu(p_a,p_b,k) &= -B_\mu(p_b,p_a,k) \;.
\end{aligned} \tag{3.17}$$

Then

$$\begin{aligned}
M_\mu^{00}(p_a,p_b,k) &= A_\mu(p_a,p_b,k) = M_\mu^{00}(p_b,p_a,k) \\
M_\mu^{0-}(p_a,p_b,k) &= -i\sqrt{2}B_\mu(p_a,p_b,k) = -M_\mu^{0-}(p_b,p_a,k) \\
M_\mu^{+-}(p_a,p_b,k) &= -A_\mu(p_a,p_b,k) - iB_\mu(p_a,p_b,k) = -M_\mu^{0-}(p_b,p_a,k) \\
&= -M_\mu^{00}(p_a,p_b,k) + \frac{1}{\sqrt{2}}M_\mu^{0-}(p_a,p_b,k) \;.
\end{aligned} \tag{3.18}$$

Using the symmetry properties of A_μ and B_μ, we can write

$$\begin{aligned}
M_\mu^{00}(p_a,p_b,k) &= -\frac{1}{2}\left(M_\mu^{+-}(p_a,p_b,k) + M_\mu^{+-}(p_b,p_a,k)\right) \\
M_\mu^{0-}(p_a,p_b,k) &= \frac{1}{\sqrt{2}}\left(M_\mu^{+-}(p_a,p_b,k) - M_\mu^{+-}(p_b,p_a,k)\right) \;.
\end{aligned} \tag{3.19}$$

This confirms our assertion that we can infer matrix elements and therefore complete dynamics of all Kl_4 processes from the decay of K^+ to two charged pions.

Before we proceed further, we label combinations of vectors

$$\begin{aligned}
P &= p_1 + p_2 \\
Q &= p_1 - p_2 \\
q &= p_l + p_\nu
\end{aligned} \tag{3.20}$$

and

$$\begin{aligned} s &= (p_1+p_2)^2 = (k-q)^2 \\ t &= (p_2+q)^2 = (k-p_1)^2 \\ u &= (p_1+q)^2 = (k-p_2)^2 \ . \end{aligned} \tag{3.21}$$

The variable s represents invariant mass squared of the dipion system, q^2 stands for the invariant mass squared of the dilepton system. The kinematical variables are constrained by an identity[1]

$$s+t+u = M_K^2 + 2M_\pi^2 + q^2 \tag{3.22}$$

and are subject to inequalities

$$\begin{aligned} M_e^2 &\leq q^2 \leq (M_K - 2M_\pi)^2 \\ 4M_\pi^2 &\leq s \leq (M_K - \sqrt{q^2})^2 \\ t_{min}(s) &\leq t \leq t_{max}(s) \\ u_{min}(s) &\leq u \leq u_{max}(s) \end{aligned} \tag{3.23}$$

with

$$\begin{aligned} t_{max,min}(s) &= \frac{1}{2}\left(M_K^2 + 2M_\pi^2 + q^2 - s \pm \lambda^{1/2}(s, M_K^2, q^2)\sigma(s)\right) \\ u_{min,max}(s) &= t_{min,max}(s) \ . \end{aligned} \tag{3.24}$$

Here we defined

$$\begin{aligned} \sigma(s) &= \sqrt{1 - \frac{4M_\pi^2}{s}} \\ \lambda(a,b,c) &= a^2+b^2+c^2-2ab-2ac-2bc \ . \end{aligned} \tag{3.25}$$

The full kinematics of the decay requires five variables, which may be divided in two groups. We need three kinematical variables to describe the matrix element $\langle \pi^a(p_1)\pi^b(p_2)|J_\mu^h|K^\alpha(k)\rangle$ and two kinematical variables to unambiguously determine directions of flight of the created leptons. As the three variables describing hadronic matrix element we can take s, t, q^2. Instead of t, we may take $\cos\theta$, angle between the momentum of π^+ and the dipion line of flight in the kaon rest system.

From u and t, we can calculate $\cos\theta$ as

$$\cos\theta = \frac{u-t}{\sigma(s)\lambda^{1/2}(s, M_K^2, q^2)} \ . \tag{3.26}$$

The constraint (3.22) then gives relations

$$\begin{aligned} t &= \frac{1}{2}\left(M_K^2 + 2M_\pi^2 + q^2 - s + \sigma(s)\lambda^{1/2}(s, M_K^2, q^2)\cos\theta\right) \\ u &= \frac{1}{2}\left(M_K^2 + 2M_\pi^2 + q^2 - s - \sigma(s)\lambda^{1/2}(s, M_K^2, q^2)\cos\theta\right) \ . \end{aligned} \tag{3.27}$$

Variable $\cos\theta$ is of a big practical importance, because experimental data are usually expressed in partial waves expansion in $\cos\theta$.

As the two kinematical variables describing leptonic current, we may choose

[1] Under the assumptions we used — isospin limit and no QED effects — all pions have a common mass and the same holds for kaons. We will denote them M_π and M_K.

- θ_l — the angle of the l^+ in center of mass system of $l^+\nu$ with respect to the dilepton line of flight in rest mass of the kaon
- ϕ — the angle between the plane formed by the pions in rest mass of the kaon and the corresponding plane formed by the dileptons.

Taking into account the vectors we have at our disposal, we can introduce three distinct formfactors of the axial current by writing[2]

$$\begin{aligned} A_\mu &= -\frac{i}{M_K}\left(P_\mu F(s,t,u;q^2) + Q_\mu G(s,t,u;q^2) + q_\mu R(s,t,u;q^2)\right) \\ V_\mu &= -\frac{H(s,t,u;q^2)}{M_K^3}\epsilon^{\lambda\mu\rho\sigma} q^\nu P^\rho Q^\sigma \ . \end{aligned} \tag{3.28}$$

As we see directly from (3.28), contribution from the formfactor R is proportional to q_μ. In decays with electrons, the influence of R on the matrix element it then suppressed by the small mass of electron and is negligible. It then has no practical value in obtaining values of constants L_1 – L_3 from experimental data on decays into electrons.

Finally, each formfactor can be expanded in powers of energy as

$$I = \frac{M_K}{F_\pi}\left(I^{(0)} + I^{(2)} + I^{(4)} + \ldots\right); \quad I = F, G, R \ , \tag{3.29}$$

where $I^{(k)}$ is a quantity of order $O(p^k)$. When we calculate in the framework of χPT, the orders of this energy expansion are related to the order of the χPT to which we must calculate Feynman diagrams — to calculate $I^{(0)}$ taking only $\mathcal{L}_2$ suffices; to get $I^{(2)}$ we must add $\mathcal{L}_4$ and so forth.

3.2 Previous theoretical calculations of K_{l4} decays

The leading order values of formfactors F, G, R were obtained by Weinberg even before χPT was first introduced in 1984 by Gasser and Leutwyler. Using method of current algebra, i.e. the commutation relations of the Noether Currents and the hypothesis of a partially conserved axial-vector current, he derived [38]

$$\begin{aligned} F &= G = \frac{M_K}{\sqrt{2}F_\pi} \\ R &= \frac{M_K}{2\sqrt{2}}\left(\frac{s+t-u}{q^2 - M_K^2} + 1\right) \ . \end{aligned} \tag{3.30}$$

Twenty-five years after Weinberg's original derivation, Bijnens [6] and independently Riggenbach et al. [39] calculated formfactors F, G of K_{l4} decays in χPT to next-to-leading order. They found a very strong dependence of the result on low energy constants L_1 – L_3 and rather small dependence on L_4 and L_9. With respect to previously used D-wave scattering lengths of $\pi\pi$ scattering, usage of semileptonic kaon decays enabled improved determination of the values of

[2]For further reference we give also definition of the formfactor H of the vector current.

L_1 – L_3. The original $O(p^4)$ calculation of formfactors was improved in [36] by investigating importance of higher order terms using dispersive analysis.

The NNLO result on the K_{l4} formfactors was published in the article [29]. Using hypothesis of resonance saturation and assuming that arguments based on large N_c hold, authors were able to improve determination of the low energy constants L_1, L_2, L_3, L_5, L_7 and L_8. The derived formulae were used also in the most current fit of low energy constants L_i [9].

The last contribution to the problematics of semileptonic kaon decays is article [40]. Unlike the previously mentioned articles which all work in the isospin limit, this article calculates formfactors with explicitly disentangled isospin breaking part. However, the results are incomplete and must be supplemented by a full treatment of the radiative decay $K_{l4\gamma}$.

3.3 Parametrization of the experimental data

In experiments we measure value of $|T^2|$ and are then not capable of measuring formfactors F, G, R, H directly. It is useful to write the theoretical predictions on decay probability in terms of specific combinations of formfactors $F_i, i = 1, \ldots 4$, which have a simple partial wave expansion. These formfactors are connected with the previously defined ones through identities [41]

$$\begin{aligned} F_1 &= M_K^2\,(\gamma F + \alpha G \cos\theta) \\ F_2 &= M_K^2\,(\beta G) \\ F_3 &= M_K^2\,(\beta\gamma H) \\ F_4 &= M_K^2\left(-\frac{\alpha}{\sigma(s)}F - \frac{q^2}{M_K^2}R - \sigma(s)\gamma G\cos\theta\right)\ . \end{aligned} \tag{3.31}$$

Above,

$$\begin{aligned} \alpha &= \sigma(s)\,\frac{M_K^2 - s - q^2}{2M_K^2} \\ \beta &= \sigma(s)\,\frac{\sqrt{sq^2}}{M_K^2} \\ \gamma &= \frac{\lambda^{1/2}(M_K^2, s, q^2)}{2M_K^2}\ . \end{aligned} \tag{3.32}$$

Symbols $\sigma(s)$ and $\lambda(a, b, c)$ were introduced before (3.25).

In terms of the newly introduced formfactors, $|T|^2$ is some function

$$|T|^2 = f(F_i, s, q^2, \cos\theta, \cos\theta_l, \phi)\ . \tag{3.33}$$

The formfactor F_4 in this formula is always multiplied by the mass of the lepton. In the reasonable limit of massless electron then F_4 drops from the formula for decay rate of kaonic decay into electron.

Expanding the remaining F_1, F_2 and F_3 into a partial wave expansion with respect to angular momentum of the dipion system, we obtain expansion into a series of Legendre functions $P_l(\cos\theta)$ and their derivatives $P_l'(\cos\theta)$ [41]

$$F_1 = M_K^2 \sum_{l=0}^{\infty} P_l(\cos\theta) F_{1,l} \exp(i\delta_l)$$

$$F_{2(3)} = M_K^2 \sum_{l=0}^{\infty} P_l'(\cos\theta) F_{2(3),l} \exp(i\delta_l) \ . \tag{3.34}$$

Through investigation of the dependence of decay probability (3.3) on variables θ_l, ϕ we are able to get enough information to extract values of combinations F_1, F_2, F_3 and their relative phases.

Under the assumption of T-invariance, the Watson theorem [42] asserts that a partial wave amplitude of definite angular momentum l and isospin I must have the phase of δ_l^I, corresponding to the amplitude of $\pi\pi$ scattering. When we reconstruct experimental values of formfactors we can thus use experimental data on phase shifts of $\pi\pi$ scattering.

Combining (3.31) and (3.34), we may write expansions of formfactors F and G as

$$\begin{aligned} F &= F_s \exp(i\delta_{f_s}) + F_p \exp(i\delta_{f_p}) \cos\theta + \mathrm{D-wave} + \dots \\ G &= G_p \exp(i\delta_{g_p}) + \mathrm{D-wave} + \dots \ . \end{aligned} \tag{3.35}$$

Here $F_s, F_p, \dots$ are purely real functions of s, q^2, phases are according to the Watson theorem the $\pi\pi$ phase shifts evaluated at s. Assuming that the phase of the p-waves are the same, $\delta_{f_p} = \delta_{g_p}$, and that the D-wave can be neglected, the results depend only on the single phase difference $\delta = \delta_{f_s} - \delta_{f_p}$.

The dependence of the functions F_s and G_p on s and q^2 is further parametrized as

$$\begin{aligned} F_s(s,q^2) &= f_s + f_s' \left(\frac{s}{4M_\pi^2} - 1 \right) + f_s'' \left(\frac{s}{4M_\pi^2} - 1 \right)^2 + f_e' \frac{q^2}{4M_\pi^2} \\ G_p(s) &= g_p + g_p' \left(\frac{s}{4M_\pi^2} - 1 \right) \ , \end{aligned} \tag{3.36}$$

which well describes presently available experimental data [41].

Chapter 4

Formfactor Calculations

4.1 Amplitude from the generating functional

In the previous chapter we explained how to build generating functional in χPT, this section is dedicated to the method of obtaining matrix element

$$\langle \pi^a(p_a)\pi^b(p_b)|A^\alpha_\mu(0)|K^\beta(k)\rangle \tag{4.1}$$

from the generating functional.

We work in a physical basis $\phi^i = (\pi^\pm, \pi^3, K^\pm, K^0, \overline{K}^0, \eta)$ which is very convenient as certain variables are in this basis represented by diagonal matrices. To distinguish axial current in momentum and space representations, we write $\tilde{A}$ for momentum representation and A for the space representation.

In our derivation, we use the fact that pseudo-Goldstone bosons are generated from the vacuum by axial currents [3],

$$\langle 0|A^i_\mu(0)|\phi_i\rangle = iF_i p_\mu \ , \tag{4.2}$$

where F_i is decay constant of given pseudo-Goldstone boson ϕ_i.

Our matrix element can then be obtained from a four point function of four axial currents

$$\begin{aligned}&\langle 0|T\tilde{A}^a_{\mu_a}(p_a)\tilde{A}^b_{\mu_b}(p_b)A^\alpha_\mu(0)\tilde{A}^{\beta\dagger}_{\mu_\beta}(k)|0\rangle = \\ &\quad = \int dx_a\, dx_b\, dx_\beta e^{ip_a\cdot x_a + ip_b\cdot x_b - ik\cdot x_\beta} \times \langle 0|TA^a_{\mu_a}(x_a)A^b_{\mu_b}(x_b)A^\alpha_\mu(0)A^{\beta\dagger}_{\mu_\beta}(x_k)|0\rangle\end{aligned} \tag{4.3}$$

through Lehmann-Symanzik-Zimmerman (LSZ) reduction formula[1]

$$\begin{aligned}&\langle 0|T\tilde{A}^a_{\mu_a}(p_a)\tilde{A}^b_{\mu_b}(p_b)A^\alpha_\mu(0)\tilde{A}^{\beta\dagger}_{\mu_\beta}(k)|0\rangle = \\ &\quad = \left(\prod_{i=a,b,\beta}\frac{i\langle 0|\tilde{A}^i_{\mu_i}|\phi_i\rangle}{p_i^2 - M_i^2}\right)\langle \pi^a(p_a)\pi^b(p_b)|A^\alpha_\mu(0)|K^\beta(k)\rangle \ + \text{reg.} \\ &\quad = \left(\prod_{i=a,b,\beta}\frac{i\cdot iF_i p_{\mu_i}}{p_i^2 - M_i^2}\right)\langle \pi^a(p_a)\pi^b(p_b)|A^\alpha_\mu(0)|K^\beta(k)\rangle \ + \text{reg.} \ .\end{aligned} \tag{4.4}$$

[1] For derivation, see [15].

Here "reg." stands for terms which are regular around the investigated pole $p_i^2 \to M_i^2$, where M_i are the physical masses of the pseudo-Goldstone bosons.

To get the four point function in the space representation, we use generating functional Z (2.20)

$$\begin{aligned}\langle 0|TA^a_{\mu_a}(x_a)A^b_{\mu_b}(x_b)A^\alpha_\mu(0)A^{\beta\dagger}_{\mu_\beta}(x_k)|0\rangle = \\ = \frac{1}{i^3}\frac{\delta^4 Z[a]}{\delta a^a_{\mu_a}(x_a)\delta a^b_{\mu_b}(x_b)\delta a^\alpha_\mu(0)\delta a^{\beta\dagger}_{\mu_\beta}(x_\beta)}\Big|_{a=0} .\end{aligned} \tag{4.5}$$

For brevity we introduced notation

$$Z[a] \equiv Z[v,a,p,s]|_{v,s,p=0} . \tag{4.6}$$

By $v,s,p=0$ we understand that only the background field part in (2.24) (represented by dots) is set to zero, so we retain masses of the quarks in our calculations.

To evaluate this functional derivative, we expand the generating functional into the powers of "classical fields" ϕ_{cl} — solutions to the classical $O(p^2)$ equations of motion:

$$\begin{aligned}Z = \sum_n \frac{1}{n!}\int d^4x_1 \dots d^4x_n Z_{i_1 i_2 \dots i_n}[v,a,p,s](x_1,\dots,x_n) \times \\ \times \phi^{i_1}_{cl}[v,a,p,s](x_1)\dots\phi^{i_n}_{cl}[v,a,p,s](x_n) .\end{aligned} \tag{4.7}$$

Coefficients $Z_{i_1\dots l_n}$ can be decomposed into contributions from various orders $O(p^k)$ in an obvious way. To order $O(p^4)$ we can write

$$\begin{aligned}Z[a] = \frac{1}{2}\int d^4x \Big[Z_{ij}(\partial\phi^i_{cl}[a] - a^i F_0)(\partial\phi^j_{cl}[a] - a^j F_0) - \\ - \mathcal{M}_{ij}\phi^i_{cl}[a]\phi^j_{cl}[a]\Big] + O(\phi^3_{cl}) + O(p^6) ,\end{aligned} \tag{4.8}$$

where Z_{ij} and $\mathcal{M}_{ij}$ contain contributions up to order $O(p^4)$. In physical basis these matrices are diagonal[2],

$$\begin{aligned} Z_{ij} &= Z_i\delta_{ij} \\ \mathcal{M}_{ij} &= \mathcal{M}_i\delta_{ij} . \end{aligned} \tag{4.9}$$

To be able to evaluate functional derivative (4.5), we need variation of the classical field with respect to the field a. One way to reach it is to employ the equations of motion. From (4.8) we can write equations of motion (resummed to the order $O(p^4)$)

$$\frac{\delta Z[a]}{\delta\phi_{cl}} = 0 \tag{4.10}$$

explicitly as

$$Z_i\partial^2\phi^i_{cl}[a] + \mathcal{M}_i\phi^i_{cl}[a] = F_0 Z_i\partial\cdot a_i + \dots . \tag{4.11}$$

[2]In the isospin limit.

From here we obtain a variation

$$\frac{\delta\phi^i_{cl}[a](x)}{\delta a^\mu_j(y)} = \frac{F_0\partial_\mu}{\partial^2 + \mathcal{M}_i/Z_i}\delta_{ij}\delta(x-y) + \dots \ . \tag{4.12}$$

This can be used to gain correlator

$$\langle 0|TA^i_\mu(x)A^j_\nu(y)|0\rangle = \frac{1}{i}\frac{\delta^2 Z[a]}{\delta a^\mu_i(x)\delta a^\nu_j(y)}\Big|_{a=0} \tag{4.13}$$

from the expansion (4.8) explicitly as

$$\langle 0|TA^i_\mu(x)A^j_\nu(y)|0\rangle = \frac{i\delta_{ij}Z_iF_0^2}{\partial^2 + \mathcal{M}_i/Z_i}\ \partial_{x,\mu}\partial_{y,\nu}\delta(x-y) + \text{reg.}\ . \tag{4.14}$$

In momentum representation this reads

$$\langle 0|T\tilde{A}^i_\mu(p)\tilde{A}^j_\nu(0)|0\rangle = \frac{iZ_iF_0^2\delta_{ij}p_\mu p_\nu}{p^2 - \mathcal{M}_i/Z_i} + \text{reg.}\ . \tag{4.15}$$

By comparison with what we expect from the LSZ formula

$$\langle 0|T\tilde{A}^i_\mu(p)\tilde{A}^j_\nu(0)|0\rangle = \frac{i\delta_{ij}F_i^2p_\mu p_\nu}{p^2 - M_i^2} + \text{reg.} \tag{4.16}$$

we can relate constants from the generating functional to physical observables

$$\begin{aligned} F_i^2 &= Z_iF_0^2 \\ F_i^2M_i^2 &= F_0^2\mathcal{M}_i \end{aligned} \tag{4.17}$$

and plug this into the field variation (4.12) to get

$$\frac{\delta\phi^i_{cl}[a](x)}{\delta a^\mu_j(y)} = \frac{F_0\partial_\mu}{\partial^2 + M_i^2}\delta_{ij}\delta(x-y) + \text{reg.}\ . \tag{4.18}$$

Knowing this variation, we can proceed to functional derivative of the generating functional. The functional derivatives in (4.5) act either on coefficients $Z_{i_1\dots i_n}$ or on the classical fields ϕ_{cl} in the expansion (4.7). To get the desired pole structure from (4.4), at least three derivatives must act on classical fields, because coefficient functions do not contain singularities from (4.4). Effectively we thus can write

$$\begin{aligned} &\frac{\delta^4 Z[a]}{\delta a^a_{\mu_a}(x_a)\delta a^b_{\mu_b}(x_b)\delta a^\alpha_\mu(0)\delta a^{\beta\dagger}_{\mu_\beta}(x_\beta)} = \\ &\quad = \left(\prod_{i=a,b,\beta}\frac{F_0\partial_{\mu_i}}{\partial^2 + M_i^2}\right)\frac{\delta}{\delta a^\alpha_\mu(0)}Z_{ab\beta^\dagger}[a](x_a,x_b,x_\beta)\Big|_{a=0} + \\ &\qquad + \left(\prod_{i=a,b,\alpha,\beta}\frac{F_0\partial_{\mu_i}}{\partial^2 + M_i^2}\right)Z_{ab\alpha\beta^\dagger}[0](x_a,x_b,x_\beta,0)\ . \end{aligned} \tag{4.19}$$

Combining (4.4) with (4.19) we obtain

$$\langle\pi^a(p_a)\pi^b(p_b)|A^\alpha_\mu(0)|K^\beta(k)\rangle =$$

$$= \frac{1}{i}\left(\prod_{i=a,b,\beta}\frac{F_0}{F_i}\right)\int d^4x_a\, d^4x_b\, d^4x_\beta e^{ip_a\cdot x_a+ip_b\cdot x_b-ik\cdot x_\beta}\times$$
$$\times\left[\frac{\delta}{\delta a^\alpha_\mu(0)}Z_{ab\beta^\dagger}[a](x_a,x_b,x_\beta)\Big|_{a=0}+\right.$$
$$\left.+\frac{iF_0q_\mu}{q^2-M^2_\alpha}Z_{ab\alpha\beta^\dagger}[0](x_a,x_b,x_\beta,0)\right] \tag{4.20}$$

which may be rewritten to

$$\langle\pi^a(p_a)\pi^b(p_b)|A^\alpha_\mu(0)|K^\beta(k)\rangle =$$
$$= \frac{1}{i}\int d^4x_a\, d^4x_b\, d^4x_\beta e^{ip_a\cdot x_a+ip_b\cdot x_b-ik\cdot x_\beta}\times$$
$$\times\left[\left(\prod_{i=a,b,\beta}\frac{F_0}{F_i}\right)\frac{\delta}{\delta a^\alpha_\mu(0)}Z_{ab\beta^\dagger}[a](x_a,x_b,x_\beta)\Big|_{a=0}+\right.$$
$$\left.+\frac{iF_\alpha q_\mu}{q^2-M^2_\alpha}\left(\prod_{i=a,b,\beta,\alpha}\frac{F_0}{F_i}\right)Z_{ab\alpha\beta^\dagger}[0](x_a,x_b,x_\beta,0)\right]. \tag{4.21}$$

This last equality constitutes basis of our calculations, it is therefore worthwhile to summarize our procedure so far:

- Expand the generating functional into the series in ϕ_{cl}.
- Find the part of the coefficient $Z_{ab\beta}$ linear in a^μ and a^μ-independent part of $Z_{ab\beta\alpha}$.
- Take the linear combination (4.21) and Fourier transform the result.

We see that we received two contributions to the calculated matrix element. The second one is proportional to q^μ and thus contributes only to the R formfactor; the first term contributes to all F, G and R.

So far our method of calculating the matrix element

$$\langle\pi^a(p_a)\pi^b(p_b)|A^\alpha_\mu(0)|K^\beta(k)\rangle \tag{4.22}$$

is "safe" in the perspective of the RχPT, because we started with the generating functional Z and performed only linear operations.

4.2 One loop corrections

In the previous section we explained how to extract value of the matrix element $\langle\pi^a(p_a)\pi^b(p_b)|A^\alpha_\mu(0)|K^\beta(k)\rangle$ from coefficients $Z_{ab\beta}$ and $Z_{ab\beta\alpha}$, in this section we show how to obtain values of these coefficients.

As already explained, the generating functional of χPT to the order $O(p^4)$ is given by an integral of the most general Lagrangian which complies with the assumed symmetry properties[3] to this order

$$\mathcal{L}_{eff} = \mathcal{L}_2 + \mathcal{L}_4\ . \tag{4.23}$$

[3]Plus terms reproducing anomalous behavior. In our calculations we do not need Wess-Zumino term, therefore we do not include it into $\mathcal{L}_{eff}$.

We may then write

$$\begin{aligned} \exp(iZ) &= \int \mathcal{D}U \exp\left(iS_{eff}\right) \\ &= \int \mathcal{D}U \exp\left(i\int d^4x(\mathcal{L}_2+\mathcal{L}_4)\right) . \end{aligned} \tag{4.24}$$

In our calculation we employed the background field method in concordance with authors of [3]. Denoting the solution to the classical $O(p^2)$ equations of motion $\overline{U}$ and its square root $\overline{u}$,

$$\overline{U} = \overline{u}^2 , \tag{4.25}$$

we can write expansion around $\overline{U}$ in a form

$$U = \overline{u}\exp\left(\frac{i\sqrt{2}\,\phi_{in}}{F_0}\right)\overline{u} \tag{4.26}$$

with $\phi_{in}(x)$ a field of traceless hermitian matrices. Used parametrization has the advantage that if we postulate transformation properties of ϕ_{in}

$$\phi_{in} \to h^\dagger \phi_{in} h , \tag{4.27}$$

where h was defined right after (2.27), then U remains invariant under the chiral group.

Similarly to what we have done, we can define quantum fields by prescription

$$\phi_{in}(x) = \begin{pmatrix} \frac{\pi^0_{in}}{\sqrt{2}} + \frac{\eta_{in}}{\sqrt{6}} & \pi^+_{in} & K^+_{in} \\ \pi^-_{in} & -\frac{\pi^0_{in}}{\sqrt{2}} + \frac{\eta_{in}}{\sqrt{6}} & K^0_{in} \\ K^-_{in} & \overline{K^0_{in}} & -\frac{2\eta_{in}}{\sqrt{6}} \end{pmatrix} \tag{4.28}$$

and "classical" fields

$$\overline{u} = \exp\left(\frac{i}{\sqrt{2}F_0}\begin{pmatrix} \frac{\pi^0_{cl}}{\sqrt{2}} + \frac{\eta_{cl}}{\sqrt{6}} & \pi^+_{cl} & K^+_{cl} \\ \pi^-_{cl} & -\frac{\pi^0_{cl}}{\sqrt{2}} + \frac{\eta_{cl}}{\sqrt{6}} & K^0_{cl} \\ K^-_{cl} & \overline{K^0_{cl}} & -\frac{2\eta_{cl}}{\sqrt{6}} \end{pmatrix}\right) . \tag{4.29}$$

We stress out that these "classical" fields are the ones that are used as expansion parameters in (4.7), which enables easy determination of $Z_{ab\beta}$ and $Z_{ab\beta\alpha}$.

In the effective action we may separate contributions coming from the solutions to the classical equations of motion and the rest by writing

$$S_{eff} = \int d^4x(\overline{\mathcal{L}_2}+\overline{\mathcal{L}_4}) + \int d^4x(\mathcal{L}_2-\overline{\mathcal{L}_2}) + \int d^4x(\mathcal{L}_4-\overline{\mathcal{L}_4}) . \tag{4.30}$$

In barred quantities we substituted fields U by $\overline{U}$. The last term in (4.30) generates contributions of an order $O(p^6)$ and can hence be dropped. The first term corresponds to the contribution of the tree diagrams [3] and is expressed precisely in the form we need to read off the coefficients from (4.7). Finally, the second term corresponds to the loop corrections with $\mathcal{L}_2$ vertices and according to the

Weinberg's counting rules must be retained at our NLO calculations. We now focus our attention to the contribution of the second term.

One way to proceed is to expand the exponentials in (4.24) into a second order in quantum fields ϕ_{in} and calculate contribution of the one-loop graphs to the generating functional by Gaussian integration over these quantum fields. This was the approach taken by the authors of [3].

We decided to take a technically different approach and calculate one-loop contributions directly by evaluating Feynman diagrams [43][4].

The classical fields have a specific position given by the (4.21) — we are searching for contributions to Z with the correct powers of "classical fields". As an easy book-keeping, we can picture the "classical" fields as external lines of the diagram. This way, only graphs with the correct set of the external lines can contribute to the coefficients $Z_{ab\beta(\alpha)}$. This is very utile, as in our case we need to calculate only graphs with the external lines corresponding to the "classical" incoming K^+ and outcoming π^+, π^- for $Z_{ab\beta}$; for $Z_{ab\beta\alpha}$ we have to add also K^-[5]. To simplify further steps, each axial current in a Lagrangian term was also pictured as an external particle coming out of the corresponding vertex. When we are interested in the first derivative of some $Z_{i_1,\ldots,i_n}$ with respect to an axial current as in (4.21), it suffices to calculate amplitude of a graph with a single additional external leg corresponding to the axial current. For obvious reasons we labeled particles represented by these lines as $W^{\pm}_{\mu}$.

The quantum fields are dynamical degrees of freedom (see the change of the integration variable in the footnote) and must be integrated out before we are able to write the final effective functional. In our method this corresponds to placing quantum fields ϕ_{in} on internal lines of loop diagrams and performing the one loop integrations. The "quantum" fields must have the same Lorentz structure as the described pseudo-Goldstone boson fields and are thus scalars, which uniqely sets the form of their propagators.

When we expand the effective Lagrangian $\mathcal{L}_{eff}$ we get sum of terms with various powers of the fields ϕ_{cl} and ϕ_{in}; each term in the Lagrangian corresponds to a certain vertex rule. From (4.30) we know that the vertex rules for quantum fields ϕ_{in} are dictated by the Lagrangian $\mathcal{L}_2 - \overline{\mathcal{L}_2}$. By plugging the expansion (4.26) into the expression for the $O(p^2)$ Lagrangian (2.41) we explicitly get

$$\begin{aligned}
\mathcal{L}_{loop} &= \mathcal{L}_2 - \overline{\mathcal{L}_2} \\
&= \frac{F_0^2}{4}\Big\langle (D_\mu \tilde{U})^\dagger \cdot D^\mu \tilde{U} - \frac{1}{2}\left(D_\mu \overline{U}\right)^\dagger \cdot D^\mu \tilde{\tilde{U}} - \frac{1}{2} D_\mu \overline{U} \cdot \left(D^\mu \tilde{\tilde{U}}\right)^\dagger \\
&- \frac{1}{2}\phi_{cl}^2 \left(\overline{u}\cdot\chi^\dagger\cdot\overline{u} + \overline{u}^\dagger\cdot\chi\cdot\overline{u}^\dagger\right)\Big\rangle + O(\phi_{in}^3)\ , \qquad (4.32)
\end{aligned}$$

[4]In the end our results are identical with the results that would be obtained by the former approach. The most important step in proving this is the change of the variable of integration from ϕ to quantum fields ϕ_{in}

$$\int \mathcal{D}\phi \exp(iS_{eff}) = \int \mathcal{D}\phi_{in} \exp(iS_{eff})\ , \qquad (4.31)$$

where we used the defining relations (4.26) and (4.29). The equivalence of Feynman rules calculation with the Gaussian integration over fields is then shown in a standard way [15].

[5]We are searching for the coefficient with $\alpha = 4 - i5$ (compare (3.9) and (3.28)). In our notation (4.29) it corresponds to K^-.

where[6]

$$\begin{aligned} D_\mu \tilde{U} &= \partial_\mu \left(\overline{u}\cdot\phi_{in}\cdot\overline{u}\right) - i\overline{u}\cdot\phi_{in}\cdot\overline{u}\cdot a_\mu - i a_\mu\cdot\overline{u}\cdot\phi_{in}\cdot\overline{u} \\ D_\mu \tilde{\tilde{U}} &= \partial_\mu \left(\overline{u}\cdot\phi_{in}^2\cdot\overline{u}\right) - i\overline{u}\cdot\phi_{in}^2\cdot\overline{u}\cdot a_\mu - i a_\mu\cdot\overline{u}\cdot\phi_{in}^2\cdot\overline{u}\ . \end{aligned} \tag{4.33}$$

We are interested exclusively in the matrix element of current A_μ^{4-i5}. Therefore, we can effectively take matrix a_μ as

$$a_\mu = \begin{pmatrix} 0 & 0 & 0 \\ 0 & 0 & 0 \\ a_\mu^{4-i5} & 0 & 0 \end{pmatrix}\ . \tag{4.34}$$

Dropping other fields from a_μ speeds up calculations notably.

In the loop Lagrangian there is no contribution linear in quantum fields, because such terms are proportional to variation of the LO action

$$S_2 = \int d^4x\, \mathcal{L}_2 \tag{4.35}$$

with respect to ϕ_{cl} and this proportionality factor is equal to zero because we chose ϕ_{cl} as solutions to the classical $O(p^2)$ equations of motion. The terms with third and higher power of the quantum fields give rise to two- and higher order loop diagrams, which are beyond our NLO precision.

From (4.32) we are also able to read off "masses" of the quantum fields ϕ_{in}. If we expand $\mathcal{L}_{loop}$ (4.32) and examine mass terms of "quantum" fields, we find out that ϕ_{in} have — to the investigated order — the same masses as pseudo-Goldstone bosons, namely

$$\begin{aligned} \overset{\circ}{M}{}^2_{\pi_{in}} &= 2\hat{m}B_0 \\ \overset{\circ}{M}{}^2_{K_{in}} &= (\hat{m}+m_s)B_0 \\ \overset{\circ}{M}{}^2_{\eta_{in}} &= \frac{2}{3}(\hat{m}+2m_s)B_0\ . \end{aligned} \tag{4.36}$$

These are the masses that must be plugged into the internal propagators of ϕ_{in}.

We have now all the ingredients to calculate loop graphs and it remains to specify calculation of the graphs without ϕ_{in} — tree graphs with vertices from $\overline{\mathcal{L}_2}$ and $\overline{\mathcal{L}_4}$. At the investigated order these graphs can have only a single vertex, because the "classical" fields do not enter internal propagators; external lines are determined as in the loop case. The Feynman rules are obtained by substituting U in $\mathcal{L}_2$ and $\mathcal{L}_4$ by the classical solution $\overline{U}$. After that, we may perform an expansion to order sufficient for reading off desired coefficients $Z_{ab\beta(\alpha)}$.

4.3 Calculations with Wolfram Mathematica

In the previous section we introduced division of fields into "classical" and "quantum" and explained their positions in the calculations. We argued that each graph must contain correct set of external lines corresponding to the "classical" fields

[6] We remind that we are interested in a matrix element of an axial current. In the following expressions we thus set $v_\mu = 0$.

taking part in the decay (K^+, π^+, π^- and either K^- or W^-). In this section we introduce a Wolfram Mathematica [44] notebook we wrote to calculate the amplitudes of the Feynman diagrams introduced in the previous section[7]. This notebook is an attachment of the thesis.

The central part of our notebook is a function **GraphContribution**, which takes information about a graph and returns the calculated amplitude.

To describe a graph, we must first provide a number N of vertices in it; each vertex is given a number from one to N[8]. In addition to this, we must provide information about which Lagrangian from $\overline{\mathcal{L}}_2, \overline{\mathcal{L}}_4, \mathcal{L}_{loop}$ to use in which vertex.

Finally, we must specify lines in the graph. Each line is uniquely given by

- Number of the initial and final vertex of the line[9]. If the particle is external incoming / outgoing, then the number of initial / final vertex of the line is set to zero.
- Type of particle on the line ($\pi^0_{cl}, K^+_{in}, W^+, \ldots$)
- Its momentum
- Its Lorentz index (for particles $W^\pm_\mu$ of the axial current) .

To calculate the amplitude of the given diagram, we must combine contributions from each vertex and line. In some cases we must also divide the provisional result by the symmetry factor of the graph.

When calculating contribution of a given vertex, the function **GraphContribution** first goes through all the lines going to / from the vertex and chooses the lines that begin or end here. To simplify further calculations, all lines are reoriented to contain only incoming particles with respect to the vertex. If there is a line containing outcoming particle ϕ with momentum p, it is "reoriented" by replacing the particle with its antiparticle and by reversing its momentum to $-p$[10]. Then we go through all lines of the vertex and extract and store information about momentum for each type of particle — eight "classical", eight "quantum" and two $W^\pm$ — and for $W^\pm$ also Lorentz indices of these particles. For example if there are two π^0_{cl} incoming to the vertex with momenta q_1, q_2, we store both these momenta in a corresponding array. This book-keeping is important because of the derivatives present in the Lagrangian, as we will see shortly. We also compute number of particles of each type so we can later easily distinguish Lagrangian terms which are relevant.

After processing information about particles interacting in the vertex, we build matrices $\overline{u}$ (according to (4.29)) and $\exp(i\sqrt{2}\phi_{in}/F_0)$. From before we know how many particles are interacting in the vertex, which gives the highest order to which we must expand the exponential. We also know which particles are not interacting in the vertex, which enables us to drop them from the very beginning to save some computation time. After the expansion we are able to build the relevant Lagrangian and keep only the terms with the correct numbers of particles.

[7] Interested reader may consult also Appendix B, where sample calculation is performed with somewhat more detail.

[8] To describe external lines, we introduced a special vertex numbered zero — see further.

[9] All lines are oriented according to the direction of momentum.

[10] Correctness of this procedure relies on an assumption of validity of CPT theorem.

There are three special things that must be taken care of — derivatives in the Lagrangian, vector index of $W^{\pm}$ and identical particles.

Because we reoriented all particles to be incoming, in the momentum representation which we are using each derivative is in the corresponding Feynman rule represented by a mere multiplication by momentum with the same factor $-i$,

$$\partial_x \phi \to -i p_{x,\phi} \phi \ . \tag{4.37}$$

If we did not reorient the particles we would have to take special care of the incoming / outcoming particles. At the vertex there may be more fields of the same type but with different momenta — typically two π^0_{in} or two η_{in}. In such case we must take care of what combination of momenta we take. In assessing the correct combination we use the Wick theorem [15] which tells us to take all "contractions" among the fields. If we have vertex with N identical particles ϕ with momenta $p_1, \ldots, p_N$ and the corresponding Lagrangian term contains m derivatives of these fields $\partial^{\mu_1}, \ldots, \partial^{\mu_m}$ then according to the theorem we must sum all possible combinations of m derivatives on N momenta. In the result the corresponding Feynman rule is proportional to

$$(-i)^m \sum_{i_1 \neq i_2 \neq \ldots \neq i_m} p^{\mu_1}_{i_1} p^{\mu_2}_{i_2} \ldots p^{\mu_m}_{i_m} \ . \tag{4.38}$$

This sum is then easily constructed from the previously created array which stores separately list of momenta for each type of particle.

This rule is somewhat more complicated for $W^{\pm}$, because derivatives of these particles effectively carry two Lorentz indices — one from the derivative and one from the axial current. In such case we must be careful during the "contraction" of such a particle, because we must match also the Lorentz index of the axial current and the matching of momenta and this Lorentz index must agree. We clarify this on an example: If in the Lagrangian we have term with $\partial_\mu W^+_\nu$ and on an external line there is an incoming W^+ with momentum p and Lorentz index α, then we multiply the constructed Feynman rule by $-i p_\mu \delta_{\alpha\nu}$ instead of simple $-i p_\mu$. In our Mathematica notebook we took care of this situation.

Finally the last complication in building the Feynman rule arises when there are some indistinguishable particles left even after we "contract" fields with derivatives. For example if the Lagrangian contained term $\eta\eta\,\partial_\mu\eta$ then after we "contract" the term with derivative we are left with two indistinguishable particles $\eta\eta$. There are two ways how to contract this, therefore we must multiply the Feynman rule by additional factor of 2. In general, if after contracting the terms with derivatives there are N indistinguishable particles left, we must add factor of $N!$ to the constructed Feynman rule. This concludes our discussion of the contributions from the vertices.

For each internal propagator of a quantum particle we earlier gave reasons for the use of a scalar propagator

$$\Delta(p) = \frac{i}{p^2 - m^2_{\phi_{in}}} \ , \tag{4.39}$$

with masses (4.36). The external lines which represent powers of "classical" fields, correspond to coefficients in the expansion of the generating functional (4.7) and as such do not contribute to the constructed Feynman rule.

Finally in our case of semileptonic kaon decays we had to take care of two situations where we had to employ symmetry factors — tadpole graphs with exchange of electrically neutral particle and bubble graphs with exchange of two identical particles. In such cases we had to divide obtained amplitude by the symmetry factor two [15]. Because more complicated symmetries were not employed in our calculations, we did not check on presence of general symmetry factors but only searched for the two situations mentioned above.

To process one loop graphs, we employed external library FeynCalc [45]. When diagrams are inputed in a convention employed by FeynCalc, it is capable of giving results of one loop graphs expressed in terms of loop functions $A_0(M^2)$ and $B_0(s, M_1^2, M_2^2)$ which are defined in the Appendix B. The calculations with FeynCalc proceed in two steps — first, amplitude of the diagram is calculated in terms of general Passarino-Veltman coefficient functions. In the next step the final expression is reduced using function **PaVeReduce** of FeynCalc to contain only A_0 and B_0.

The Passarino-Veltman reduction is the last step in calculating the amplitudes of diagrams, which are now expressed in terms of momenta p_1, p_2, q of the outcoming pions and dilepton; low energy constants from the χPT Lagrangian F_0, $B_0 m_q$, L_i and loop functions A_0, B_0.

4.4 Formfactors

In previous sections we introduced the technique of calculating coefficients $Z_{i_1 \ldots i_n}$ in the expansion (4.7) using Feynman diagrams. Then we explained how we implemented this technique into our Mathematica notebook which calculates amplitudes of respective Feynman diagrams of one-loop RχPT. In this section we put all this together and give theoretical formulae for the formfactors of semileptonic kaon decay.

Above we used Weinberg's formula and discussed that to NLO we must include tree graphs where one of the vertices may be from $\overline{\mathcal{L}_4}$ and remaining vertices must come from $\overline{\mathcal{L}_2}$ and one-loop graphs with vertices from $\mathcal{L}_{loop}$. Diagrams that at given order contribute to formfactors F, G, R are schematically pictured in the Figures 2 (contributions to $Z_{ab\beta}$ linear in a^μ) and 3 (contributions to $Z_{ab\beta\alpha}$).

For calculations of the diagrams we used the Mathematica notebook introduced in the previous section.

To arrive at the correct NLO expression for the matrix element

$$\langle \pi^a(p_1)\pi^b(p_2)|J_\mu^h|K^\beta(k)\rangle \tag{4.40}$$

in χPT, amplitudes of the one particle irreducible diagrams must be multiplied by

$$\frac{1}{i}\prod_{i=a,b,\beta}\frac{F_0}{F_i} \tag{4.41}$$

and amplitudes of the pole diagrams must be multiplied by

$$\frac{F_\alpha q_\mu}{q^2 - M_\alpha^2}\prod_{i=a,b,\beta,\alpha}\frac{F_0}{F_i}\ , \tag{4.42}$$

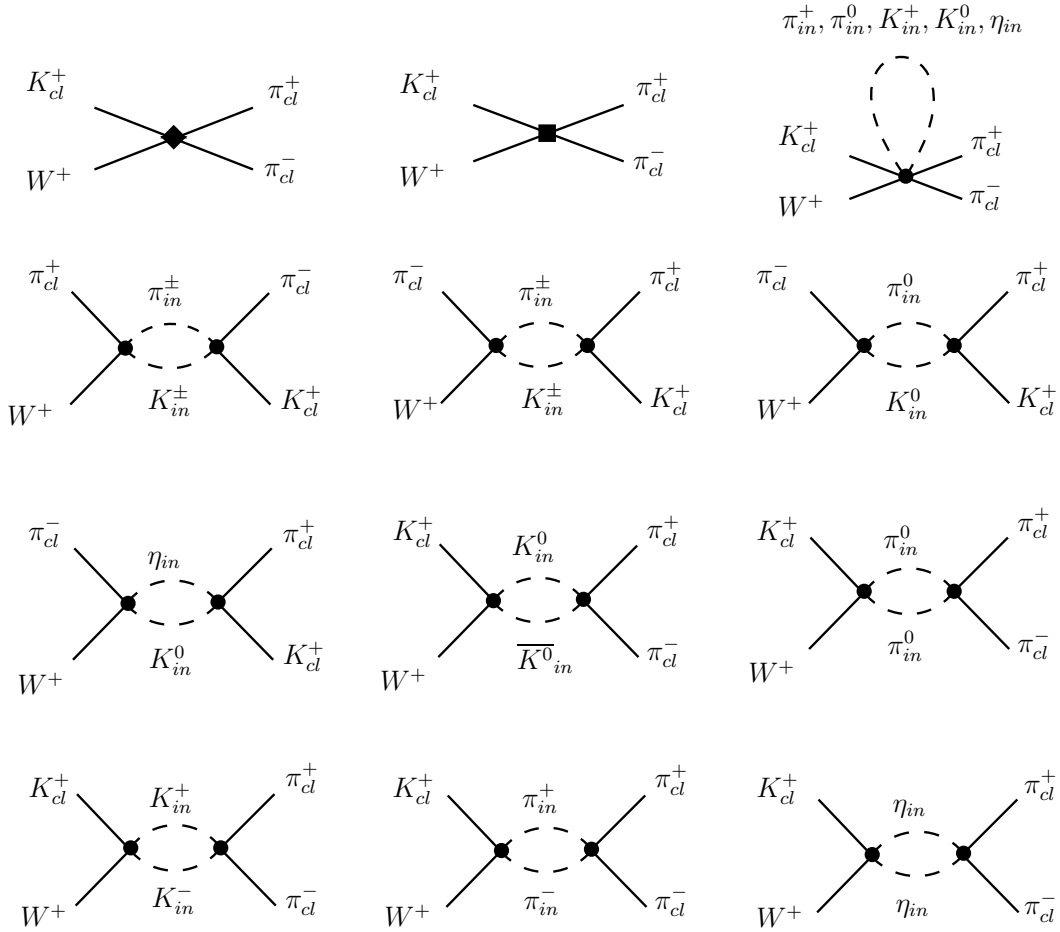

Figure 2: Feynman diagrams which contribute to coefficient $Z_{ab\beta}$ (4.7) and are linear in a^μ (contain single W^+). Diamond vertex corresponds to $\mathcal{L}_2$, boxed vertex corresponds to $\mathcal{L}_4$ and circles stand for vertices from $\mathcal{L}_{loop}$. "Classical" particles are drawn with solid lines, "quantum" particles with dashed lines.

as indicated in (4.21). Finally, the employed convention (3.28) states that to get theoretical predictions on the formfactors, we must multiply the derived result for investigated matrix element by a factor iM_K and take coefficients standing in front of vectors P^μ, Q^μ and q^μ. This completes our calculations of the formfactors. However, we introduced some modifications before quoting the final result.

The formfactors may be rewritten to a more legible form by using mass shell conditions

$$\begin{aligned} p_1^2 = p_2^2 &= M_\pi^2 \\ (p_1 + p_2 + q)^2 &= M_K^2 \ , \end{aligned} \tag{4.43}$$

which together with definitions (3.21) and constraint (3.22) enable us to express

$$\begin{aligned} p_1 \cdot p_2 &= \frac{s}{2} - M_\pi^2 \\ p_1 \cdot q &= \frac{u - M_\pi^2 - q^2}{2} \\ p_2 \cdot q &= \frac{t - M_\pi^2 - q^2}{2} \ . \end{aligned} \tag{4.44}$$

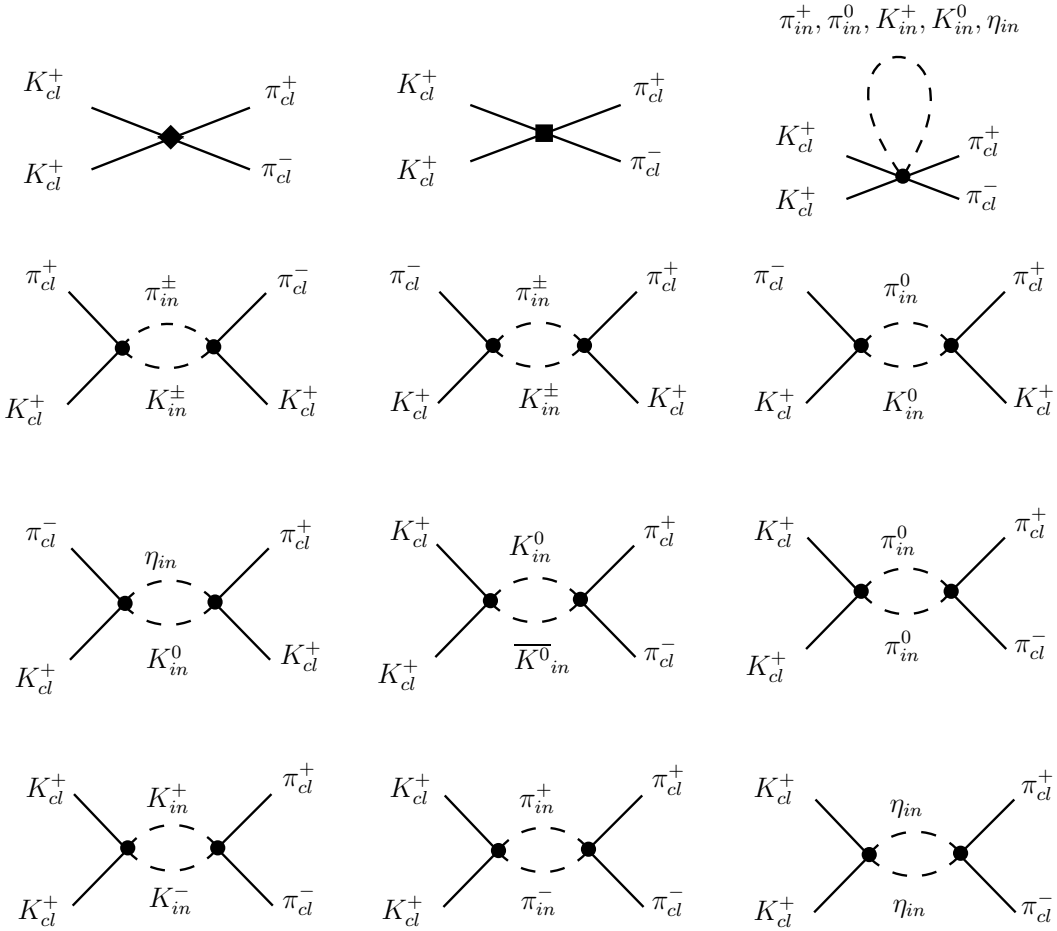

Figure 3: Feynman diagrams which contribute to coefficient $Z_{ab\beta\alpha}$. Diamond vertex corresponds to $\mathcal{L}_2$, boxed vertex corresponds to $\mathcal{L}_4$ and circles stand for vertices from $\mathcal{L}_{loop}$. "Classical" particles are drawn with solid lines, "quantum" particles with dashed lines.

Further we may use (2.44) and replace $B_0 m_q$ by $O(p^2)$ masses of pion and kaon

$$\begin{aligned} B_0\hat{m} &= \frac{\overset{\circ}{M}{}^2_\pi}{2} \\ B_0 m_s &= \overset{\circ}{M}{}^2_K - \frac{\overset{\circ}{M}{}^2_\pi}{2} \ . \end{aligned} \tag{4.45}$$

Our final change is rewriting the one loop functions A_0 and B_0 to scalar bubble $J^r_{PQ}(s)$ (defined in the Appendix B) and derived functions. Using formulae given in the Appendix B, we may write

$$\begin{aligned} A_0(s) &\to s(1 + B_0(0,s,s)) \\ B_0(s, \overset{\circ}{M}{}^2_P, \overset{\circ}{M}{}^2_Q) &\to 16\pi^2 J^r_{\overset{\circ}{M}_P, \overset{\circ}{M}_Q}(s) \ . \end{aligned} \tag{4.46}$$

In accord with our previous discussion on RχPT, to get correct positions of branching points we then substitute LO masses $\overset{\circ}{M}_P$ in arguments of J^r with their physical counterparts M_P. This replacement constitute our transition from the "strict" chiral expansion to "bare" chiral expansion.

Then we replace[11]

$$\frac{J^r_{PQ}(s)}{s^2} = \frac{J^r_{PQ}(0) + sJ^{r'}_{PQ}(0) + \overline{\overline{J}}_{PQ}(s)}{s^2} \ , \tag{4.47}$$

which simplifies some of the fractions in the result. Finally, to separate constant part of J^r from the unitary part that depends on kinematical variables we use

$$J^r_{PQ}(s) = J^r_{PQ}(0) + \overline{J}_{PQ}(s) \ . \tag{4.48}$$

After performing all steps mentioned above, we arrive at the following results for formfactors F and G:

Formfactor F may be at NLO written as

$$F_{NLO}(s,t;u;q^2) = \frac{M_K}{\sqrt{2}F_\pi}\left(\frac{F_\pi}{F_K}\right)\left[Z + \frac{1}{F_\pi^2}\left(P_F(s,t;u;q^2) + U_F(s,t;u)\right)\right] \ , \tag{4.49}$$

where the contribution $U_F(s,t;u)$ denotes the unitary correction generated by the one loop graphs which appear at order E^4 in the low energy expansion and $P_F(s,t;u;q^2)$ stands for polynomial in s,t,u and q^2 and contains contributions from tree graphs in the order $O(p^4)$ and constant part of the one loop graphs. They are explicitly

$$\begin{aligned}
U_F(s,t;u) = &\left(\frac{3}{2}\overset{\circ}{M}{}^2_\pi - 2M_\pi^2 + s\right)\overline{J}_{\pi\pi}(s) + \frac{3}{4}\left(s - 2M_\pi^2 + 2\overset{\circ}{M}{}^2_\pi\right)\overline{J}_{KK}(s) + \\
&+ \frac{1}{2}\overset{\circ}{M}{}^2_\pi\overline{J}_{\eta\eta}(s) - \frac{1}{36}\Delta_{K\pi}\overset{\circ}{\Delta}{}^2_{K\pi}\left(\frac{\overline{\overline{J}}_{K\eta}(t)}{t^2} + 9\frac{\overline{\overline{J}}_{K\pi}(t)}{t^2}\right) + \\
&+ \left(\frac{1}{8}\overset{\circ}{\Sigma}_{\eta K}M_K^2 + \frac{1}{12}M_\pi^2\left(2\overset{\circ}{M}{}^2_\pi - 5\overset{\circ}{M}{}^2_K\right) + \frac{1}{8}\overset{\circ}{\Delta}_{\eta K}\overset{\circ}{M}{}^2_K\right)\frac{\overline{J}_{K\eta}(t)}{t} + \\
&+ \left(\frac{1}{8}\overset{\circ}{\Sigma}_{K\pi}M_K^2 + \frac{1}{4}M_\pi^2\left(2\overset{\circ}{M}{}^2_\pi - 3\overset{\circ}{M}{}^2_K\right) + \frac{3}{8}\overset{\circ}{\Delta}_{K\pi}\overset{\circ}{M}{}^2_K\right)\frac{\overline{J}_{K\pi}(t)}{t} + \\
&+ \frac{1}{8}\left(M_K^2 + 2M_\pi^2 - 7\overset{\circ}{M}{}^2_K\right)\overline{J}_{K\eta}(t) + \\
&+ \frac{1}{8}\left(5M_K^2 + 6M_\pi^2 - 3\overset{\circ}{M}{}^2_K - 8\overset{\circ}{M}{}^2_\pi - 4t\right)\overline{J}_{K\pi}(t) + \\
&+ \frac{1}{2}\left(M_K^2 + M_\pi^2 - u\right)\overline{J}_{K\pi}(u)
\end{aligned} \tag{4.50}$$

and

$$\begin{aligned}
P_F(s,t;u;q^2) = &\ 32L_1\left(s - 2M_\pi^2\right) + 8L_2\left(s - q^2 + M_K^2\right) + \\
&+ 4L_3\left(M_K^2 - 3M_\pi^2 + 2s - t\right) + \\
&+ 8L_4\left(5\overset{\circ}{M}{}^2_\pi + 2\overset{\circ}{M}{}^2_K\right) + 4L_5\left(2\overset{\circ}{M}{}^2_\pi + \overset{\circ}{M}{}^2_K\right) + 2L_9q^2 + \\
&+ s\left(\frac{3}{4}J^r{}_{KK}(0) + \frac{1}{2}J^r{}_{K\pi}(0) + J^r{}_{\pi\pi}(0) - \frac{1}{128\pi^2}\right) + \\
&+ \frac{1}{128\pi^2}(t-u) + q^2\left(-\frac{1}{2}J^r{}_{K\pi}(0) + \frac{1}{128\pi^2}\right) +
\end{aligned}$$

[11] The introduced shortened notation $J^r_{PQ}, \overline{J}_{PQ}$ and $\overline{\overline{J}}_{PQ}$ represents functions with (physical) masses M_P and M_Q in place of arguments m_P and m_Q.

$$
\begin{aligned}
&+\frac{1}{4}M_\pi^2\left(J^r{}_{K\eta}(0)-6J^r{}_{KK}(0)+J^r{}_{K\pi}(0)-8J^r{}_{\pi\pi}(0)+\frac{1}{12\pi^2}\right)+\\
&+\frac{1}{8}M_K^2\left(J^r{}_{K\eta}(0)+5J^r{}_{K\pi}(0)+\frac{1}{48\pi^2}\right)+\\
&+\frac{1}{4}\overset{\circ}{M}{}_\pi^2\left(J^r{}_{\eta\eta}(0)+6J^r{}_{KK}(0)-4J^r{}_{K\pi}(0)+13J^r{}_{\pi\pi}(0)+\frac{5}{16\pi^2}\right)+\\
&+\frac{1}{8}\overset{\circ}{M}{}_K^2\left(8J^r{}_{\eta\eta}(0)-7J^r{}_{K\eta}(0)+16J^r{}_{KK}(0)-3J^r{}_{K\pi}(0)+\frac{7}{8\pi^2}\right)\ .
\end{aligned}
\tag{4.51}
$$

Here we introduced for brevity

$$
\begin{aligned}
\Delta_{PQ} &= M_P^2-M_Q^2\\
\Sigma_{PQ} &= M_P^2+M_Q^2\\
\overset{\circ}{\Delta}_{PQ} &= \overset{\circ}{M}{}_P^2-\overset{\circ}{M}{}_Q^2\\
\overset{\circ}{\Sigma}_{PQ} &= \overset{\circ}{M}{}_P^2+\overset{\circ}{M}{}_Q^2
\end{aligned}
\tag{4.52}
$$

and earlier we defined

$$
Z = \frac{F_0^2}{F_\pi^2}\ . \tag{4.53}
$$

Similar division of the result is possible for the G formfactor. Namely,

$$
G_{NLO}(s,t;u;q^2)=\frac{M_K}{\sqrt{2}F_\pi}\left(\frac{F_\pi}{F_K}\right)\left[Z+\frac{1}{F_\pi^2}\left(P_G(s,t;u;q^2)+U_G(s,t;u)\right)\right] \tag{4.54}
$$

with unitary corrections

$$
\begin{aligned}
U_G(s,t;u) &= \frac{1}{12}\left(s-4\overset{\circ}{M}{}_K^2\right)\overline{J}_{K,K}(s)+\frac{1}{6}\left(s-4\overset{\circ}{M}{}_\pi^2\right)\overline{J}_{\pi,\pi}(s)+\\
&+\frac{1}{36}\Delta_{K\pi}\overset{\circ}{\Delta}_{K\pi}\left(\frac{\overline{\overline{J}}_{K\eta}(t)}{t^2}+9\frac{\overline{\overline{J}}_{K\pi}(t)}{t^2}\right)+\\
&+\left(-\frac{1}{8}\overset{\circ}{\Sigma}_{\eta K}M_K^2+\frac{1}{12}M_\pi^2\left(5\overset{\circ}{M}{}_K^2-2\overset{\circ}{M}{}_\pi^2\right)-\frac{1}{24}\overset{\circ}{\Delta}_{\eta K}\left(\overset{\circ}{M}{}_K^2+2\overset{\circ}{M}{}_\pi^2\right)\right)\frac{\overline{J}_{K,\eta}(t)}{t}+\\
&+\left(-\frac{1}{8}\overset{\circ}{\Sigma}_{K\pi}M_K^2+\frac{1}{4}M_\pi^2\left(3\overset{\circ}{M}{}_K^2-2\overset{\circ}{M}{}_\pi^2\right)-\frac{1}{8}\overset{\circ}{\Delta}_{K\pi}\left(\overset{\circ}{M}{}_K^2+2\overset{\circ}{M}{}_\pi^2\right)\right)\frac{\overline{J}_{K,\pi}(t)}{t}+\\
&+\frac{1}{24}\left(-7\overset{\circ}{M}{}_K^2-3M_K^2+4\overset{\circ}{M}{}_\pi^2-6M_\pi^2+6t\right)\overline{J}_{K,\eta}(t)+\\
&+\frac{1}{8}\left(-\overset{\circ}{M}{}_K^2-5M_K^2+4\overset{\circ}{M}{}_\pi^2-6M_\pi^2+6t\right)\overline{J}_{K,\pi}(t)+\\
&+\frac{1}{2}\left(M_K^2+M_\pi^2-u\right)\overline{J}_{K,\pi}(u)
\end{aligned}
\tag{4.55}
$$

and polynomial part

$$
\begin{aligned}
P_G(s,t;u;q^2) &= 8L_2(t-u)+4L_3(t-M_K^2-M_\pi^2)+\\
&+8L_4\left(2\overset{\circ}{M}{}_K^2+\overset{\circ}{M}{}_\pi^2\right)+4L_5\left(\overset{\circ}{M}{}_K^2+2\overset{\circ}{M}{}_\pi^2\right)+2L_9q^2+
\end{aligned}
$$

$$
\begin{aligned}
&+ s\left(-\frac{1}{8}J^r{}_{K,\eta}(0) - \frac{1}{8}J^r{}_{K,\pi}(0) + \frac{1}{12}J^r{}_{K,K}(0) + \frac{1}{6}J^r{}_{\pi,\pi}(0) + \frac{1}{128\pi^2}\right) + \\
&+ (t-u)\left(\frac{1}{8}J^r{}_{K,\eta}(0) + \frac{5}{8}J^r{}_{K,\pi}(0) + \frac{1}{384\pi^2}\right) + \\
&+ q^2\left(\frac{1}{8}J^r{}_{K,\eta}(0) + \frac{1}{8}J^r{}_{K,\pi}(0) + \frac{1}{384\pi^2}\right) + \frac{M_K^2}{128\pi^2} + \\
&+ \mathring{M}_K^{\,2}\left(\frac{1}{3}J^r{}_{\eta,\eta}(0) - \frac{5}{24}J^r{}_{K,\eta}(0) + \frac{3}{2}J^r{}_{K,K}(0) + \frac{1}{8}J^r{}_{K,\pi}(0) + \frac{17}{192\pi^2}\right) + \\
&+ \mathring{M}_\pi^{\,2}\left(-\frac{1}{12}J^r{}_{\eta,\eta}(0) + \frac{1}{12}J^r{}_{K,\eta}(0) + \frac{1}{4}J^r{}_{K,\pi}(0) + \frac{7}{4}J^r{}_{\pi,\pi}(0) + \frac{19}{192\pi^2}\right) .
\end{aligned}
\tag{4.56}
$$

We checked we arrive at the result obtained by the standard χPT [36] after we substitute LO parameters by inversions of (2.74), (2.75) and (2.76) and keep only terms to NLO.

As another check we investigated explicit scale invariance of the result by changing μ — we changed value of the L_i's according to[12]

$$
L_i^r(\mu_1) = L_i^r(\mu_2) + \frac{\Gamma_i}{16\pi^2}\log\frac{\mu_1}{\mu_2} , \tag{4.57}
$$

and $J^r_{PQ}(0)$ according to formulae given in the Appendix B and checked that all contributions cancel.

[12]The logarithmic running is implied by (2.51), constants Γ_i were derived in [3].

Chapter 5

Obtaining the $L_1 - L_3$

5.1 Resummed result

Everything so far is correct from the point of view of RχPT, as we started with generating functional Z and used only linear operations to get theoretical predictions on formfactors F_{NLO} and G_{NLO}. To get the final predictions on the theoretical values of these formfactors we must perform three more operations.

In the "bare" expansion from previous chapter we must express remaining LO masses and LO pion decay constant F_0 in terms of physical values and X, Z, r (see (2.91))

$$\begin{aligned} F_0^2 &= Z F_\pi^2 \\ \overset{\circ}{M}{}_\pi^2 &= Y M_\pi^2 \\ \overset{\circ}{M}{}_K^2 &= \frac{r+1}{2} Y M_\pi^2 \\ \overset{\circ}{M}{}_\eta^2 &= \frac{2r+1}{3} Y M_\pi^2 \ . \end{aligned} \tag{5.1}$$

At the same time we must reexpress low energy constants L_4, L_5 and L_9 in terms of masses and decay constants according to Appendix C. Finally, we must parametrize our ignorance of higher order contributions by introducing higher order remainders. After all these steps, our theoretical predictions on the values of formfactors read schematically

$$\begin{aligned} F_{th} &= F_{NLO}(X, Z, r, \delta_{F_\pi}, \delta_{F_K}, L_1, L_2, L_3) + F_{th}\, \delta_F \\ G_{th} &= G_{NLO}(X, Z, r, \delta_{F_\pi}, \delta_{F_K}, L_1, L_2, L_3) + G_{th}\, \delta_G \ . \end{aligned} \tag{5.2}$$

Now we have theoretical expressions for formfactors F and G formulated in terms of physical constants; X, Z, r; higher order remainders and three unknown constants $L_1 - L_3$. By comparison of our theoretical predictions with experimental values of formfactors we are able to determine the values of these low energy constants in terms of the remaining quantities, as we show in the following section.

5.2 Isolating $L_1 - L_3$

While formfactor F depends on all three low-energy constants $L_1 - L_3$, formfactor G depends only on L_2 and L_3. The situation gets even simpler if we investigate

formfactors at the point $\cos\theta = 0$. Then we have (3.27)

$$u = t = \frac{1}{2}\left(M_K^2 + 2M_\pi^2 + q^2 - s\right) \tag{5.3}$$

and L_2 dependence of the G formfactor vanishes. In such case G is function of only L_3 and comparison of theoretical prediction on G with the experimental values can be used to isolate L_3.

For further simplification we extrapolated the experimental data to the point $q^2 = 0$ where formfactors are functions of single kinematical parameter s[1]. In the considered limit this kinematical parameter is bounded by inequalities (3.23)

$$4M_\pi^2 \leq s \leq M_K^2 \ . \tag{5.4}$$

Our theoretical prediction on formfactor G can be split into part which depends on L_3 explicitly and the part which is independent of L_3

$$G_{th} = \overline{G_{NLO}} + K_3 L_3 + G_{th}\delta_G \ , \tag{5.5}$$

where from (4.54) and (4.56) we can read off[2]

$$K_3 = -\frac{\sqrt{2}M_K}{F_\pi^2 F_K} \cdot (s + M_K^2) \tag{5.6}$$

and we defined

$$\overline{G_{NLO}} = G_{NLO}\Big|_{L_3=0} \ , \tag{5.7}$$

which is independent of low energy constant L_3.

If we now set our theoretical prediction on G equal to experimentally measured value G_{exp} by setting

$$G_{exp} = G_{th} \tag{5.8}$$

at some value s_G of kinematical variable s and then substitute this to (5.5), we obtain

$$L_3 \ = \ \frac{G_{exp}(1-\delta_G) - \overline{G_{NLO}}}{K_3} \ . \tag{5.9}$$

All quantities at (5.9) are evaluated at $s = s_G$.

Plugging in from definition of K_3 we get

$$L_3 \ = \ \frac{F_\pi^2 F_K}{\sqrt{2}M_K(s_G + M_K^2)}\left(\overline{G_{NLO}} - G_{exp}(1-\delta_G)\right) \ . \tag{5.10}$$

Everything on the right hand side can be expressed using only experimentally measureable data, X, Z, r and higher order remainders and (5.10) thus constitutes our final result on reparametrization of L_3.

With this result, we can replace each L_3 by the expression (5.10) as we did in case of L_4 – L_9. Specifically we can do this in our theoretical result for F formfactor, which then depends only on two unknown constants L_1 and L_2.

[1] Just to remind — the formfactors depend in general on three parameters. Two of these we constrained, so we are left with one degree of freedom.

[2] This holds only for $\cos\theta = 0$.

Because formfactors are in general complex numbers and the same holds for our theoretical predictions, formula (5.10) gives us in general complex L_3. If this were true then our Lagrangian (2.48) would not be Hermitian. The simplest way how to resolve this is to compare only real parts of theoretical predictions and experimental values which is the way we used — in the rest of this thesis, we work exclusively with real parts of complex expressions. Especially, we plug in only real parts of expressions A_{exp} and $\overline{A_{NLO}}$ to final formulae for low energy constants L_1 – L_3, such as (5.10). We do not do anything wrong from the perspective of the RχPT as taking real part is a linear operation.

Situation with L_1 and L_2 is a little more complicated. One way we could pin down the L_2 would be to relax the constraint $\cos\theta = 0$ and use again comparison of theoretical prediction with experimental value of G formfactor for some nonzero value of $\cos\theta$. However, the change in values of G induced by relaxing constraint $\cos\theta = 0$ are expected to be small and we would introduce a large error into our calculations. We decided to take another way instead and reexpress the L_1 and L_2 solely from the values of formfactor F.

Because we are reexpressing two low energy constants, we need two pieces of experimental data. We have basically two possibilities:

- Compare theoretical prediction of the formfactor F with its experimental value at two distinct s (s_A, s_B).
- Compare value of the formfactor at s_F and the slope of the formfactor $\frac{dF}{ds}$ at (possibly different) point s_S.

Now we derive formulae for L_1 and L_2 in both ways.

5.2.1 First strategy to reexpress L_1 and L_2

In this way we use theoretical prediction on experimental values of F at two distinct points s_A and s_B. As we did in the case of G formfactor, we can split the theoretical predictions into the part independent of L_1 and L_2 and the rest,

$$\begin{aligned} F_{A,th} &= \overline{F_{A,NLO}} + K_{A1}L_1 + K_{A2}L_2 + F_{A,th}\,\delta_A \\ F_{B,th} &= \overline{F_{B,NLO}} + K_{B1}L_1 + K_{B2}L_2 + F_{B,th}\,\delta_B\ . \end{aligned} \tag{5.11}$$

Above we introduced following quantities: $F_{A(B),th}$ are our final theoretical results on values of F at $s_{A(B)}$ and $\delta_{A(B)}$ are corresponding higher order remainders. Values of constants K_{A1}, K_{A2}, K_{B1} and K_{B2} may be read off from (4.49) and (4.51) as

$$\begin{aligned} K_{A1} &= \frac{\sqrt{2}M_K}{F_\pi^2 F_K}\cdot 16(s_A - 2M_\pi^2) \\ K_{A2} &= \frac{\sqrt{2}M_K}{F_\pi^2 F_K}\cdot 4(s_A + M_K^2) \\ K_{B1} &= \frac{\sqrt{2}M_K}{F_\pi^2 F_K}\cdot 16(s_B - 2M_\pi^2) \\ K_{B2} &= \frac{\sqrt{2}M_K}{F_\pi^2 F_K}\cdot 4(s_B + M_K^2)\ . \end{aligned} \tag{5.12}$$

Finally,

$$\begin{aligned}\overline{F_{A,NLO}} &= F_{NLO}\Big|_{L_1=L_2=0} \\ \overline{F_{B,NLO}} &= F_{NLO}\Big|_{L_1=L_2=0} ,\end{aligned} \tag{5.13}$$

where F_{NLO} is evaluated at s_A on the first line and at s_B on the second line.

Setting theoretical predictions equal to their respective experimental values

$$F_{A(B),th} = F_{A(B),exp} \tag{5.14}$$

we can use (5.11) and solve the system of two linear equations to get

$$\begin{aligned}L_1 &= \frac{K_{A2}(\overline{F_{B,NLO}} - F_{B,exp}(1-\delta_B)) - K_{B2}(\overline{F_{A,NLO}} - F_{A,exp}(1-\delta_A))}{K_{A1}K_{B2} - K_{A2}K_{B1}} \\ L_2 &= \frac{K_{B1}(\overline{F_{A,NLO}} - F_{A,exp}(1-\delta_A)) - K_{A1}(\overline{F_{B,NLO}} - F_{B,exp}(1-\delta_B))}{K_{A1}K_{B2} - K_{A2}K_{B1}} .\end{aligned} \tag{5.15}$$

Using definitions (5.12) we get the final result

$$\begin{aligned}L_1 &= \frac{F_K F_\pi^2}{16\sqrt{2}M_K}\frac{(s_A+M_K^2)(\overline{F_{B,NLO}} - F_{B,exp}) - (s_B+M_K^2)(\overline{F_{A,NLO}} - F_{A,exp})}{(s_A-s_B)(M_K^2+2M_\pi^2)} \\ &\quad + \frac{F_K F_\pi^2}{16\sqrt{2}M_K}\frac{(s_A+M_K^2)F_{B,exp}\,\delta_B - (s_B+M_K^2)F_{A,exp}\,\delta_A}{(s_A-s_B)(M_K^2+2M_\pi^2)} \\ L_2 &= \frac{F_K F_\pi^2}{4\sqrt{2}M_K}\frac{(s_B-2M_\pi^2)(\overline{F_{A,NLO}} - F_{A,exp}) - (s_A-2M_\pi^2)(\overline{F_{B,NLO}} - F_{B,exp})}{(s_A-s_B)(M_K^2+2M_\pi^2)} \\ &\quad + \frac{F_K F_\pi^2}{4\sqrt{2}M_K}\frac{(s_B-2M_\pi^2)F_{A,exp}\,\delta_A - (s_A-2M_\pi^2)F_{B,exp}\,\delta_B}{(s_A-s_B)(M_K^2+2M_\pi^2)}\end{aligned} \tag{5.16}$$

As before for L_3, we again arrived at a result that is expressed only through experimentally obtainable constants, X, Z, r and higher order remainders δ_W[3]. Here and in what follows we under the shorthand notation δ_W understand the set of $\delta_A, \delta_B, \delta_F, \delta_G, \delta_S, \delta_{F_\pi}, \delta_K$ (δ_F and δ_S are introduced in the next section).

5.2.2 Second strategy to reexpress L_1 and L_2

The second way to isolate L_1 and L_2 is to use value of the formfactor at s_F and the slope of the formfactor $S = \frac{dF}{ds}$ at point s_S. Because we are working in the limit of zero $\cos\theta$ and q^2, F depends on a single variable and the derivative has a uniquely defined sense.

Before proceeding further, we must specify our theoretical prediction on $\frac{dF}{ds}$. From (4.49) we see that this derivative can be to NLO split into two parts,

$$S_{NLO}(s) = \frac{dF}{ds}\Big|_s = \frac{M_K}{\sqrt{2}F_\pi^2 F_K}\left(\frac{dU_F(s,t_F;u_F)}{ds} + \frac{dP_F(s,t_F,u_F)}{ds}\right) , \tag{5.17}$$

[3]We once again stress out that the L_3 in (5.10) has been reparametrized and as such drops from all formulae, therefore also from formulae for $F_{A(B),NLO}$.

where we plugged in expressions for t and u in the used approximation (5.3)

$$t_F = u_F = \frac{1}{2}\left(M_K^2 + 2M_\pi^2 - s\right) \ . \tag{5.18}$$

Unitary part was defined in (4.50) and explicit form of its derivative is not interesting in our case. Here we quote only derivative of the polynomial part of the F formfactors as this is the one containing the low energy constants:

$$\frac{dP_F(s,t_F,u_F)}{ds} = \frac{3}{4}J^r_{KK}(0) + \frac{1}{2}J^r_{K\pi}(0) + J^r_{\pi\pi}(0) + 32L_1 + 8L_2 + 10L_3 - \frac{1}{128\pi^2} \ . \tag{5.19}$$

As in the previous case we in our theoretical predictions of the formfactor and its derivative isolate dependence on low-energy constants L_1, L_2 which we want to reparametrize,

$$\begin{aligned} F_{th} &= \overline{F_{NLO}} + K_{F1}L_1 + K_{F2}L_2 + F_{th}\,\delta_F \\ S_{th} &= \overline{S_{NLO}} + K_{S1}L_1 + K_{S2}L_2 + S_{th}\,\delta_S \ . \end{aligned} \tag{5.20}$$

Similarly to the previous case, F_{th} and S_{th} are our final theoretical results on values of $F(s_F)$ and $S(s_S)$ and δ_F, δ_S are corresponding higher order remainders. Values of constants K_{F1}, K_{F2}, K_{S1} and K_{S2} may be read off from (4.49), (4.51), (5.17) and (5.19) as

$$\begin{aligned} K_{F1} &= \frac{\sqrt{2}M_K}{F_\pi^2 F_K}\cdot 16(s_F - 2M_\pi^2) \\ K_{F2} &= \frac{\sqrt{2}M_K}{F_\pi^2 F_K}\cdot 4(s_F + M_K^2) \\ K_{S1} &= \frac{\sqrt{2}M_K}{F_\pi^2 F_K}\cdot 16 \\ K_{S2} &= \frac{\sqrt{2}M_K}{F_\pi^2 F_K}\cdot 4 \end{aligned} \tag{5.21}$$

and parts independent on $L_{1,2}$ are

$$\begin{aligned} \overline{F_{NLO}} &= F_{NLO}\Big|_{L_1=L_2=0} \\ \overline{S_{NLO}} &= S_{NLO}\Big|_{L_1=L_2=0} \ , \end{aligned} \tag{5.22}$$

where F_{NLO} is evaluated at s_F and S_{NLO} is evaluated at s_S.

Knowledge of experimental values F_{exp}, S_{exp} enables us to reduce L_1 and L_2 from (5.20) as

$$\begin{aligned} L_1 &= \frac{K_{F2}(\overline{S_{NLO}} - S_{exp}(1-\delta_S)) - K_{S2}(\overline{F_{NLO}} - F_{exp}(1-\delta_F))}{K_{F1}K_{S2} - K_{F2}K_{S1}} \\ L_2 &= \frac{K_{S1}(\overline{F_{NLO}} - F_{exp}(1-\delta_F)) - K_{F1}(\overline{S_{NLO}} - S_{exp}(1-\delta_S))}{K_{F1}K_{S2} - K_{F2}K_{S1}} \ , \end{aligned} \tag{5.23}$$

which simplifies to

$$L_1 = \frac{F_K F_\pi^2}{16\sqrt{2}M_K}\frac{\overline{F_{NLO}} - F_{exp}(1-\delta_F) - (s_F + M_K^2)(\overline{S_{NLO}} - S_{exp}(1-\delta_S))}{(M_K^2 + 2M_\pi^2)}$$

$$L_2 \;=\; \frac{F_K F_\pi^2}{4\sqrt{2}M_K}\frac{(s_F-2M_\pi^2)(\overline{S_{NLO}}-S_{exp}(1-\delta_S))-(\overline{F_{NLO}}-F_{exp}(1-\delta_F))}{(M_K^2+2M_\pi^2)}\,. \tag{5.24}$$

This last result constitutes a second possibility how to parametrize L_1 and L_2 in terms of physical observables, X, Z, r and higher order remainders.

5.3 Values of low energy constants

Goal of this section is to present results on values of the low energy constants; their values are obtained from formulae (5.10), (5.16) and (5.24). In this section we do not investigate influence of the higher order remainders δ_W on the result therefore we now for a while set all higher order remainders equal to zero. With this choice, L_1 – L_3 depend only on experimental input and values of X, Z, r.

The experimental values we used in place of $F_{exp}, G_{exp}, S_{exp}$ were already partly discussed in the third chapter. There we expanded the formfactors into partial waves (3.35) and parametrized partial waves in the expansion as a series (3.36).

Numerical values of the coefficients in (3.36) are taken from the measurements of the experiment NA48/2 on decays $K^\pm \to \pi^+\pi^- e^\pm \nu$ [8]:

Coefficient	Value
f_s	5.705 ± 0.035
f_s'	0.867 ± 0.050
f_s''	-0.416 ± 0.053
f_e'	0.388 ± 0.053
g_p	4.952 ± 0.086
g_p'	0.508 ± 0.122

Table 5: Coefficient parametrizing the formfactors

Experimental values of phase shifts we used come from the E865 measurement [32]. More specific details about the parametrization can be found in Appendix E. Figure 4 on the next page displays s-dependence of real parts of F and G for $\cos\theta = q^2 = 0$.

When we specified experimental values of formfactors and neglected remainders, the low energy constants L_1 – L_3 depend through (5.10), (5.16) and (5.24) on only three parameters X, Z, r . Following table summarizes some representative values we found in the literature. For easier further reference we labeled each set of X, Z, r; labels D and E stand for respective central values.

Label	Source	X	Z	r
A	Standard $O(p^2)$ χPT	1	1	25.9
B	From $O(p^4)$ L_i [35]	0.902	0.865	25.2
C	From $O(p^6)$ L_i [35]	0.726	0.734	25.9
D	Lattice calculations [33] (PACS - CS)	0.59 ± 0.21	0.66 ± 0.09	26.5 ± 2.3
E	Lattice calculations [33] (RBC/UKQCD)	0.20 ± 0.14	0.46 ± 0.04	23.2 ± 1.5

Table 6: Representative values of X, Z, r from the literature

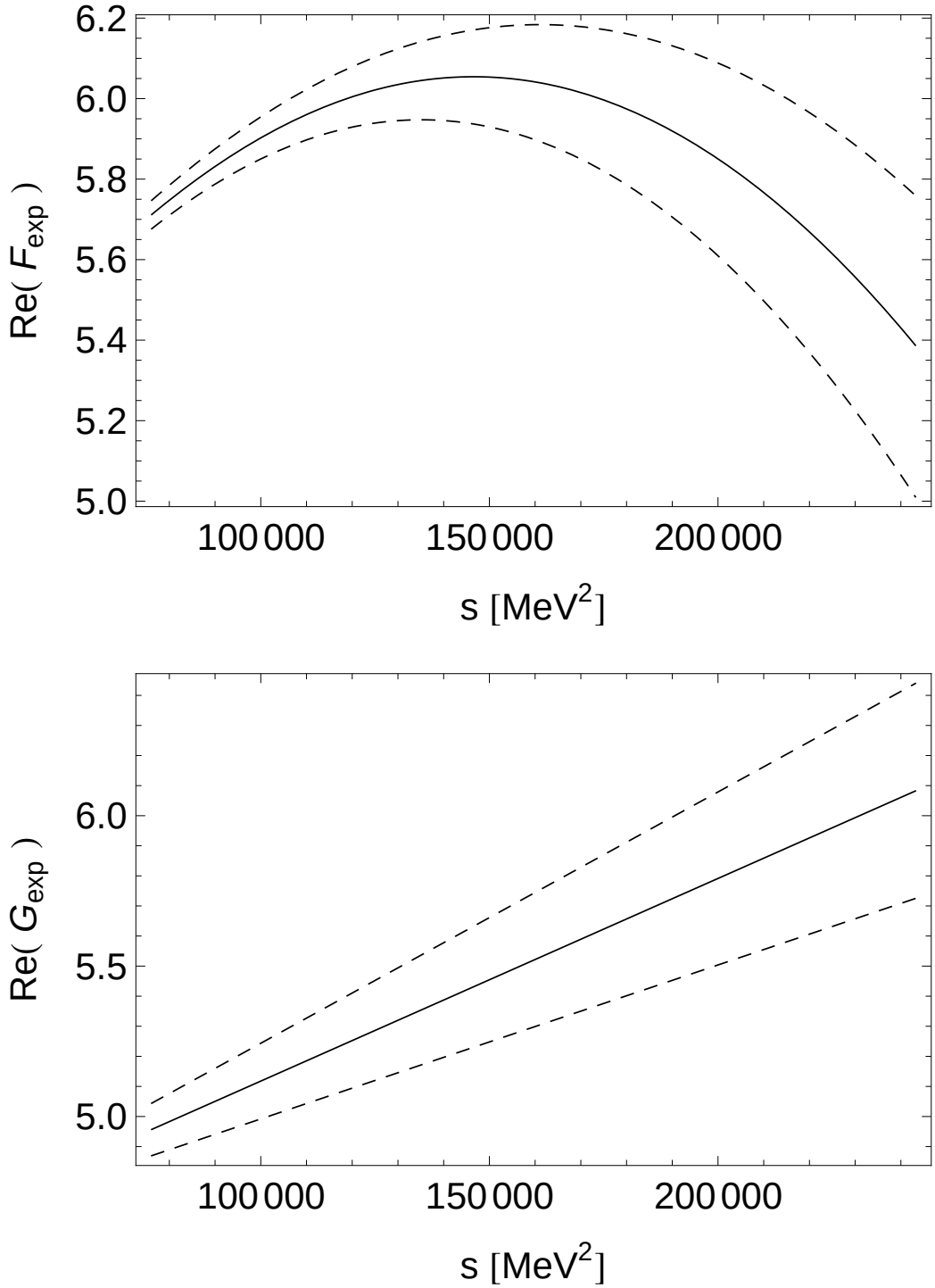

Figure 4: Real parts of experimental values of formfactors F, G for $\cos\theta = 0$, $q^2 = 0$. The formfactors are parametrized according to (3.35) and (3.36). Values of used coefficients of the partial wave expansion are listed in Table 5; values of phase shifts are taken from [32]. Dashed lines represent the experimental error.

The standard $O(p^2)$ χPT gives $X, Z = 1$; for ratio of quark masses we used LO expression (2.47). Values from the article [35] were obtained by inversions of formulae from Appendix C - instead of reparametrization of low energy constants L_i in terms of X, Z, r it is possible to start with values of L_i fitted in the framework of the standard χPT and calculate X, Z, r from these as a first approximation. Authors of [35] used two experimental sets of low energy constants (one obtained

from $O(p^4)$ fit and one obtained from $O(p^6)$ fit), therefore we quote two values from a single article. Finally the last two values come from lattice simulations of QCD[4].

If we now take these values and plug them into (5.10) and (5.16), we get for the choice $s_A = 4M_\pi^2$, $s_B = M_K^2$[5], $s_G = 4M_\pi^2$ following values of low energy constants[6]

Set of X, Z, r	$10^3\, L_1$	$10^3\, L_2$	$10^3\, L_3$
A	0.16	2.56	-4.37
B	0.19	2.48	-4.38
C	0.19	2.41	-4.35
D	0.18	2.37	-4.28
E	0.06	2.12	-3.75

Table 7: Values of L_1 – L_3 obtained using the first strategy (with no remainders)

As the experimental input we took corresponding central values. Values of masses and decay constants we used are summarized in Appendix D.

Similarly in the second strategy for obtaining low energy constants (5.16), we for the choice $s_F = s_S = s_G = 4M_\pi^2$ get

Set of X, Z, r	$10^3\, L_1$	$10^3\, L_2$	$10^3\, L_3$
A	1.04	2.14	-4.37
B	1.07	2.06	-4.38
C	1.07	2.00	-4.35
D	1.05	1.96	-4.28
E	0.89	1.73	-3.75

Table 8: Values of L_1 – L_3 obtained using the second strategy (with no remainders)

In both cases we see that the results on the low energy constants within each table are not very different except for the last set of X, Z, r where we can see some deviations caused by the small values of X, Z. By comparing the two tables we see that each gives rather different prediction on L_1, L_2. As we show in the next section, the difference can be explained in a satisfactory manner after taking into account the presence of the higher order remainders δ_W.

We will draw dependence of L_1 – L_3 on X, Z and r in the following section after we present an estimate on the theoretical error caused by the presence of higher order remainders δ_W.

5.4 Theoretical error from δ_W

As a first guess on the size of the remainders of quantities calculated at NLO we expect (2.83)

$$\delta_W \sim 0.1 \ . \tag{5.25}$$

[4]These values were already mentioned in the section on RχPT.

[5]There are indications ([9]) that the chiral series does not converge well for large values of s. More on this can be found in following sections.

[6]To remind - we took real parts of experimental values and theoretical predictions.

However, the derivative of the F formfactor dF/ds is at LO equal to zero and starts its chiral expansion at NLO[7]. Therefore for this quantity we expect remainder δ_S of higher value

$$\delta_S \sim \frac{M_K^2}{\Lambda_H^2} \sim 0.3 \ . \tag{5.26}$$

To get an estimate on errors of $L_1 - L_3$ we can treat the remainders as normal-distributed random numbers with standard deviation equal to 0.3 for dF/ds and to 0.1 in other cases. In all cases the distributions must be centered at zero as we have no hint about the sign of the remainders. Because we have no particular information about the remainders, we consider them to be mutually independent.

The errors on $L_1 - L_3$ can be then obtained by purely algebraic combination of errors introduced by various remainders[8] added in quadrature. An alternative way is to use Monte Carlo method. In this case we generate random values of the remainders and plug these into the formulae (5.10) and (5.16) or (5.24). With this approach we generate large number of sets of $L_1 - L_3$, corresponding to various values of the remainders. The sought-after estimate on the error of L_1 can be then calculated as a standard deviation of the set of generated values of L_1; the other two low energy constants can be taken care of in the same way.

Because of the resummed approach, the low energy constants $L_1 - L_3$ depend on the remainders linearly. The proportionality constants depend on r but are independent of X and Z. As the r-dependence of the error of the low energy constants ΔL_i caused by the existence of remainders is very weak, we quote here the values of this error for standard LO value $r = 25.9$ for both strategies how to obtain low energy constants.

Way how to obtain $L_1 - L_3$	$10^3 \Delta L_1$	$10^3 \Delta L_2$	$10^3 \Delta L_3$
First strategy ((5.16))	0.80	1.18	2.38
Second strategy ((5.24))	0.64	1.08	2.38

Table 9: Errors of L_i

These errors change by less then 0.5% when we calculate them for $r = 22$ instead of $r = 25.9$; r-dependence of the errors ΔL_i is therefore really negligible.

High values of errors on low energy constants $L_1 - L_3$ confirm our previous assertion that data in Tables 7 and 8 are compatible within the margin of error. Because the second strategy of determining L_1 and L_2 seems to be less affected by the error from the remainders and because of the aforementioned potential problems with χPT at high values of s, in the rest of the text we use exclusively the second strategy of obtaining $L_1 - L_2$.

So far we did not discuss experimental errors and we do it now. From Table 5 we can read off that the errors of the experimental values of the formfactor F and its derivative at threshold are roughly 1% and 6%. We may consider these values as additional sources of uncertainties expressed through the remainders δ_F and δ_S. If we add the experimental errors in quadrature with our previous estimates 10% and 30%, we arrive at values 10.05% and 30.6%. This increase is rather small; therefore we will stick to our previous estimates of 10 and 30%.

[7] To LO is F constant, see (3.30).

[8] In our case there are in total five remainders — $\delta_{F_\pi}, \delta_{F_K}, \delta_G$ and either δ_A, δ_B or δ_F, δ_S.

When we calculate relative error on experimental value of F at M_K^2 (F_B), we find out that the relative experimental uncertainty is about 6%. This value increases our estimate on δ_B to 12%, after adding the two errors in quadrature. This constitutes another argument on why we should be using second strategy to obtain values of L_1 and L_2.

When we now have an estimate on errors, we can plot dependence of the low energy constants on unknown values of X, Z and r — the results are displayed in Figures 5, 6 and 7. As the "standard" combination we took values obtained from PACS - CS lattice calculations [33]

$$X^{std} = 0.59, Z^{std} = 0.66, r^{std} = 26.5 \tag{5.27}$$

and each graph draws dependence on one of the parameters. The investigated ranges are

$$\begin{aligned} 0 \leq &\quad X &&\leq 1 \\ 0.2 \leq &\quad Z &&\leq 1.2 \\ 14 \leq &\quad r &&\leq 35\ . \end{aligned} \tag{5.28}$$

The solid line on each graph shows theoretical prediction on the value of the low energy constant with zero higher order remainders; dotted lines represent boundaries of errors arising from direct and indirect remainders.

We see that dependence on X, Z, r is noticeable, however it is smaller than error caused by the unknown higher order remainders (except for very low values of Z). To get a better feeling for how much each component contributes to the final error, we successively set all remainders but one equal to zero and calculated error coming from the only nonzero remainder[9]. Moreover, to find out influence of unknown values of X, Z, r we investigated how much values of L_i change if we replace the standard values $X^{std}, Z^{std}, r^{std}$ one after another with $X^{new} = 0.8$, $Z^{new} = 0.75$ or $r^{new} = 28.8$[10]. These are values of X, Z, r at the endpoints of the intervals suggested for X, Z, r by the article [33] (see Table 6). In this latter case we took as an error on the low energy constant

$$\left| L_i(X^{new}, Z^{std}, r^{std}) - L_i(X^{std}, Z^{std}, r^{std}) \right| \tag{5.29}$$

and so on. Our findings are summarized in the Table 10 and graphically depicted in the Figure 8.

Situation	$10^3\,\Delta L_1$	$10^3\,\Delta L_2$	$10^3\,\Delta L_3$
$\delta_{F_\pi} = 0.1$	0.19	0.54	1.03
$\delta_{F_K} = 0.1$	0.09	0.38	0.61
$\delta_F = 0.1$	0.17	0.67	0.00
$\delta_G = 0.1$	0.52	0.52	2.07
$\delta_S = 0.3$	0.27	0.13	0.00
$X^{new} = 0.8$	0.14	0.02	0.34
$Z^{new} = 0.75$	0.06	0.04	0.11
$r^{new} = 28.8$	0.02	0.04	0.10

Table 10: Sources of ΔL_i

[9]The standard deviations of the nonzero remainders were kept at value 0.1 or 0.3, depending on which remainder it was.

[10]Each time we change only one of X, Z, r.

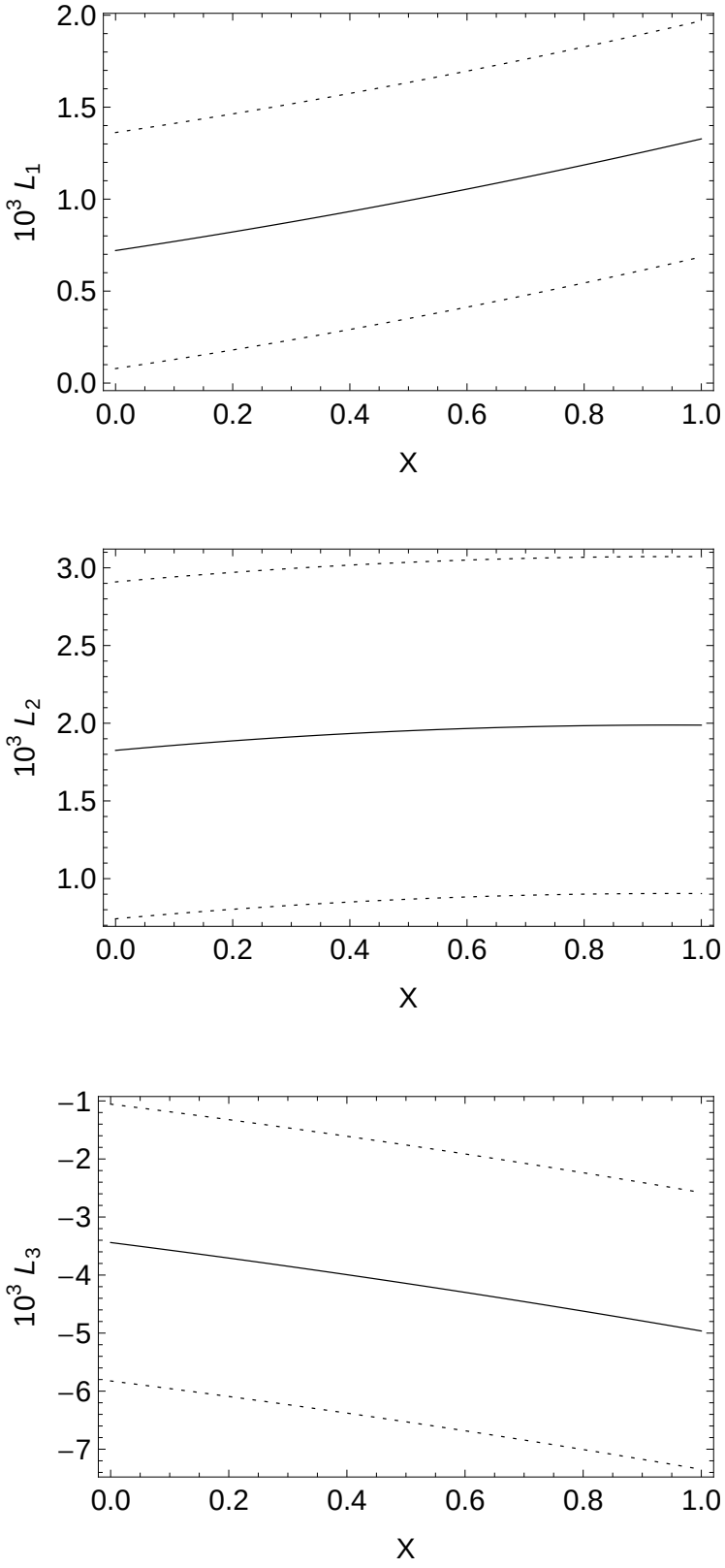

Figure 5: Dependence of L_1 – L_3 on unknown value of X. Constants L_1 – L_3 were determined from the experimental data by means of the formulae (5.10) and (5.24). Each graph is plotted for $Z = 0.66$ and $r = 26.5$. Dotted lines represent errors of L_1 – L_3 arising from higher order remainders. The remainder δ_S was assumed to be 30% and all other remainders $\delta_F, \delta_G, \delta_{F_\pi}, \delta_{F_K}$ were assumed to be 10%. The errors induced by the remainders were added in quadrature.

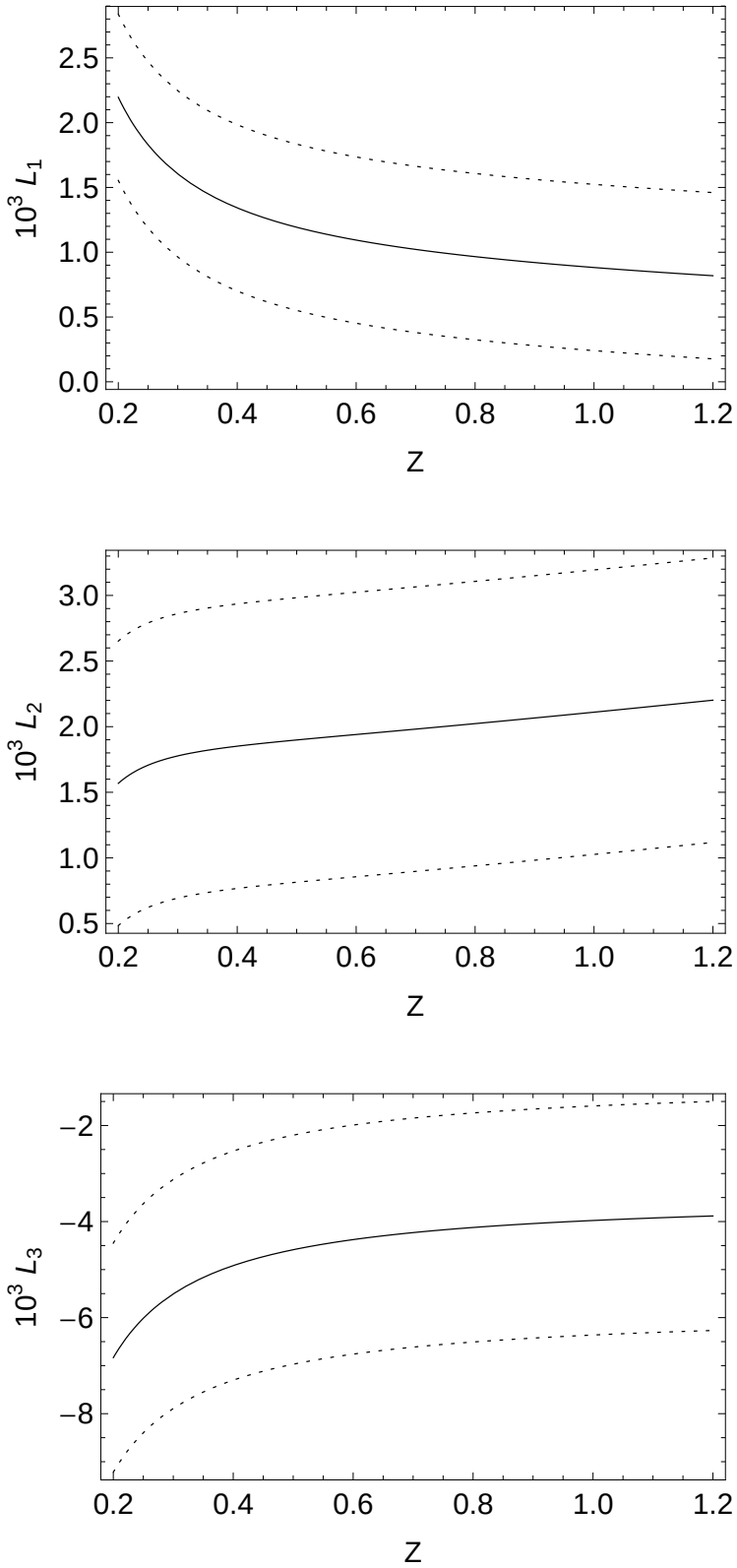

Figure 6: Dependence of L_1 – L_3 on unknown value of Z. Constants L_1 – L_3 were determined from the experimental data by means of the formulae (5.10) and (5.24). Each graph is plotted for $X = 0.59$ and $r = 26.5$. Dotted lines represent errors of L_1 – L_3 arising from higher order remainders. The remainder δ_S was assumed to be 30% and all other remainders $\delta_F, \delta_G, \delta_{F_\pi}, \delta_{F_K}$ were assumed to be 10%. The errors induced by the remainders were added in quadrature.

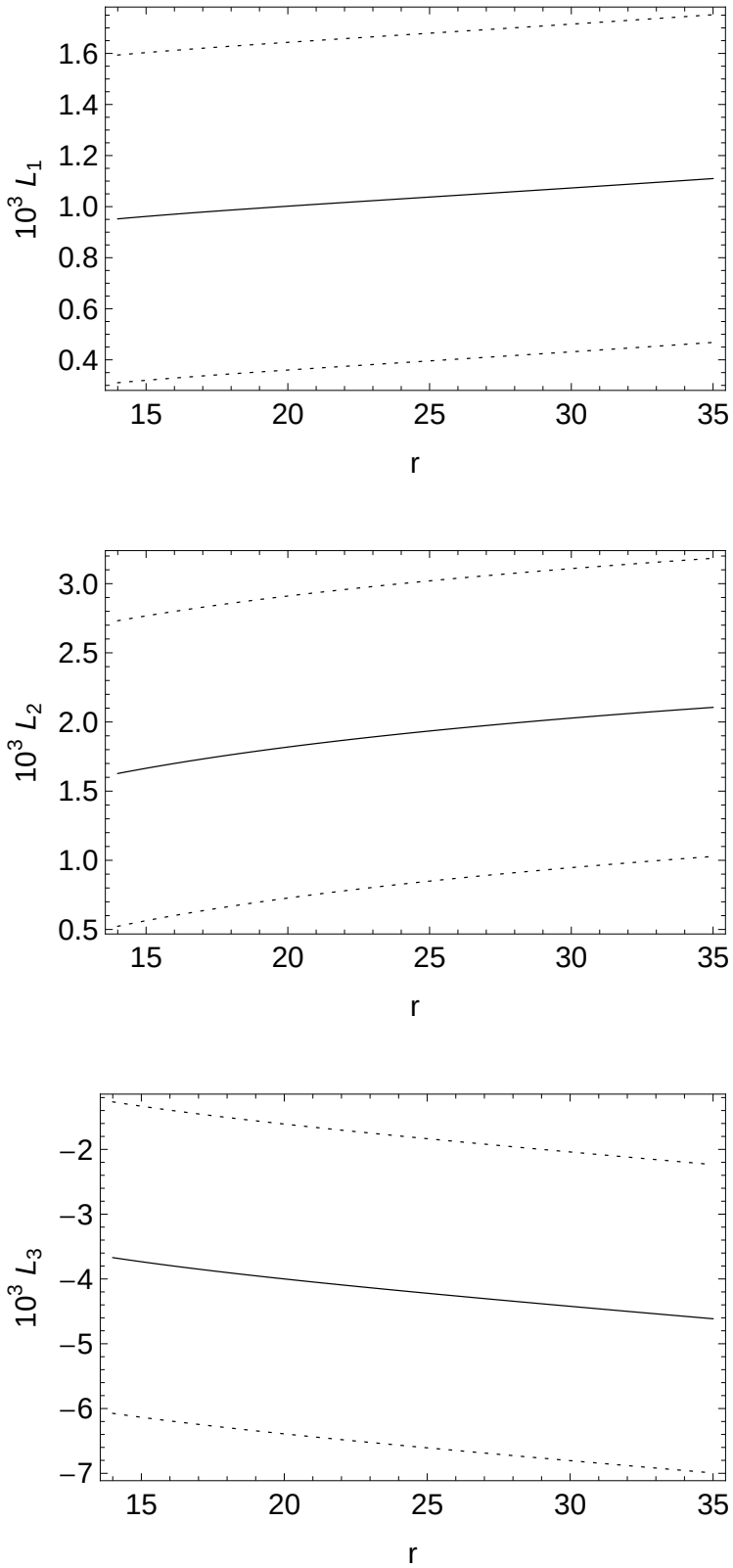

Figure 7: Dependence of L_1 – L_3 on unknown value of r. Constants L_1 – L_3 were determined from the experimental data by means of the formulae (5.10) and (5.24). Each graph is plotted for $X = 0.59$ and $Z = 0.66$. Dotted lines represent errors of L_1 – L_3 arising from higher order remainders. The remainder δ_S was assumed to be 30% and all other remainders $\delta_F, \delta_G, \delta_{F_\pi}, \delta_{F_K}$ were assumed to be 10%. The errors induced by the remainders were added in quadrature.

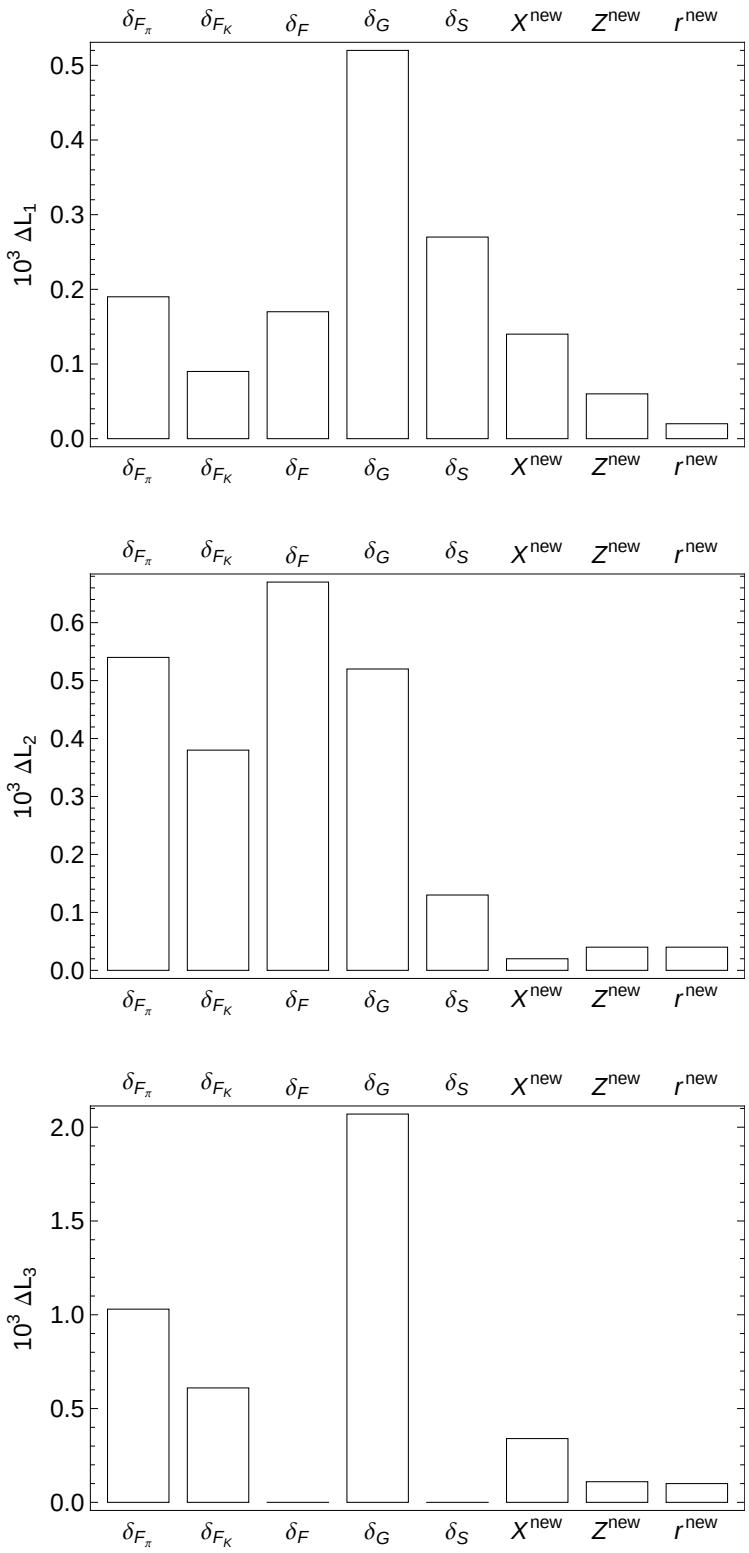

Figure 8: Graphical depiction of how much direct and indirect remainders and unknown values of X, Z, r contribute to theoretical error on low energy constants L_1 – L_3 obtained from (5.10) and (5.16). To calculate uncertainties of the remainders, we took successively δ_S equal to 0.3 / other remainders equal to 0.1 and surveyed how values of L_1 – L_3 change under effect of each of the remainders. To probe effect of various X, Z, r we started with $X = 0.59, Z = 0.66, r = 26.5$ and changed in turn X to 0.8, Z to 0.75 and r to 28.8 and again noted induced change in L_1 – L_3.

On the basis of values given in the Table 10 we can claim that dependence of the low energy constants L_1 – L_3 on X, Z and r is indeed very small[11]. This on one side shows that knowledge of precise values of X, Z, r is not very important to obtain values of these low energy constants; on the other hand it is caused by the fact that error introduced by the remainders is rather big.

5.5 Quadratic remainders

In this section we want to compare our full theoretical prediction on the formfactors with the experimental values and decide if we come to similar conclusions as authors of [29] which observed unsatisfactory convergence for large s.

We took $X^{std}, Z^{std}, r^{std}$ corresponding to set D and fixed their values throughout this comparison. Then we parametrized the direct higher order remainders as polynomials[12]

$$\begin{aligned} \Delta_F(s) &= F_{th}(s)\,\delta_F(s) = c_0 + c_1(s-4M_\pi^2) + c_2(s-4M_\pi^2)^2 \\ \Delta_G(s) &= G_{th}(s)\,\delta_G(s) = d_0 + d_1(s-4M_\pi^2) + d_2(s-4M_\pi^2)^2\ , \end{aligned} \tag{5.30}$$

where magnitudes of the parameters c_i, d_i can be estimated by the dimensional analysis as

$$\begin{aligned} c_0, d_0 &\sim \frac{M_K}{\sqrt{2}F_\pi}\frac{M_K^4}{\Lambda_H^4} = 0.23 \\ c_1, d_1 &\sim \frac{M_K}{\sqrt{2}F_\pi}\frac{M_K^2}{\Lambda_H^4} = 9.3\cdot 10^{-7}\,\mathrm{MeV}^{-2} \\ c_2, d_2 &\sim \frac{M_K}{\sqrt{2}F_\pi}\frac{1}{\Lambda_H^4} = 3.8\cdot 10^{-12}\,\mathrm{MeV}^{-4}\ . \end{aligned} \tag{5.31}$$

In these formulae we estimated F_{th}, G_{th} by theoretical values of the formfactors F, G to LO within the standard χPT (3.30). We neglected remainders of orders higher than quadratic in s, which turns out to be a reliable description as experimental data are described by a quadratic function (3.36) and our NLO results are for any values of low energy constants also very well described by a quadratic polynomial.

These parameters are related to the indirect remainders $\delta_F, \delta_G, \delta_S$ used before through relations

$$\begin{aligned} c_0 &= F_{exp}\Big|_{s=4M_\pi^2}\delta_F \\ d_0 &= G_{exp}\Big|_{s=4M_\pi^2}\delta_G \\ c_1 &= S_{exp}\Big|_{s=4M_\pi^2}\delta_S\ . \end{aligned} \tag{5.32}$$

[11] We checked that decreasing values of X, Z, r in the range set by the set D from Table 6 instead of increasing them leads to similar conclusions.

[12] We found this idea in [34]. It should not surprise the reader that the remainders depend on s as their size is affected by the value of s at which we compare NLO calculations with the experiment.

In all these relations real parts of experimental values are taken, as argued above. Because of relations (5.32) our full theoretical predictions

$$\begin{aligned} F_{th}(s) &= F_{NLO}(s) + \Delta_F(s) \\ G_{th}(s) &= G_{NLO}(s) + \Delta_G(s) \end{aligned} \tag{5.33}$$

depend only on two remainders $\delta_{F_\pi}, \delta_{F_K}$ and six constants c_0, c_1, c_2, d_0, d_1 and d_2[13].

It can be easily checked explicitly that the full theoretical prediction on formfactor F depends only on value of c_2, which follows directly from the technique we used in reparametrizing L_1 and L_2. With this in mind we can now plot the full theoretical prediction on F and compare it with the experimental data; the result is plotted in the Figure 9. The solid line corresponds to $c_2 = 0$, gray area is bounded by theoretical predictions for $c_2 = \pm 3.8 \cdot 10^{-12}\,\mathrm{MeV}^{-4}$ which is the value suggested by the dimensional analysis (5.31).

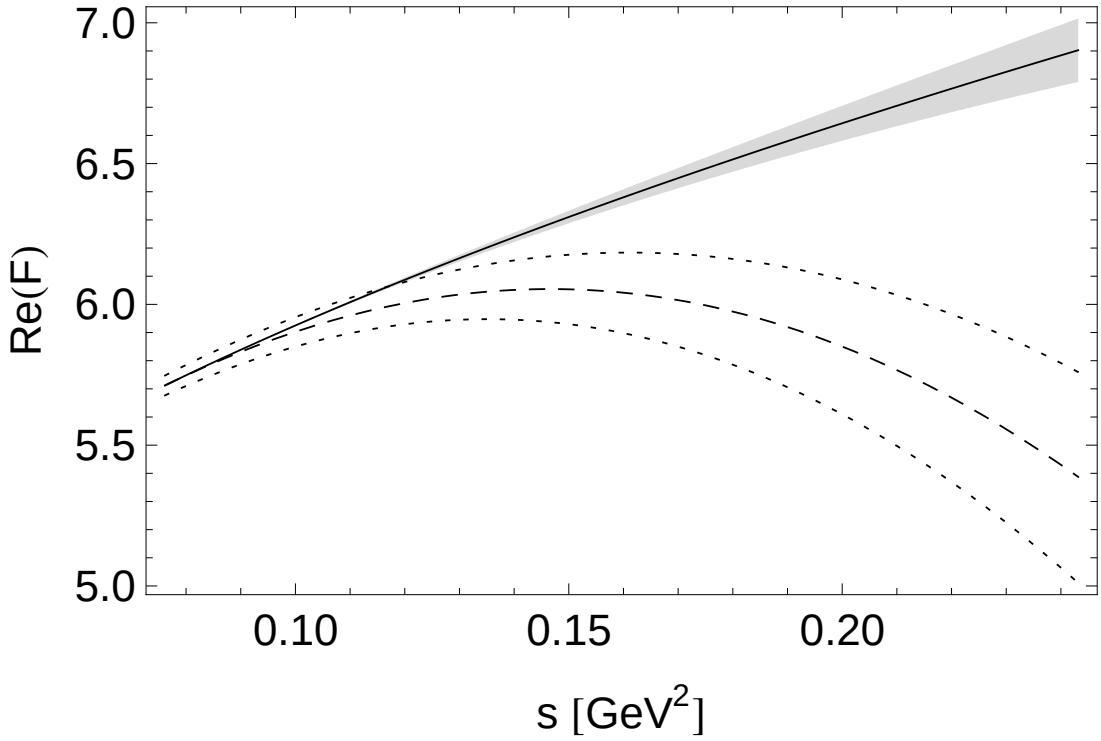

Figure 9: Comparison of our full theoretical prediction of real part of the formfactor F with experimental values for $\cos\theta = q^2 = 0$. Theoretical prediction is calculated as NLO contribution plus higher order remainders[14] (5.33). We took $X = 0.59, Z = 0.66$ and $r = 26.5$ and reparametrized values of low energy constants L_1 – L_3 (5.10), (5.24). Higher order remainders were rewritten using (5.32) (see text for further information). The full line corresponds to $c_2 = 0$, gray strip is bounded by theoretical predictions for $c_2 = \pm 3.8 \cdot 10^{-12}\,\mathrm{MeV}^{-4}$. The experimental values are parametrized according to (3.35) and (3.36). Values of used coefficients of the partial wave expansion are listed in Table 5; values of phase shifts are taken from [32]. Dashed lines represent experimental data, dotted lines their errors.

[13]It is understood that in (5.33) all L_1 – L_3 were replaced according to formulae (5.10) and (5.24)

[14]We stress out that this picture includes higher order remainders and thus says nothing about the overall convergence of our NLO predictions.

Full formfactor G_{th} (5.33) depends on five variables $\delta_{F_\pi}, \delta_{F_K}, d_0, d_1, d_2$. To plot error of our theoretical prediction, we estimated sizes of δ_{F_π} and δ_{F_K} as 10% and took values of d_i from (5.31). We added all these effects in quadrature and we got the result drawn of Figure 10.

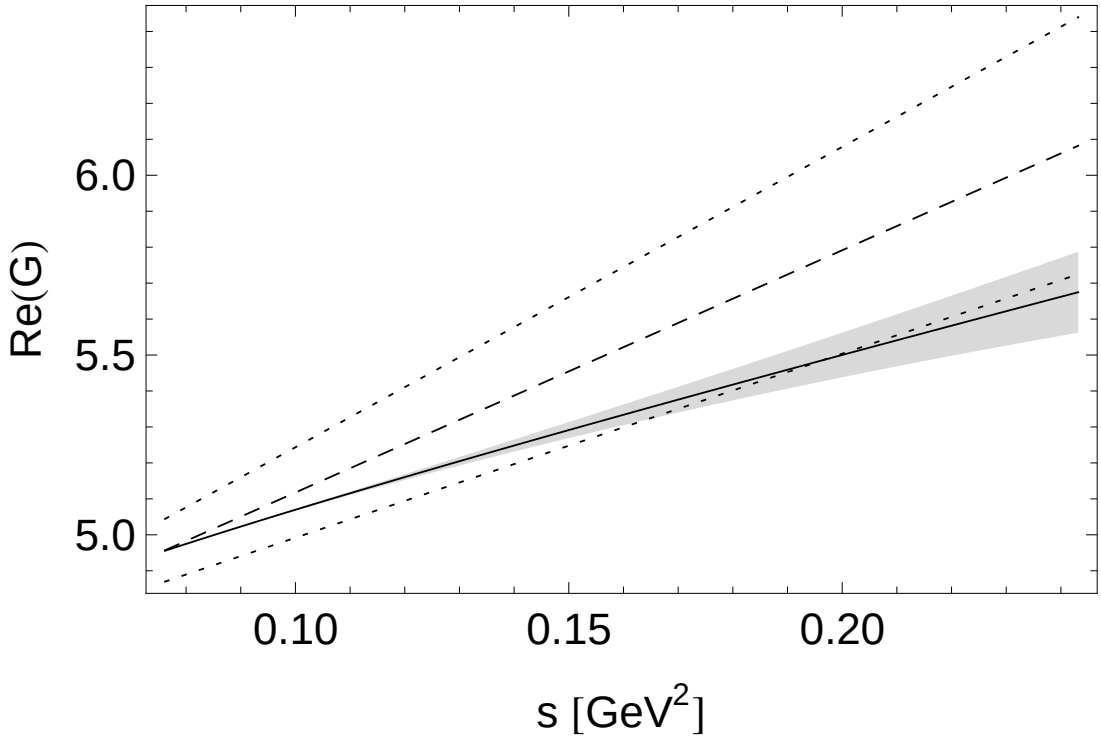

Figure 10: Comparison of our theoretical prediction of real part of the formfactor G with experimental values for $\cos\theta = q^2 = 0$. Theoretical prediction is calculated as NLO contribution plus higher order remainders[15] (5.33). We took $X = 0.59, Z = 0.66$ and $r = 26.5$ and reparametrized values of low energy constants L_1 – L_3 (5.10), (5.24). Higher order remainders were rewritten using (5.32). The full line corresponds to $\delta_{F_\pi} = \delta_{F_K} = d_0 = d_1 = d_2 = 0$, gray strip is bounded by theoretical predictions with $\delta_{F_\pi} = \delta_{F_K} = 0.1$ and d_i according to (5.31) added in quadrature. The experimental values are parametrized according to (3.35) and (3.36). Values of used coefficients of the partial wave expansion are listed in Table 5; values of phase shifts are taken from [32]. Dashed lines represent experimental data, dotted lines their errors.

We see that our prediction on formfactor G agrees with the experimental data rather well. For the F formfactor, the situation is different. Because of our technique of reparametrization of L_1 and L_2, the prediction fits experimental data around the threshold. However, for growing s we can see ever increasing discrepancy which for the largest values of s reaches 30%. From this chapter we know that this discrepancy can be soothed only by quadratic term[16] in the expansion of the higher order remainder (5.30).

From the experimental data we are able to "determine" the value of c_2. It

[15] We stress out that this picture includes higher order remainders and thus says nothing about the overall convergence of our NLO predictions.

[16] Or possibly higher terms which we assume small.

suffices to take the function

$$F_{exp} - F_{NLO} \tag{5.34}$$

which corresponds to $F_{exp}\,\delta_F$ and fit it with the quadratic function (5.30). The result after resummation of L_1 – L_3 does not depend on $c_0, c_1, \delta_{F_\pi}, \delta_{F_K}$ because these contribute only to constant terms and the terms linear in s. For values $X = 0.59, Z = 0.66, r = 26.5$ we get $c_2 = 6.05 \cdot 10^{-11}\,\mathrm{MeV}^{-4}$, for other sets from Table 6 we get values of c_2 within three percent of this result. If we include error on the experimental data, we get an estimate

$$10^{11} c_2 \in (5.2, 7.0)\,\mathrm{MeV}^{-4}\ . \tag{5.35}$$

Clearly, our estimate based on dimensional analysis was far from being correct. With respect to overall size of the higher order remainders ($F_{exp}\,\delta_F$) there are two possible scenarios. It is possible that large contribution of the quadratic part of the remainder $c_2(s - 4M_\pi^2)^2$ is compensated by contributions of the constant and linear part in (5.30) to give a small overall value of δ_F in accordance with our expectations. For example for $c_0 = -0.2$, $c_1 = -7 \cdot 10^{-6}\,\mathrm{MeV}^{-2}$ we get relative error δ_F smaller than seven percent in the whole allowed kinematical range.

However, we incline to believe that the problem of unsatisfactory matching between theory and experiment is caused by poor convergence of the chiral series for large s.

One of the arguments for this assertion is based on the standard $O(p^6)$ calculations of the formfactor F. If we take NNLO expressions for the formfactor [29] and use values of the low energy constants L_i from the newest fit [9], we obtain theoretical result which is compared to experimental values on Figure 11.

We see that NNLO expression has similar problems to describe the F formfactor truthfully, despite we would expect errors further suppressed by another factor of $M_K^2/\Lambda_H^2 \sim 0.3$. If we used low energy constants L_i corresponding to[17] $X = 0.59, Z = 0.66$ and $r = 26.5$, the discrepancy between (standard) χPT with our values of low energy constants and the experiment is even larger. Because the higher order remainder is not saturated even at NNLO it thus seems likely that the chiral series of the RχPT does not converge well around $s = M_K^2$.

Second argument suggesting poor convergence of the chiral series is the problems with explaining large curvature of the experimental data. Instead of performing fit of $F_{exp} - F_{NLO}$ with quadratic polynomial it is equally possible to expand our theoretical prediction into the Legendre polynomials on the allowed kinematical range $(4M_\pi^2, M_K^2)$

$$F_{th}(s) = \alpha_{0,th} P_0\left(\frac{s - s_1}{s_2}\right) + \alpha_{1,th} P_1\left(\frac{s - s_1}{s_2}\right) + \alpha_{2,th} P_2\left(\frac{s - s_1}{s_2}\right) \tag{5.36}$$

with

$$\begin{aligned} s_1 &= \frac{M_K^2 + 4M_\pi^2}{2} \\ s_2 &= \frac{M_K^2 - 4M_\pi^2}{2}\ . \end{aligned} \tag{5.37}$$

[17] Constants L_1 – L_3 are determined through calculations above, L_4 – L_9 using formulae from Appendix C.

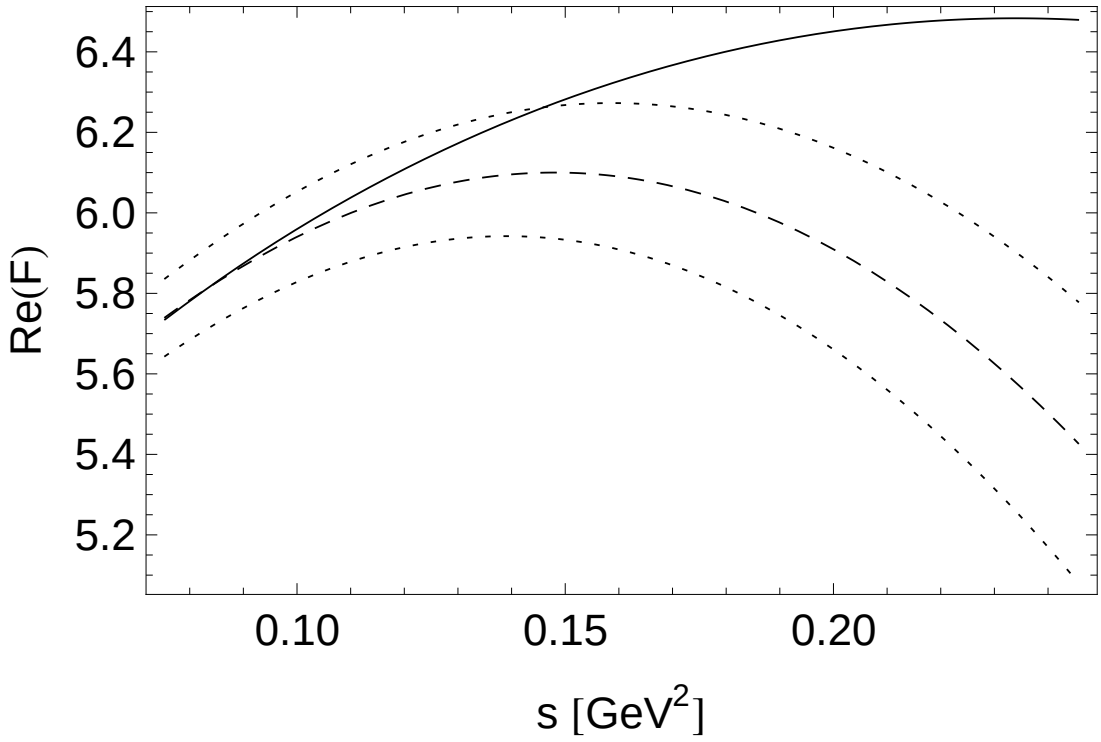

Figure 11: Comparison of NNLO theoretical prediction [29] of real part of the formfactor F with experimental values. The curve of theoretical prediction was plotted for the values of the low energy constants L_i according to [9]; we set $\cos\theta = q^2 = 0$. The experimental values are parametrized according to (3.35) and (3.36). Values of used coefficients of the partial wave expansion are listed in Table 5; values of phase shifts are taken from [32]. Dashed lines represent experimental values, dotted lines error of the experimental data.

In the expansion above we neglected higher terms as both experimental data and our NLO theoretical predictions are well described by quadratic polynomials for any values of low energy constants. Each of the constants $\alpha_{i,th}$ can be in an obvious way written as a sum of contributions from LO $\alpha_{i,th}^{LO}$, NLO $\alpha_{i,th}^{NLO}$ and similarly for higher orders. The coefficients $\alpha_{i,th}$ can be obtained from F through linear operation (projection on P_i) and we thus expect their good convergence in RχPT.

When we calculate contributions to $\alpha_{2,th}$ from leading and next-to-leading order by projections of respective theoretical formulae on P_2 we get[18]

$$\begin{aligned} \alpha_{i,th}^{LO} &= 0 \\ \alpha_{2,th}^{NLO} &= -8.84\ . \end{aligned} \tag{5.38}$$

We performed calculations for $X = 0.59, Z = 0.66, r = 26.5$; value of $\alpha_{2,th}^{NLO}$ does not depend on precise values of X, Z, r much and precise values of X, Z, r are therefore irrelevant for our purpose.

In comparison, value of the coefficient $\beta_{2,exp}$ of the respective expansion of the

[18]Because values of L_i affect only terms that are linear and constant in s, the value of $\alpha_{2,th}^{NLO}$ is independent of L_i.

experimental result

$$F_{exp}(s) = \beta_{0,exp} P_0\left(\frac{s-s_1}{s_2}\right) + \beta_{1,exp} P_1\left(\frac{s-s_1}{s_2}\right) + \beta_{2,exp} P_2\left(\frac{s-s_1}{s_2}\right) \quad (5.39)$$

can be obtained from experimental data as

$$\beta_{2,exp} \;=\; -63.04\ . \quad (5.40)$$

We can see that our assumption about good convergence is very severely violated, as our theoretical prediction $\alpha_{2,th}^{NLO}$ is far away from the corresponding experimental value $\beta_{2,exp}$.

These convergence problems seem to have natural explanation in the presence of the Sigma resonance ($f_0(500)$) with mass[19] [46]

$$M_\sigma = ((441 \pm 4) - i(272 \pm 6))\ \text{MeV} \quad (5.41)$$

close to the mass of the kaon. Because of this, K_{l4} decays with large s can have nontrivial contribution from processes with exchange of the σ, which could lead to significant contributions to F and G.

Recently, Soto, Talavera and Tarrús [47] came with an improvement of two-flavor χPT which includes σ as a dynamical degree of freedom. The improvement — called χPT_S — lies in representing σ by a singlet field S. It is counted as a quantity of order $O(p)$ and its mass is also considered $M_\sigma \sim O(p)$. This counting is introduced to indicate that processes with an exchange of sigma are suppressed. Because of this counting, no loop graphs with sigma contribute to the calculated formfactors at NLO.

The symmetry of χPT then at NLO allows four additional Lagrangian terms containing sigma,

$$\mathcal{L}_\sigma = \left(F_0 c_{1d} S + c_{2d} S^2\right) \langle D_\mu U D^\mu U^\dagger \rangle + \left(F_0 c_{1m} S + c_{2m} S^2\right) \langle \chi^\dagger U + \chi U^\dagger \rangle\ . \quad (5.42)$$

The generalization of the approach to the case of $SU(3) \times SU(3)$ χPT is still missing in the literature and it would be beyond the scope of this thesis to do so here. Instead we simply mimic the method of [47] which necessarily brings about errors. Despite it we believe this procedure can shed some light on our problem of badly converging K_{l4} formfactors.

Following [47] we add an $SU(3) \times SU(3)$ singlet field[20] S into our theory and count it as a quantity of order $O(p)$. Its interactions with pseudo-Goldstone bosons of χPT are governed by the Lagrangian (5.42). This allows one additional Feynman diagram contribute to the K_{l4} decays, displayed in Figure 12.

This diagram then constitutes additional contribution to the coefficient $Z_{ab\beta}$ and thus to the values of formfactors (4.21). The calculation of the diagram is straightforward with the resulting contribution to the formfactor reading

$$F_\sigma = \frac{16\sqrt{2} F_0^2 M_K}{F_\pi^2 F_K} \frac{1}{s - M_\sigma^2} \left(c_{1d}^2 \left(M_\pi^2 - \frac{s}{2}\right) - c_{1d} c_{1m} \overset{\circ}{M}{}_\pi^2\right)\ . \quad (5.43)$$

[19] Value of $\sqrt{s}$ at the pole.

[20] In the full treatment, σ would be probably included as a member of an octet.

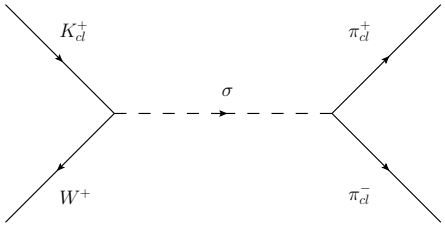

Figure 12: An extra Feynman diagram that contributes to formfactors F, G in the NLO calculations. This graph appears after addition of σ as an explicit degree of freedom into RχPT. Because in $\chi\mathrm{PT_S}$ each σ is counted as $O(p)$, only tree graphs with single sigma exchange can contribute in NLO.

For values of coupling constants $c_{1m,1d}$ we turn once again to the article [47]. There authors showed that chiral symmetry constraints value of c_{1m} at tree level to zero,

$$c_{1m} = 0 \ . \tag{5.44}$$

We will therefore neglect it which simplifies our result to

$$F_\sigma = \frac{16\sqrt{2}F_0^2 M_K}{F_\pi^2 F_K} \frac{c_{1d}^2}{s - M_\sigma^2} \left(M_\pi^2 - \frac{s}{2} \right) \ . \tag{5.45}$$

Through relating value of c_{1d} to the sigma decay width it is in the $SU(2) \times SU(2)$ $\chi\mathrm{PT_S}$ possible to show [47] that

$$c_{1d}^2 = 0.457 \, \frac{F_0^2}{F_\pi^2} = 0.457 \, Z \ . \tag{5.46}$$

Because we have no better estimate in hand, we use value of c_{1d} from (5.46).

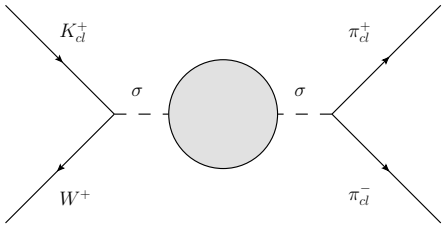

Figure 13: Taking M_σ as complex number — full experimental value on $\sqrt{s}$ at the pole — instead of only the real part corresponds to evaluating resummed Feynman diagram drawn on this figure instead of the diagram from Figure 12.

Before evaluating (5.45) we must specify also the value of M_σ we plugged in. We decided to take the full complex value (5.41), which physically corresponds to evaluating diagram in Figure 13 instead of the diagram from Figure 12. This assures that we do not encounter a singularity for any real s in the kinematic region under consideration, which would happen if we took only the real part of M_σ.

In this settings, we may add contribution F_σ to our previous result[21] F_{NLO}

[21] Note that in the full treatment including σ would lead to different values of constants L_i as can be seen for example from the misfit between theory and experiment on the threshold. Here we try to show that we are able to reproduce large curvature of F and thus neglect this effect.

and compare how well the sum agrees with experimental data. In Figure 14 we plot resulting comparisons for $X = 0.59, r = 26.5$ and $Z = 0.4, 0.5$ and 0.6.

From the figures we can nicely see that adding σ as an explicit degree of freedom enables us — for certain values of parameters — to find better agreement between theoretical investigations of K_{l4} decays and the relevant experiments. Specifically we are able to describe large curvature of F formfactor which seems to contradict predictions of the standard χPT or its resummed form. However, we must keep in mind that we did not perform an thorough investigation of the $\chi\mathrm{PT_S}$. We included σ as a singlet, approximated $c_{1d,1m}$ by their respective $SU(2) \times SU(2)$ $\chi\mathrm{PT_S}$ values and used only LO calculations with σ. Therefore, caution is in place and more investigations are necessary.

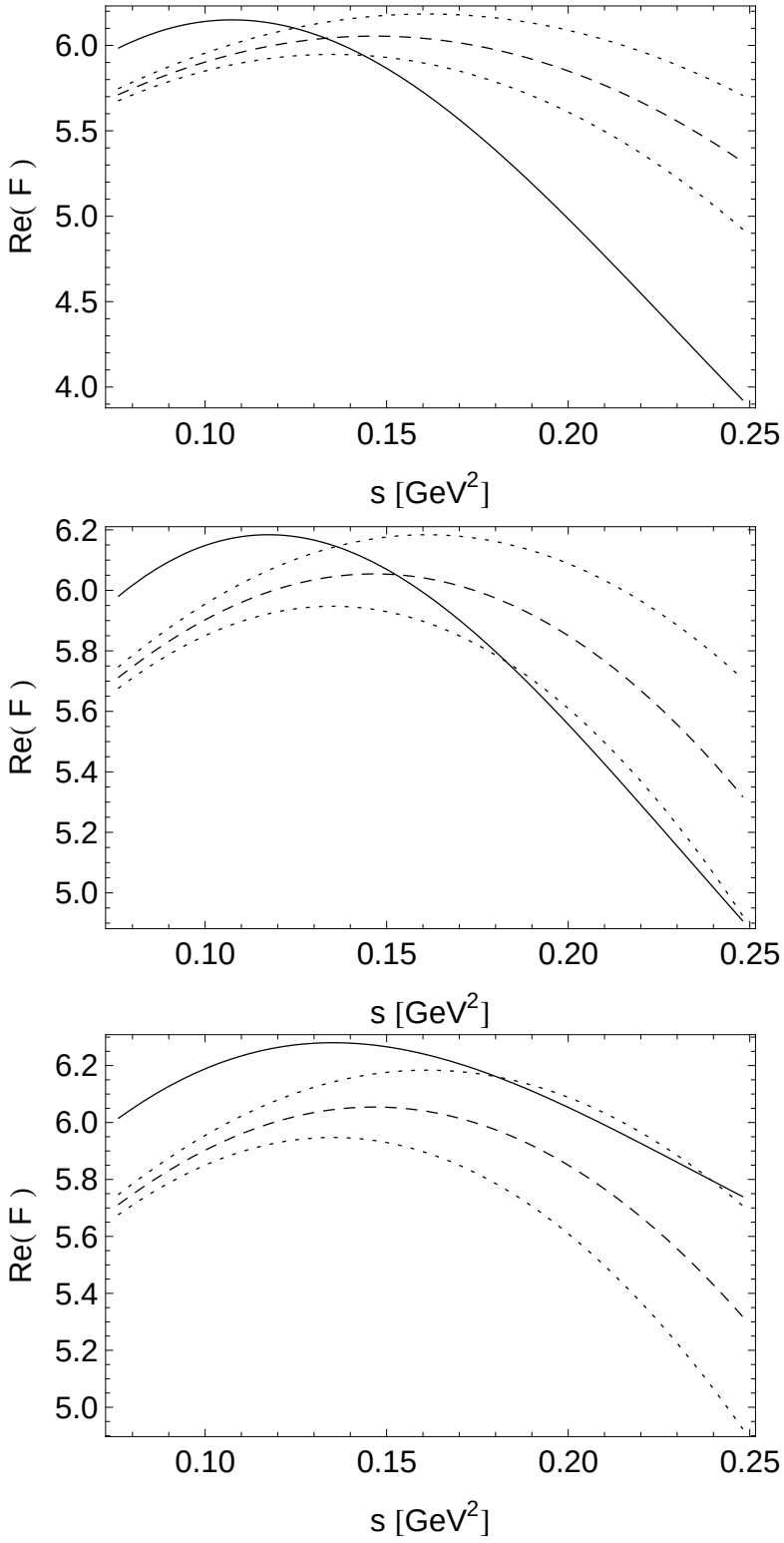

Figure 14: Comparison of theoretical predictions on real part of formfactor F with experimental values for $\cos\theta = q^2 = 0$. Theoretical predictions are calculated as sum of contribution of sigma exchange (5.43) and (4.49). Constants for sigma interactions were taken from $SU(2) \times SU(2)$ $\chi\mathrm{PT_S}$ (5.44), (5.46). Theoretical curves are drawn for $X = 0.59, r = 26.5$ and $Z = 0.6$ (upper figure), $Z = 0.5$ (middle figure) and $Z = 0.4$ (lower figure); as low energy constants we plugged in $L_1 = 1.05 \cdot 10^{-3}$, $L_2 = 1.96 \cdot 10^{-3}$, $L_3 = -4.28 \cdot 10^{-3}$. Dashed lines represent experimental values, dotted lines error of the experimental data.

Conclusion

In the first part of the thesis we introduced the reader into the problematic of effective field theories, Chiral Perturbation theory and semileptonic K_{l4} decays. Specific attention was given to emphasizing possibility of a scenario with suppressed chiral order parameters Σ, F and the Resummed Chiral Perturbation Theory — resummed formulation of χPT capable of correct manipulations with chiral series in this scenario — was discussed in detail.

Our first original result is the derivation of expressions for formfactors F, G of semileptonic kaon decay $K^+ \to \pi^+\pi^- l^+\nu_l$ in the RχPT. Our calculations were performed to order $O(p^4)$ and in the isospin limit. We employed so called background field method and reformulated it into a language of Feynman diagrams with explicitly distinguished "classical" and "quantum" fields, corresponding to external particles and quantum fluctuations. The method was for convenience rewritten into a form of a Mathematica notebook which can be used to calculate various tree and one-loop processes within RχPT. Explicit formulae for formfactors F, G are given and correctness of our calculation is checked by comparison with results of the standard χPT.

After that we present two strategies how to reparametrize low energy constants L_1 – L_3, which concludes the efforts to reparametrize all low energy constants L_i of RχPT in terms of physical observables, parameters X, Z, r and higher order remainders[22]. Several arguments lead us to favor second of the strategies, which uses value and derivative of F at threshold instead of value of F at two distinct points. With help of recent experimental data values of low energy constants are obtained for several sets of X, Z, r.

Starting with dimensional analysis, higher order remainders are estimated to be 30% for slope of the formfactor and 10% for other remainders. The errors on L_i induced by these remainders do not depend on X and Z and their r-dependence is only very small. Our final result on low energy constants L_1 – L_3 for used values of X, Z, r read[23]

Set of X, Z, r	$10^3\, L_1$	$10^3\, L_2$	$10^3\, L_3$
A	1.04 ± 0.64	2.14 ± 1.08	-4.37 ± 2.38
B	1.07 ± 0.64	2.06 ± 1.08	-4.38 ± 2.38
C	1.07 ± 0.64	2.00 ± 1.08	-4.35 ± 2.38
D	1.05 ± 0.64	1.96 ± 1.08	-4.28 ± 2.38
E	0.89 ± 0.64	1.73 ± 1.08	-3.75 ± 2.38

Table 11: Final values of L_1 – L_3

[22] Other low energy constants were reparametrized before, see Appendix C

[23] The sets of X, Z, r are defined in Table 6.

Unfortunately, the results are too imprecise to decide whether value of $2L_1 - L_2$ is suppressed according to Zweig rule or attains large nonzero value as authors of [9] found. We are however able to compare our findings with values from this article, which are

$$\begin{aligned} 10^3 L_1 &= 0.88 \pm 0.09 \\ 10^3 L_2 &= 0.61 \pm 0.20 \\ 10^3 L_3 &= -3.04 \pm 0.43 \ . \end{aligned} \tag{5.47}$$

We see that these L_1 and L_3 agree with our values within the margin of error, however the agreement for L_2 is not very good. One possible explanation of this is that higher order remainders are larger than expected; other eventuality is that scenario with suppressed order parameters of the spontaneous symmetry breakdown of the symmetry is valid and the standard treatment of χPT is inappropriate. Unfortunately, the error on our calculations is too large to make a final conclusion.

We also investigated how much $L_1 - L_3$ depend on values of X, Z, r and plotted their respective dependencies; the dependencies are rather small in comparison with error brought about by higher order remainders.

In the end we focused on convergence of chiral series of F formfactor for large values of s and in accordance with previous investigations in standard χPT we found large discrepancy between theory and experiment caused by inability of NLO RχPT to generate sufficient curvature of the formfactor. It is possible that despite the discrepancy in describing the curvature of the formfactor the overall theoretical error of our NLO calculations is small. However, we are inclined to believe that the correct explanation of this phenomenon lies in a poor convergence of the chiral series for values of s close to the kaon mass. On a very simplified model which includes sigma resonance as an explicit degree of freedom we show that for certain configurations of parameters the Feynman graphs with exchange of σ can generate contributions which supply the missing curvature; full inclusion of the σ could thus vastly improve the theoretical predictions.

Further research should contain calculation of formfactors to NNLO in RχPT, which would significantly decrease the error introduced by higher order remainders and largely improved the predictive capability about values of the low-energy constants $L_1 - L_3$. On the other hand it must be kept in mind that NNLO results contain large number of $O(p^6)$ low energy constants C_i [9], which must be provided in some way. Second possible improvement lies in including isospin breaking effects and electromagnetic corrections, which were both neglected in this work. Finally, it is desirable to further investigate the possibility of improving the χPT by an explicit inclusion of σ, which could dramatically improve matching between theory and experiment for larger s.

Appendix A

The scalar bubble

The scalar bubble is a function that arises in the amplitudes of loop graphs. It is defned as [35]

$$\begin{aligned} J_{m_P,m_Q}(q^2) &= -i\int \frac{d^dk}{(2\pi)^d}\frac{1}{(k^2-m_P^2+i0)((k-q)^2-m_Q^2+i0)} \\ &= -2\lambda_\infty + J^r_{m_P,m_Q}(q^2)\ . \end{aligned} \tag{A.1}$$

After the indicated split, function $J^r_{m_P,m_Q}(q^2)$ contains no singularity in the limit $d \to 4$. The singular part

$$\lambda_\infty = \frac{\mu^{d-4}}{(4\pi)^2}\left(\frac{1}{d-4} - \frac{1}{2}(\log(4\pi)+\Gamma'(1)+1)\right)\ . \tag{A.2}$$

appears in the renormalization of the low energy constants L_i (2.51). At this place we can thus see explicitly, how infinities which must be renormalized enter our calculations.

The scalar bubble differs from the function B_0 used by the FeynCalc by a simple rescaling

$$B_0(q^2, m_P^2, m_Q^2) = 16\pi^2 J_{m_P,m_Q}(q^2)\ . \tag{A.3}$$

From FeynCalc manual [45] we can read off a relation

$$A_0(m_P^2) = m_P^2(1 + B_0(0, m_P^2, m_P^2))\ . \tag{A.4}$$

It is customary to separate J^r into constant part and the Chew-Mandelstam function $\overline{J}_{PQ}$

$$J^r_{m_P,m_Q}(s) = J^r_{m_P,m_Q}(0) + \overline{J}_{m_P,m_Q}(s)\ . \tag{A.5}$$

The constant part can be calculated as a limit for $s \to 0$ and reads

$$J^r_{m_P,m_Q}(0) = -\frac{1}{16\pi^2}\frac{m_P^2\log(m_P^2/\mu^2) - m_Q^2\log(m_Q^2/\mu^2)}{m_P^2 - m_Q^2} \tag{A.6}$$

or in the case of the same masses

$$J^r_{m_P,m_P}(0) = -\frac{1}{16\pi^2}\left(\log\frac{m_P^2}{\mu^2} + 1\right)\ . \tag{A.7}$$

Here we remind that our calculations were performed at $\mu = 770\,\mathrm{MeV}$.

The Chew-Mendelstam function is given by an integral

$$\overline{J}_{m_P,m_Q}(s) = \frac{s}{16\pi^2}\int_{(m_P+m_Q)^2}^{\infty}\frac{dx}{x}\frac{\lambda^{1/2}(x,m_P^2,m_Q^2)}{x}\frac{1}{x-s} \tag{A.8}$$

with λ function defined in (3.25). This integral may be calculated explicitly as

$$\begin{aligned}\overline{J}_{m_P,m_Q}(s) = \frac{1}{32\pi^2}\Bigg(2 + \frac{\Delta_{PQ}}{s}\log\frac{m_Q^2}{m_P^2} - \frac{\Sigma_{PQ}}{\Delta_{PQ}}\log\frac{m_Q^2}{m_P^2} + \\ + 2\frac{(s-(m_P-m_Q))^2}{s}\sigma_{PQ}(s)\log\frac{\sigma_{PQ}(s)-1}{\sigma_{PQ}(s)+1}\Bigg)\end{aligned} \tag{A.9}$$

In the limit $m_P \to m_Q$ we get

$$\overline{J}_{m_P,m_P}(s) = \frac{1}{16\pi^2}\left(2 + \sigma_{PP}(s)\log\frac{\sigma_{PP}(s)-1}{\sigma_{PP}(s)+1}\right) . \tag{A.10}$$

In the previous expressions

$$\begin{aligned}\Delta_{PQ} &= m_P^2 - m_Q^2 \\ \Sigma_{PQ} &= m_P^2 + m_Q^2 \\ \sigma_{PQ}(s) &= \sqrt{\frac{s-(m_P+m_Q)^2}{s+(m_P+m_Q)^2}} .\end{aligned} \tag{A.11}$$

The Chew-Mandelstam function is special in that ratio $\overline{J}_{m_P,m_Q}(s)/s$ is finite in the limit $s \to 0$.

Similarly we can define $\overline{\overline{J}}$ as

$$\overline{\overline{J}}_{m_P,m_Q}(s) = J^r_{m_P,m_Q}(s) - J^r_{m_P,m_Q}(0) - sJ^{r'}_{m_P,m_Q}(0) ; \tag{A.12}$$

in the limit $s \to 0$ we then have finite ratio $\overline{\overline{J}}_{PQ}(s)/s^2$.

Appendix B

Sample Mathematica input and processing of a graph

In this appendix we show the process of evaluating a Feynman diagram using our Mathematica notebook. As a sample diagram we take diagram from Figure 15. On the diagram we marked momenta given to each particle in brackets — particles on external legs have momenta according to our convention (3.1) after taking in mind that W^+ decays into the two leptons with total momentum q. Momenta of "quantum" particles are constrained by only conservation of momentum. For better orientation we write with each vertex a number given to it in our notebook.

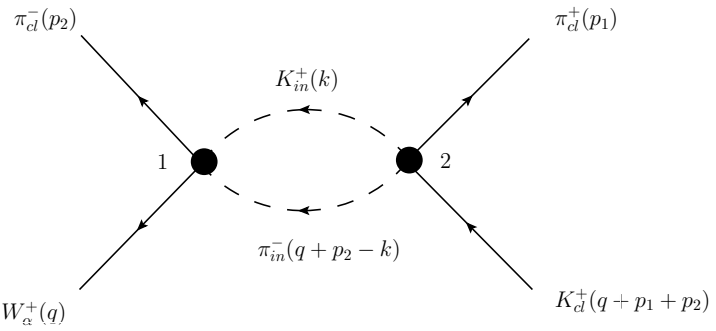

Figure 15: Sample Feynman diagram on which we show the use of the Mathematica notebook we wrote for evaluation of RχPT graphs to one loop order. Direction of arrows indicates flow of momentum

Description of the diagram would begin with description of the lines[1]

Line1 = {1, 0, π^-_{cl}**,** p_2**, , 0};**
Line2 = {1, 0, W^+**,** q**,** α**, 0};**
Line3 = {2, 1, K^+_{in}**,** k**, , 1};**
Line4 = {2, 1, π^-_{in}**,** p_2+q-k**, , 1};**
Line5 = {0, 2, K^+_{cl}**,** p_1+p_2+q**, , 0};**
Line6 = {2, 0, π^+_{cl}**,** p_1**, , 0};**
Lines = {Line1, Line2, Line3, Line4, eLine5, eLine6};

[1]Boldface text represents Mathematica input/output. Particle types and momenta were in these extracts written in the way they appear in this thesis instead of their symbolic representations used in the notebook (for example $K^+ \sim$ **KPlus**).

The first two numbers in each line stand for the vertices from and to which the line goes. If one of the vertices is zero, it means the particle is external. Next two items label the type of particle on the line and its momentum in the given orientation. Fifth item stands for the Lorentz index carried by the vector particles; for scalar particles it does not play any role. Finally the last 0 or 1 decide if the line is external or internal.

After this we finish specification of the graph by writing

Graph = {2, Lines, {3, 3}, k};

The number two tells us how many vertices the graph has. Then follows specification of the lines we discussed above. Next item describes which Lagrangian should be used in each vertex; specification goes from vertex one. The Lagrangians are numbered as

- 1 corresponds to $\mathcal{L}_2$
- 2 corresponds to $\mathcal{L}_4$
- 3 corresponds to $\mathcal{L}_{loop}$

In the specified graph we thus have two vertices from $\mathcal{L}_{loop}$. The last item on the List specifies loop momenta for FeynCalc.

With this specification we can run the calculation with command

GraphContribution[Graph];

The function **GraphContribution** starts with evaluating contributions from both vertices.

We start with the vertex number 1, which is displayed on the left part of the Figure 16. First we select lines that start or end in this vertex and reorient all outcoming lines into incoming. This reorientation is performed by switching numbers of initial and final vertex, inversing momenta and replacing particle with an antiparticle. Result of such switch is on the right side of the Figure 16.

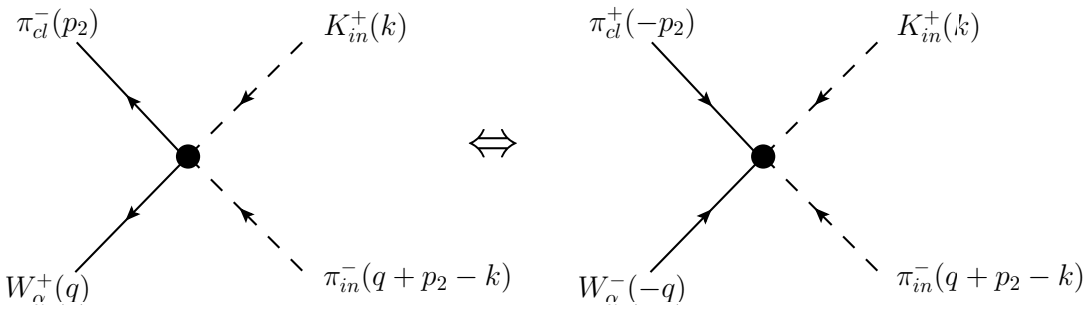

Figure 16: Preparations for calculations of contribution of the first vertex of the investigated diagram. On the left we have original form of the vertex; on the right the same vertex after orienting all lines as incoming.

As a next step we go through these lines and create a table of interacting particles, their momenta and possibly vector indexes. Because of the contraction procedure we must keep information about momenta and vector indexes together.

Particle type	Momentum / (Momentum, Lorentz index)
π^+_{cl}	$-p_2$
W^-	$(-q, \alpha)$
K^+_{in}	k
π^-_{in}	$q + p_2 - k$

Table 12: Information about particles interacting in the vertex 1

Now we can start to build the relevant Lagrangian. From the definition of the graph we know that at this vertex we must use $\mathcal{L}_{loop}$. There are four interacting particles, therefore we can expand exponentials in definitions of u (4.25) into fourth order and plug them into ${\mathcal{L}_{loop}}^2$ (4.32). In the resulting expansion we substitute each field derivative according to

$$\partial_\mu \phi \to -ip_{\phi,\mu}\, \phi \ . \tag{B.1}$$

This deserves further comment: Motivation of this replacement lies in isolating the field ϕ from the more complex structure because then we are able to find relevant Lagrangian terms simply by calling Mathematica function **Coefficient**. For example in our case we would call schematically[3]

Coefficient[**ExpandedLagrangian,** $\pi^+_{cl} W^- K^+_{in} \pi^-_{in}$]**;**

Here, **ExpandedLagrangian** stands for $\mathcal{L}_{loop}$ with expanded exponentials and with derivatives substituted with respective momenta and **Coefficient** is standard Mathematica function for isolating coefficients of a polynomial.

The substitution (B.1) is sound, because we oriented all particles as incoming. Had we not done it, we would have to decide about sign in (B.1) each time because we would not know if the particle is annihilated or created in the vertex.

Finally, to be able to use function **Coefficient**, we must separate information about Lorentz structure also for the $W^\pm$ fields in the Lagrangian. This is done by subsitutions which may be for W^+ schematically written

$$\begin{aligned} W^+_\mu &\to W^+ \,\mathbf{WPlusIndex}[\mu] \\ \partial_\alpha W^+_\mu &\to -iW^+ \,\mathbf{WPlusDerivative}[\mu, \alpha] \ . \end{aligned} \tag{B.2}$$

Analogous substitutions are performed for W^-. By these substitutions we again achieved separation of information about the particle content $W^\pm$ of the given Lagrangian term from its Lorentz structure, which enables us to select relevant Lagrangian terms by mere **Coefficient** in the way indicated above.

The contribution of the first vertex after performing all indicated steps reads[4]

$$-\frac{i\,\mathbf{WMinusIndex}[\mu_1]}{2\sqrt{2}F_0}\left(p_{K^+_{in},\mu_1} - p_{\pi^-_{in},\mu_1} + 2p_{\pi^+_{in},\mu_1}\right) \tag{B.3}$$

which in the standard notation corresponds to Lagrangian term

$$\frac{W^-_{\mu_1}}{2\sqrt{2}F_0}\left(\pi^+_{cl}\pi^-_{in}\partial^{\mu_1}K^+_{in} - \pi^+_{cl}K^+_{in}\partial^{\mu_1}\pi^-_{in} + 2K^+_{in}\pi^-_{in}\partial^{\mu_1}\pi^+_{in}\right) \ . \tag{B.4}$$

[2]Vector particles $W^\pm_\mu$ are symbolically written as **WPlus**[μ]**, WMinus**[μ]

[3]More on a position of $W^\pm$ in a moment.

[4]We had to distinguish between Lorentz indices of Lagrangian terms in distinct vertices. We did this by writing number of respective vertex as a subscript to corresponding Lorentz indices.

To evaluate the given vertex, we must now match momenta of the "classical" and "quantum" particles from Table 12 with momenta terms from the Lagrangian (B.3). In this case the result is simple and reads

$$\frac{i\,\mathbf{WMinusIndex}[\mu_1]}{2\sqrt{2}F_0}\,(2k-q+p_2)_{\mu_1}\ . \tag{B.5}$$

If there were more identical particles, we would have to use combination (4.38) instead.

The calculation is finalized by contracting vector particles. In this case it is simple and consists in replacing μ_1 in all expressions with α (for α, see Table 12) to yield final vertex rule

$$\frac{i}{2\sqrt{2}F_0}\,(2k-q+p_2)_{\alpha}\ . \tag{B.6}$$

If any of the Lagrangian terms contained $\mathbf{WMinusDerivative}[\mu_\mathbf{1},\nu_\mathbf{1}]$, we would have to replace μ_1 with α and in addition multiply the result for the processed term by $(-q)_{\nu_1}$, which is momentum of the only W^- in the interaction.

Because there are no uncontracted identical particles left[5], we are finished with the first vertex.

The same procedure is done for the vertex number two (Figure 17).

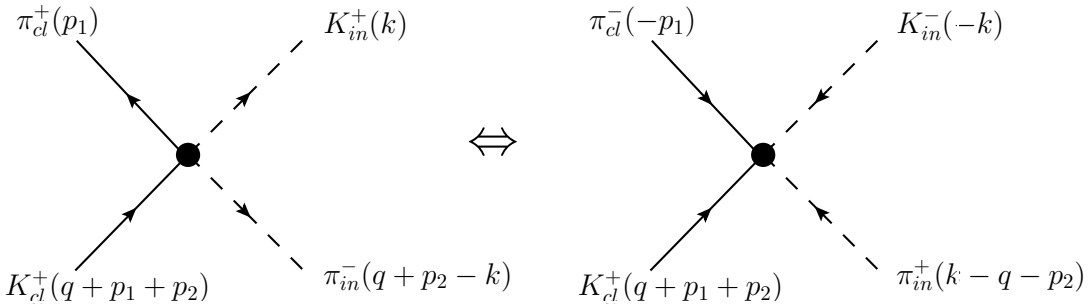

Figure 17: Preparations for calculations of contribution of the second vertex of the investigated diagram. On the left we have original form of the vertex; on the right the same vertex after orienting all lines as incoming.

Again we reorient the relevant lines, extract information about particles going to the vertex, find the relevant Lagrangian term and then match the momenta (derivatives) from the Lagrangian to the interacting particles. This evaluation contains no novelties and we thus do not go thrugh it in detail again and only quote the final vertex rule

$$\frac{B_0 m_s + 3B_0\hat{m} + 2k\cdot(2p_1+p_2+q) - 4p_1\cdot(p_2+q) - 2p_2\cdot q - 2p_1^2 - p_2^2 - q^2}{4F_0^2}\ . \tag{B.7}$$

External lines contribute nothig; both internal lines are in the loop and their contribution is set proportional to

$$\mathbf{FeynAmpDenominator}\left[\mathbf{PD}\left[k,\ B_0(m_s+\hat{m})\right]\right] \tag{B.8}$$

[5]This would happen if the Lagrangian contained terms like $\pi^0\pi^0, \eta\eta\partial\eta, \ldots$

and

$$\textbf{FeynAmpDenominator}\left[\textbf{PD}\left[q+p_2-k,\, 2B_0\hat{m}\right]\right]\ . \tag{B.9}$$

This form of the propagator is forced by the FeynCalc package. We plug in $O(p^2)$ masses of the "quantum" particles which corresponds to calculating "strict" chiral series; the transformation of the result to "bare" chiral series is performed later as mentioned in the main text.

After the program checks that there are no tadpoles or bubbles which would give a symmetry factor, it combines (B.8), (B.9), (B.6) and (B.7) together and multiplies it with a phase $(i)^4$ — one factor i for each vertex and each internal line.

The result **Result** is plugged into the FeynCalc through command

$$\textbf{PaVeReduce[OneLoop[k, Result],A0ToB0} \rightarrow \textbf{True]}\ .$$

Here k indicates the loop momenta we specified in the definition of the graph; the option **A0ToB0** means that all loop functions in the output are expressed in terms of $A_0(m_1)$ and $B_0(s, m_1, m_2)$ from the Appendix A. To arrive at the physical result we then have to divide the result by $16\pi^2$ due to conventions used by FeynCalc.

After all these steps, we obtain (rather long) expression which contains only momenta $p_{1,2}$ and q, Lagrangian constants $F_0, B_0 m_s, B_0\hat{m}$ and L_i and loop functions $A_0(m_1), B_0(s, m_1, m_2)$ and can be further simplified through steps described in the main text.

This concludes this Appendix, we hope that after reading it the reader has now much better picture of how our Mathematica notebook works.

Appendix C

Resummed low energy constants $L_4 - L_9$

Resummation of the low energy constants L_4 – L_9 was done before, here we quote the final formulae.

Resummed expressions for L_4 – L_8 were first given in the article [5], here we quote formulae from [35]. The resummation of L_4 and L_5 was obtained from the expansions of "good" variables F_K^2 and F_π^2. The result reads[1]

$$\begin{aligned}
4\overset{\circ}{M}{}_\pi^2 L_4 &= \frac{1}{2}(1-Z-\eta(r))\frac{F_\pi^2}{r+2} + \frac{2F_K^2\delta_{F_K} - (r+1)F_\pi^2\delta_{F_\pi}}{2(r+2)(r-1)} - \\
&- \frac{M_\pi^2}{4(r+2)(r-1)}\frac{X}{Z}\Big[(4r+1)J^r_{\pi\pi}(0) + (r-2)(r+1)J^r_{KK}(0) - \\
&\qquad - (2r+1)J^r_{\eta\eta}(0) + \frac{(r+2)(r-1)}{16\pi^2}\Big] , \\
4\overset{\circ}{M}{}_\pi^2 L_5 &= \frac{1}{2}F_\pi^2\eta(r) - \frac{F_K^2\delta_{F_K} - F_\pi^2\delta_{F_\pi}}{(r-1)} + \\
&+ \frac{M_\pi^2}{4(r-1)}\frac{X}{Z}[5J^r_{\pi\pi}(0) - (r+1)J^r_{KK}(0) - (2r+1)J^r_{\eta\eta}(0) - \frac{3(r-1)}{16\pi^2}] .
\end{aligned} \tag{C.1}$$

Newly introduced quantities are defined as

$$\begin{aligned}
r_2^* &= 2\frac{F_K^2M_K^2}{F_\pi^2M_\pi^2} - 1 \\
\epsilon(r) &= 2\frac{r_2^* - r}{r^2-1} \\
\eta(r) &= \frac{2}{r-1}\left(\frac{F_K^2}{F_\pi^2} - 1\right) \\
\Delta_{GMO} &= \frac{3F_\eta^2M_\eta^2 + F_\pi^2M_\pi^2 - 4F_K^2M_K^2}{F_\pi^2M_\pi^2} .
\end{aligned} \tag{C.2}$$

[1] For brevity we wrote δ_A instead of δ_{A^2}, i. e. under δ_{F_π} we understand $\delta_{F_\pi^2}$

From the "good" observables $F_P^2 M_P^2$ we can resum another three low energy constants

$$
\begin{aligned}
4\overset{\circ}{M}{}_\pi^4 L_6 &= \frac{1}{4}\frac{F_\pi^2 M_\pi^2}{r+2}(1-X-\varepsilon(r)) \\
&-\frac{M_\pi^4}{72(r-1)(r+2)}\left(\frac{X}{Z}\right)^2 [27r J^r_{\pi\pi}(0)+9(r+1)(r-2)J^r_{KK}(0) \\
&+(2r+1)(r-4)J^r_{\eta\eta}(0)+\frac{11(r-1)(r+2)}{16\pi^2}] \\
&-\frac{F_\pi^2 M_\pi^2 \delta_{F_\pi M_\pi}[(r+1)^2]-4F_K^2 M_K^2 \delta_{F_K M_K}}{4(r^2-1)(r+2)} \\
4\overset{\circ}{M}{}_\pi^4 L_7 &= -\frac{1}{8}F_\pi^2 M_\pi^2\left(\varepsilon(r)-\frac{\Delta_{GMO}}{(r-1)^2}\right) \\
&-\frac{3(1+r)F_\eta^2 M_\eta^2 \delta_{F_\eta M_\eta}+(2r^2+r-1)F_\pi^2 M_\pi^2 \delta_{F_\pi M_\pi}-8rF_K^2 M_K^2 \delta_{F_K M_K}}{8(r-1)^2(r+1)} \\
4\overset{\circ}{M}{}_\pi^4 L_8 &= \frac{1}{4}F_\pi^2 M_\pi^2 \varepsilon(r) \\
&+\frac{M_\pi^4}{24(r-1)}\left(\frac{X}{Z}\right)^2 [9J^r_{\pi\pi}(0)-3(r+1)J^r_{KK}(0)-(2r+1)J^r_{\eta\eta}(0)-\frac{5(r-1)}{16\pi^2}] \\
&-\frac{2F_K^2 M_K^2 \delta_{F_K M_K}-(r+1)F_\pi^2 M_\pi^2 \delta_{F_\pi M_\pi}}{2(r^2-1)}.
\end{aligned}
\tag{C.3}
$$

Resummation of L_9 was performed in [33] with the result

$$
\begin{aligned}
L_9 = \frac{1}{32\pi^2}&\left[\frac{1}{6}\log\frac{\overset{\circ}{M}{}_\pi^2}{\mu^2}+\frac{1}{12}\log\frac{\overset{\circ}{M}{}_K^2}{\mu^2}\right]+\frac{F_\pi^2}{12}\langle r^2\rangle_V^\pi(1-e_V^\pi)+ \\
&+\frac{1}{32\pi^2}\left[\frac{1}{12}+\frac{1}{9}Y+\frac{M_\pi^2}{36M_K^2}(r+1)Y\right],
\end{aligned}
\tag{C.4}
$$

where $\langle r^2\rangle_V^\pi$ is pion electromagnetic radius and e_V^π is corresponding higher order remainder.

Appendix D

Physical constants for resummation

Here we quote physical values of masses and decay constants of pseudoscalar mesons we used in our calculations. Because we worked in the isospin limit and neglected QED effects all pions have the same mass and decay constant and the same is true for kaons. As common pion and kaon masses we used arithmetic average of masses of charged and neutral particles.

Values we used are [10]

$$\begin{aligned} M_\pi &= 137.3\,\mathrm{MeV} \\ M_K &= 495.6\,\mathrm{MeV} \\ M_\eta &= 547.9\,\mathrm{MeV} \\ F_\pi &= 92.2\,\mathrm{MeV} \\ F_K &= 110.4\,\mathrm{MeV}\ . \end{aligned} \tag{D.1}$$

For resummed low energy constant we need also experimental value of the pion electromagnetic radius [33]

$$\langle r^2 \rangle_V^\pi = 0.451 \pm 0.031\,\mathrm{fm}^2\ . \tag{D.2}$$

Appendix E

Phase shifts of $\pi\pi$ scattering

In the elastic region of $\pi\pi$ scattering, partial wave amplitudes of isospin amplitudes T^I depend on the square of center of mass energy of the pions s as [48]

$$T_l^I(s) = \frac{1}{2i}\sqrt{\frac{s}{s-4M_\pi^2}}\left(\exp(2i\delta_l^I(s)) - 1\right) \ . \tag{E.1}$$

Here, δ_l^I are phase shifts.

Partial wave amplitudes and phase shift have following properties [48]:

- At the treshold we can write partial wave amplitudes as a series

$$\mathrm{Re}\left(T_l^I(s)\right) = q^{2l}\left(a_l^I + \overline{b}_l^I q^2 + \ldots\right) \ , \tag{E.2}$$

  where

$$q^2 = \frac{s}{4M_\pi^2} - 1 \ . \tag{E.3}$$

- The phase shifts δ_0^0 and δ_1^1 reach $\pi/2$ at known values m_σ, m_ρ,

$$\delta_0^0(\sqrt{s} = m_\sigma) = \delta_1^1(\sqrt{s} = m_\rho) = \frac{\pi}{2} \ . \tag{E.4}$$

- Below $s \approx 1\,\mathrm{GeV}^2$ is

$$a_1^1(s) = \sqrt{\frac{s}{s-4M_\pi^2}}\, q^{-2}\frac{s-m_\rho^2}{4M_\pi^2 - m_\rho^2}\tan\delta_1^1(s) \tag{E.5}$$

  very smooth and the same — with less accuracy — holds for a_2^0.

Schenk [48] found a simple parametrization of $\pi\pi$ scattering phase shifts that satisfies these three conditions, namely

$$\tan\delta_l^I(s) = \sqrt{1-\frac{4M_\pi^2}{s}}\, q^{2l}\left(a_l^I + b_l^I q^2 + c_l^I q^4 + d_l^I q^6\right)\frac{4M_\pi^2 - s_l^I}{s - s_l^I} \ . \tag{E.6}$$

The $\pi\pi$ scattering phase shifts satisfy so-called Roy equations [49]. Solutions to these dispersive equations depend on four parameters $a_0^0, a_0^2, \theta_0, \theta_1$ — two S-wave scattering lengths and two phases at conveniently chosen matching point s_0.

In [32] authors related Schenk parameters $a_l^I, b_l^I, c_l^I, d_l^I$ to four parameters describing solutions of the Roy equation through $(X = a, b, c, d)$

$$X_l^I = z_1 + z_2 u + z_3 v + z_4 u^2 + z_5 v^2 + z_6 uv + z_7 u^3 + z_8 u^2 v + z_9 uv^2 + z_1 0 v^3 \ , \quad \text{(E.7)}$$

where

$$u = \frac{a_0^0}{p_0}, \quad v = \frac{a_0^2}{p_2} - 1, \quad p_0 = 0.225, \quad p_2 = -0.03706 \ . \quad \text{(E.8)}$$

Values of coefficients z_i were obtained from numerical solutions to Roy equations and can be found in the Appendix B of the article [32].

Finally the values of s_0^0 and s_1^1 are fixed by the boundary conditions

$$\delta_0^0(s_0) = \theta_0, \quad \delta_1^1(s_0) = \theta_1 \ . \quad \text{(E.9)}$$

Bibliography

[1] V. Cirigliano et al., "Kaon Decays in the Standard Model", *Rev. Mod. Phys.*, vol. 84, p. 399, 2012.

[2] G. Buchalla et al., "B, D and K decays", *Eur. Phys. J.*, vol. C57, p. 309, 2008.

[3] J. Gasser, H. Leutwyler, "Chiral Perturbation Theory: Expansions in the Mass of the Strange Quark", *Nucl. Phys.*, vol. B250, p. 465, 1985.

[4] S. Scherer, "Introduction to Chiral Perturbation Theory", *Adv. Nucl. Phys.*, vol. 27, p. 277, 2003.

[5] S. Descotes-Genon et al., "Resumming QCD vacuum fluctuations in three-flavour Chiral Perturbation Theory", *Eur. Phys. J.*, vol. C34, p. 201, 2003.

[6] J. Bijnens, "K_{l4} Decays and the Low-energy Expansion", *Nucl. Phys.*, vol. B337, p. 635, 1990.

[7] Peter Truöl, "New Results on Rare and Forbidden Semileptonic K^+ Decays", 2000, arXiv:0012012v1 [hep-ex].

[8] The NA48/2 Collaboration, "New measurement of the $K^\pm \to \pi^+\pi^- e^\pm \nu$ (K_{e4}) decay Branching Ratio and Hadronic Form Factors", 2012, arXiv:1206.7065v1 [hep-ex].

[9] J. Bijnens, I. Jemos, "A new global fit of the L_i^r at next-to-next-to-leading order in Chiral Perturbation Theory", 2011, arXiv:1103.5945v2 [hep-ph].

[10] J. Beringer et al. (Particle Data Group), "2012 Review of Particle Physics", *Phys. Rev.*, vol. D86, p. 010001, 2012.

[11] T. Appelquist, J. Carazzone, "Infrared singularities and massive fields", *Phys. Rev.*, vol. D11, p. 2856, 1975.

[12] B. Grzadkowski et al., "Natural relations and Appelquist-Carazzone decoupling theorem", *Phys. Rev.*, vol. D29, p. 1476, 1984.

[13] S. Weinberg, "Phenomenological Lagrangians", *Physica*, vol. 96A, p. 327, 1979.

[14] A.Pich, "Effective Field Theory", 1998, arXiv:9806303v1 [hep-th].

[15] M. E. Peskin, D. V. Schroeder, "An Introduction To Quantum Field Theory (Frontiers in Physics)", Perseus Books Publishing, Reading, 1995.

[16] W. Greiner et al., "Quantum Chromodynamics", Springer, Berlin, 2002.

[17] J. L. Kneur, A. Neveu, "Λ_{MS}^{QCD} from Renormalization Group Optimized Perturbation", 2011, arXiv:1108.3501v1 [hep-ph].

[18] G. Ecker, "The Standard Model At Low Energies", 1993, arXiv:9309268v1 [hep-ph].

[19] C. Vafa, E. Witten, "Restrictions on symmetry breaking in vector-like gauge theories", *Nucl. Phys.*, vol. B234, p. 173, 1984.

[20] S. Coleman, E. Witten, "Chiral-Symmetry Breakdown in Large-N Chromodynamics", *Phys. Rev. Lett.*, vol. 45, p. 100, 1980.

[21] J. Goldstone, "Field theories with $\ll$ Superconductor $\gg$ solutions", *Il Nuovo Cimento*, vol. 19, p. 154, 1961.

[22] H. Leutwyler, "On the Foundations of Chiral Perturbation Theory", *Ann. Phys.*, vol. 235, p. 165, 1994.

[23] J. Wess, B. Zumino, "Consequences of anomalous Ward identities", *Phys. Lett.*, vol. B37, p. 95, 1971.

[24] E. Witten, "Global aspects of current algebra", *Nucl. Phys.*, vol. B223, p. 422, 1983.

[25] J. Bijnens et al., "Chiral perturbation theory for anomalous processes", *Z. Phys.*, vol. C46, p. 599, 1990.

[26] J. Bijnens et al., "Nambu-Jona-Lasinio-like models and the low-energy effective action of QCD", *Nucl. Phys.*, vol. B350, p. 501, 1993.

[27] G. Ecker et al., "The role of resonances in chiral perturbation theory ", *Nucl. Phys.*, vol. B321, p. 311, 1989.

[28] S. Myinta, C. Rebbia, "Derivation of chiral lagrangians from lattice QCD", *Nucl. Phys. Proc. Suppl.*, vol. 34, p. 213, 1994.

[29] G. Amoros et al., "$K_{\ell 4}$ Form-Factors and π-π Scattering"", *Nucl. Phys.*, vol. B585, p. 293, 2000.

[30] D. B. Kaplan, A. V. Manohar, "Current-Mass Ratios of the Light Quarks", *Phys. Rev. Lett.*, vol. 56, p. 2004, 1086.

[31] S.-Z. Jiang et al., "Computation of the p6 order chiral Lagrangian coefficients from the underlying theory of QCD", *Phys. Rev.*, vol. D81, p. 014001, 2010.

[32] S. Descotes-Genon et al., "Analysis and interpretation of new low-energy Pi-Pi scattering data", *Eur. Phys. J.*, vol. C24, p. 469, 2002.

[33] V. Bernard et al., "Chiral dynamics with strange quarks in the light of recent lattice simulations", *JHEP*, vol. 2011, p. 107, 2011.

[34] S. Descotes-Genon, "Low-energy pi-pi and pi-K scatterings revisited in three-flavour resummed chiral perturbation theory", *Eur. Phys. J.*, vol. C52, p. 141, 2007.

[35] M. Kolesár, J. Novotný, "$\pi\eta$ scattering and the resummation of vacuum fluctuation in three-flavour χPT", *Eur. Phys. J.*, vol. C56, p. 231, 2008.

[36] J. Bijnens et al., "K_{l4} Decays Beyond One Loop", *Nucl. Phys.*, vol. B427, p. 427, 1994.

[37] F. Halzen, A. D. Martin, "Quarks and Leptons: An Introductory Course in Modern Particle Physics", John Wiley & Sons, New York, 1984.

[38] S. Weinberg, "Current-Commutator Calculation of the K_{l4} Form Factors", *Phys. Rev. Lett.*, vol. 17, p. 336, 1966.

[39] C.Riggenbach et al., "Chiral symmetry and the large-N_c limit in K_{l4} decays", *Phys. Rev.*, vol. D43, p. 127, 1991.

[40] A. Nehme, "Isospin Breaking in $K_{\ell 4}$ Decays of the Neutral Kaon", *Nucl. Phys.*, vol. B682, p. 289, 2004.

[41] The NA48/2 Collaboration, "Precise tests of low energy QCD from K_{e4} decay properties", *Eur. Phys. J.*, vol. C70, p. 635, 2010.

[42] K. M. Watson, "The Effect of Final State Interactions on Reaction Cross Sections", *Phys. Rev.*, vol. 88, p. 1163, 1952.

[43] L. F. Abbott, "The Background Field Method Beyond One Loop", *Nucl. Phys.*, vol. B185, p. 189, 1981.

[44] Wolfram Research, Inc., "Mathematica", Version 7.0, Champaign, IL (2008).

[45] R. Mertig, "FeynCalc", `http://www.feyncalc.org/`, 07/29/2012.

[46] I. Caprini et al., "Mass and width of the lowest resonance in QCD", *Phys. Rev. Lett.*, vol. 96, p. 132001, 2006.

[47] J.Soto et al., "Chiral effective theory with a light scalar and lattice QCD", 2011, arXiv:1110.6156v2 [hep-ph].

[48] A. Schenk, "Absorption and Dispersion of Pions at Finite Temperature", *Nucl. Phys.*, vol. B363, p. 97, 1991.

[49] S. M. Roy, "Exact integral equation for pion-pion scattering involving only physical region partial waves", *Phys. Lett.*, vol. B36, p. 353, 1971.

List of Tables

List of Abbreviations

LO	leading order
NLO	next-to-leading order
NNLO	next-to-next-to-leading order
QCD	Quantum Chromodynamics
QED	Quantum Electrodynamics
χPT	Chiral Perturbation Theory
RχPT	Resummed Chiral Perturbation Theory
$\chi\mathrm{PT}_\mathrm{S}$	Chiral Perturbatin Theory with a light scalar (σ)

Attachments

Included is a file "MathematicaNotebook.nb" which contains our Mathematica notebook which may be used for calculation of various Feynman diagrams of RχPT to one loop.